Materiomics: Deciphering topographic cues for cell-surface interactions

Hemant Vijaykumar Unadkat

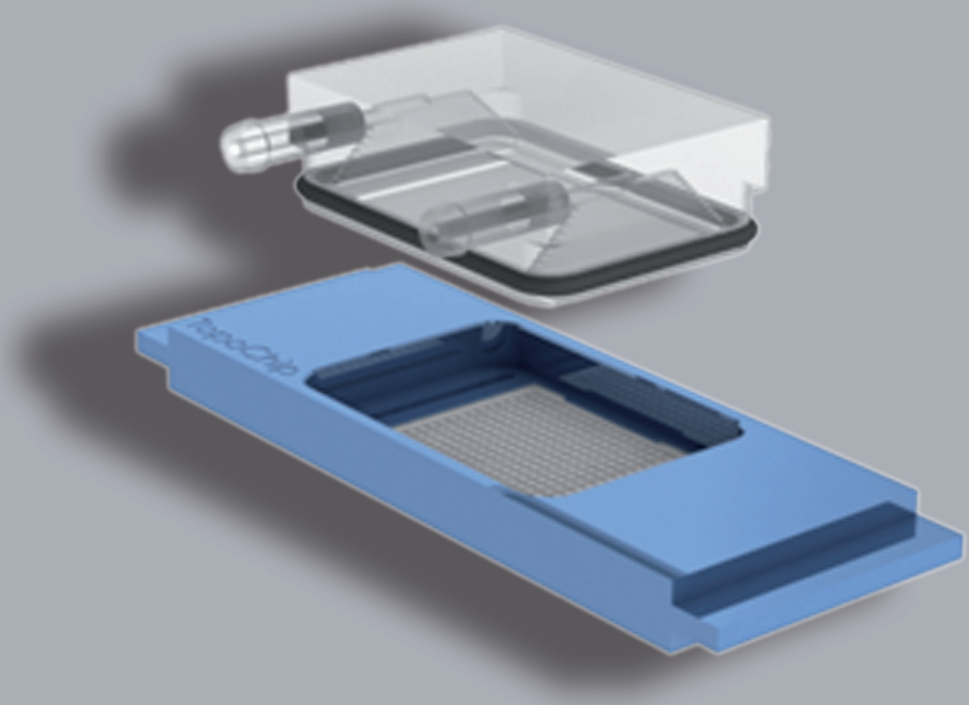

Materiomics: Deciphering topographic cues for cell-surface interactions

Hemant Vijaykumar Unadkat

PhD thesis
University of Twente

Members of the committee

Chairman	Prof. Dr. Gerard van der Steenhoven	University of Twente
Promotor	Prof. Dr. Jan Feijen	University of Twente
Assistant Promotor	Dr. Roman Truckenmuller	University of Twente
Members	Prof. Dr. Vinod Subramaniam (bio-imaging)	University of Twente
	Prof. Dr. Marc Uetz (discrete mathematics)	University of Twente
	Prof. Dr. Jan Eijkel (micro- and nanofluidics)	University of Twente
	Prof. Dr. Ruud Bank (cell-materials interaction)	University of Groningen
	Prof. Dr. Leo Koole (biomaterials)	University of Maastricht

MATERIOMICS: DECIPHERING TOPOGRAPHIC CUES FOR CELL-SURFACE INTERACTIONS

DISSERTATION

to obtain

the degree of doctor at the University of Twente,

on the authority of the rector magnificus,

prof. dr. H. Brinksma,

on account of the decision of the graduation committee,

to be publicly defended

on Wednesday the 29th of February 2012 at 14:45 hrs.

by

Hemant Vijaykumar Unadkat

born on the 6th of April 1979

in Nagpur, India

This thesis has been approved by:

Promotor: Prof. Dr. Jan Feijen

Assistant Promotor: Dr. Roman Truckenmuller

©Copyright 2012, Hemant Unadkat, Gadchiroli, India

Neither this book nor its parts may be reproduced without prior written consent from the author

ISBN: 978-90-365-3321-8

Contents

Publications

1. *Unadkat, H. V.*; Hulsman, M.; Cornelissen, K.; Papenburg, B. J.; Truckenmüller, R. K.; Post, G. F.; Carpenter, A. E.; Wessling, M.; Uetz, M.; Reinders, M. J. T.; Stamatialis, D.; van Blitterswijk, C. A.; de Boer, J. **An algorithm-based topographical biomaterials library to instruct cell fate** *Proceedings of the National Academy of Sciences* 108, 16565-16570 (2011)
    a. Research Highlight*:* **Nature 478, 9; 2011, Nature Methods 8, 900; (2011), Nature Materials 10, 808; (2011)**
2. Truckenmüller, R. K.; Giselbrecht, S.; Escalante-Marun, M.; Groenendijk, M.; Papenburg, B.; Rivron, N.; *Unadkat, H.*; Saile, V.; Subramaniam, V.; van den Berg, A.; van Blitterswijk, C. A.; Wessling, M.; de Boer, J.; Stamatialis, D.; **Fabrication of cell container arrays with overlaid surface topographies.** *Biomedical Microdevices, 1-13*
3. *Unadkat, H. V.*; Rewagad, R.; Hulsman, M.; Hulshof, G. F. B.; Truckenmüller, R. K.; Stamatialis, D.; Eijkel, J.C. T.; van den Berg, A.; van Blitterswijk, C. A.; de Boer, J. **A modular versatile chip carrier for high throughput screening of cell-biomaterial interactions** (Submitted)
4. *Unadkat, H. V.*; Groen, N.; Doorn, J.; Fischer, B.; Barradas, A. M. C.; Hulsman, M.; van de Peppel, J.; Moroni, L.; van Leeuwen, J. P. T.; Reinders, M. J. T.; van Blitterswijk, C. A.; de Boer, J. **High content imaging as a novel tool for automated analysis of biomaterial-induced cellular responses** (Submitted)

Patents

1. WO 2009/058015. **High throughput screening methods and apparatus for analyzing interactions between surfaces with different topographies and the environment** International Patent Application.
2. P92753US00 **Surface topographies inducing mesenchymal stromal cell proliferation and differentiation** US Provisional Filed by University of Twente 23 September 2010.
3. P93576US00 **A seeding and culturing device for high throughput screening of biomaterials** US Provisional Filed by University of Twente 15 December 2010.

Book Chapter

Hemant Unadkat, Robert Gauvin, Clemens van Blitterswijk, Ali Khademhosseini, Jan de Boer, Roman Truckenmüller **Microfabrication techniques in Materiomics,** *Materiomics: High throughput screening of biomaterial properties*, Ed: Jan de Boer and Clemens van Blitterswijk; Cambridge University Press (In press)

Chapter 1

Introduction and aim of this thesis

Directing or modulating behaviour of cells is a vital phenomenon for tissue engineering and regenerative medicine and hence understanding of its control is crucial for evoking the required regenerative responses from the tissue being repaired or replaced. Biomaterials which can dictate the behaviour of cells or in other words instructive materials are being brought to clinical applications. These materials are believed to rely on a fundamental phenomenon in cell biology called mechano-transduction which is a process by which cells convert mechanical stimuli into chemical responses. More than a century ago, a surgeon and anatomist Julius Wolff hypothesised that the structure of bone tissue is influenced by the mechanical environment (1). In his observation Wolff noted that in cancellous bone, the trabeculae matched the principal stress lines caused by daily physical loading. Around the same time Thompson and other researchers also proposed that shape of tissues and organs during embryonic development is regulated by the mechanical forces that they experience (2-3).

Lately, it has become increasingly evident that, mechanical forces can regulate a wide array of biological processes, from cell proliferation and differentiation to tissue mass homeostasis and complex inflammatory cascades (4-8). In vivo these mechanical forces which regulate cell behaviour arise from cell-cell contact, extracellular matrix and interstitial fluids amongst others. Mechanical forces inside a cell can also be modulated by using traditional pharmacologic methods to directly target the force sensing and generating machinery primarily the actin-myosin complex. Several pharmacologic agents such as blebbistatin which inhibit the modulators of contractility, including the molecular motor myosin II are known (9). Similarly, molecular-genetic methods have also been used effectively to target pathways known to play a role in actin-myosin complex modulation.

In addition to these molecular and genetic methods biophysical approaches have attracted the attention of researchers. For instance it is known that by varying the stiffness of the substrate that cells grow on,

one can modulate the behaviour of cells (10-11). The cellular response to the stiffness of a substrate can be easily studied by growing cells on polymeric hydrogels. It is easy to fabricate these gels with varying stiffness by changing the degree of crosslinking. One such way to modulate the behaviour of cells is by using surface topographies. It is known for a long time that cells orient and often move rapidly along fibres of 5-50 µm in diameter. This phenomenon which is known as 'contact guidance' was first described by Paul Weiss in 1945 (12).

It is now known that surface topography can regulate cellular responses from initial attachment and migration through to differentiation and production of new tissue. This finding has brought us to the era of smart or instructive biomaterials which can dictate the response of surrounding tissue by presenting optimal surface characteristics. With these advancements, the topography of implantable biomaterials is critical for integration of materials within the human body. Technological advances in the field of materials processing have provided us with immense possibilities by which characteristics of materials such as stiffness and topographies can be altered in a precise and reproducible manner. However, until now it has been difficult to identify the best material surface for desired cell behaviour as techniques to study the behaviour of cells on these multitudes of variations in surface topographies did not exist.

This thesis is intended at introducing the field of Materiomics. Materiomics as we define it is high throughput screening of natural and synthetic materials and their properties. In this thesis we have tried to provide a systematic overview of steps required for Materiomics technology development with a pilot example of the TopoChip system. The TopoChip system is meant for high-throughput screening of cellular interactions with surface topographies. Over the years it has been shown in the literature that by modifying the topography of the implant surface a desired response from the surrounding tissue or implanted cells (when a cell seeded scaffold is implanted) can be evoked. For instance, in relation to bone formation, this response can either be in the form of osteoconduction or osteoinduction.

In chapter 2, we describe microfabrication techniques and their relation and application to the field of Materiomics.

Chapter 3 provides the paradigm of Materiomics. In this chapter we present the TopoChip technology which sheds light on the interaction of mesenchymal stem cells with surface topographies.

Over the years as high-throughput screening systems progressed, microfluidics became an essential part of these systems. For instance DNA microarrays, which were initially available on conventional glass slides, saw a rapid transition with the development in microfluidics. The old generation of arrays could only be used for hybridisation and imaging. Today, microarrays with robust fluid handling capabilities thereby reducing the errors and improved reliability of results are available. In chapter 4 the integration and application of microfluidics for the TopoChip platform are described.

Robust and reliable biological assays which prohibit omission of essential information are key for the success of high throughput screening systems. In chapter 5, we describe how morphometric phenotypical information from cells can inform us about changes in gene repertoire of cells when grown on different biomaterials.

In Chapter 6, we provide the conclusions and describe some additional examples of systems, which in the future may prove important in the progress of Materiomics.

References

1. Wolff J (1892) *Das Gesetz der Transformation der Knochen* (Hirschwald, Berlin,) pp xii, 152 p.
2. Roux W (1895) *Gesammelte Abhandlungen über Entwicklungsmechanik der Organismen* (W. Engelmann, Leipzig,) p 2 vol.
3. Thompson DAW (1917) *On growth and form* (University press, Cambridge) pp xv, 793 p.
4. Chien S, Li S, & Shyy YJ (1998) Effects of mechanical forces on signal transduction and gene expression in endothelial cells. *Hypertension* 31(1 Pt 2):162-169 .
5. Chowdhury F*, et al.* (2010) Material properties of the cell dictate stress-induced spreading and differentiation in embryonic stem cells. *Nat Mater* 9(1):82-88 .
6. Davies PF, Remuzzi A, Gordon EJ, Dewey CF, Jr., & Gimbrone MA, Jr. (1986) Turbulent fluid shear stress induces vascular endothelial cell turnover in vitro. *Proc Natl Acad Sci U S A* 83(7):2114-2117 .
7. McBeath R, Pirone DM, Nelson CM, Bhadriraju K, & Chen CS (2004) Cell shape, cytoskeletal tension, and RhoA regulate stem cell lineage commitment. *Dev Cell* 6(4):483-495 .
8. Yamawaki H, Pan S, Lee RT, & Berk BC (2005) Fluid shear stress inhibits vascular inflammation by decreasing thioredoxin-interacting protein in endothelial cells. *J Clin Invest* 115(3):733-738 .
9. Walker A*, et al.* (2010) Non-muscle myosin II regulates survival threshold of pluripotent stem cells. *Nat Commun* 1:71.
10. Folkman J & Moscona A (1978) Role of cell shape in growth control. *Nature* 273(5661):345-349.
11. Huebsch N*, et al.* (2010) Harnessing traction-mediated manipulation of the cell/matrix interface to control stem-cell fate. *Nat Mater* 9(6):518-526.
12. Weiss P (1945) Experiments on cell and axon orientation in vitro: The role of colloidal exudates in tissue organization. *Journal of Experimental Zoology* 100(3):353-386.

Chapter 2

Microfabrication techniques in Materiomics

Microfabrication techniques in Materiomics

Hemant Unadkat*, Robert Gauvin*, Clemens van Blitterswijk, Ali Khademhosseini, Jan de Boer, Roman Truckenmüller

* These authors contributed equally to this chapter

Scope:

The present chapter deals with an overview of basic micro- and nanofabrication techniques. The goal is to explain to the reader how such techniques can be utilized for the study of Materiomics. The basic processes used in microfabrication, amongst others including photolithography, etching and micromolding, are explained. Some classical examples of these techniques as applied to Materiomics are highlighted. Furthermore, possible uses of such techniques for understanding the interplay between cells and materials are also discussed.

1. Introduction

1.1. Overview

Techniques used to fabricate structures or devices in the range of micrometer sizes and smaller are commonly referred to as microfabrication techniques. Microfabrication techniques, initially meant for the electronics industry, have found wide range of applications in diverse fields such as chemical engineering and life sciences. Since the early 1990s, application of microfabrication technologies for the chemical and biological analysis has been termed as micro total analysis systems (μTAS) (1). The earliest use of microfabrication technologies was reported in the early 20th century when vacuum tubes started to be replaced by integrated circuits (ICs). However, the first reported use of microfabrication technology in the field of microfluidics was in 1979 (2). For the first time, microfabrication technologies were applied to fabricate a gas-chromatographic air analyzer on a silicon wafer.

Microfabrication technologies offer the advantages of ultra precision engineering and fabrication processes. Microfabricated devices meant for μTAS initially offered the advantage of sample analysis but over the years the evolution in these technologies has led to the added advantage of sample preparation, fluid handling, separation systems, cell handling, and cell culturing in an integrated manner (1).

Pertaining to the evolving field of Materiomics, microfabrication technologies can be used for two major applications. On one hand, can be used for the fabrication of metamaterials, and on the other, they are ideal for fabrication of systems for high-throughput screening of material properties.

1.2.Materiomics and μTAS

Materiomics can be defined as large-scale studies of structure, properties and function of natural and synthetic materials. A large-scale study commonly referred to as high-throughput screening (HTS) relies on studying thousands of different properties or different types of materials. Microfabrication enables fabrication of miniaturized devices thereby facilitating the accommodation of, for instance, thousands of different materials or test conditions on the same platform. This enables us to study the behavior and characteristics of all these materials and test conditions within one experiment.

μTAS approaches have been adapted to be applied to multiple disciplines such as pharmacology, genetics and proteomics. In pharmacology, for instance, properties of thousands of different compounds are studied in order to discover the most promising drug candidate. This HTS approach has led to the discovery of new drugs for various diseases, although the action of these compounds pertaining to a given disease was originally unknown. Similarly, HTS of gene activity can be monitored by widely used microarray technologies. The new generation of microarrays and HTS systems also provides exceptional possibilities such as fluid handling in integrated devices, greatly improving the reading capabilities and the quality of results.

The use of μTAS in the evolving field of Materiomics provides the possibility to miniaturize the devices. These miniaturized devices are equipped with enhanced functionalities (3) such as the ability to handle very large sample number, portability and easy readings, and allow us to study properties which previously could not be investigated.

1.3.Materiomics and metamaterials

Immense efforts have recently been dedicated towards the development of metamaterials. These classes of materials are artificially engineered to display properties which may not be inherent in nature. For instance, this field has provided us with materials having a negative refractive index, a property

which is not found in natural materials(4). Such classes of materials gain their property by virtue of their structure rather than composition. A plethora of microfabrication techniques are currently being investigated for the fabrication of metamaterials. The combination of microfabrication techniques with Materiomics will ultimately allow us to manufacture arrays of such materials to be evaluated in a high-throughput manner.

1.4.Advantages of microfabrication in Materiomics

Advantages of the application of microtechnologies for the fabrication of devices or systems to study material properties include cost efficiency, high performance, precision-based design flexibility, miniaturization and automated analysis. Miniaturization involves convergence of multiple disciplines, for instance, fluid dynamics, material sciences, chemical engineering and life sciences, that need to be carefully studied and applied in order for such a system to be functional. By decreasing the size or amount of material required, the dimensions of the device also decrease, providing us with a device that allows us to perform high-throughput screening, offers us portability and aids us to design high-density arrays on a small scale while reducing the cost and consuming less energy and materials. However, these devices can be used to evaluate biological behavior in a less invasive manner and can help us to test thousands of different materials and surface properties of biomaterials without the burden related to *in vivo* assays.

2. Basic techniques

2.1. Photolithography

Lithography literally means writing on stone and has its origin in Greek. The term photolithography particularly refers to transferring geometric patterns into a photosensitive material via selective exposure to light. Fig. 1 shows an exemplary photolithography process followed by a subtractive pattern transfer process in the form of etching (5-6).

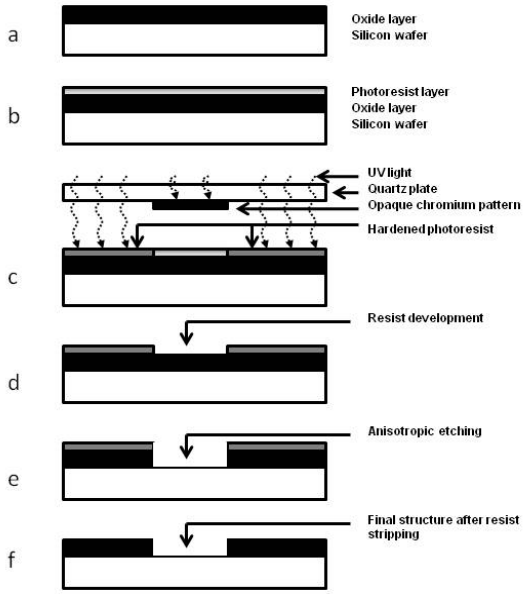

Figure 1 Schematic representation of traditional photolithography and subtractive pattern transfer process using a silicon wafer

The first step in photolithography typically involves coating a silicon wafer with a photoresist. Two types of photoresists can be used i.e., positive and negative resists. Here we describe the process using a negative photoresist and an oxidized silicon wafer as an example. A chromium glass photomask which can be fabricated by laser direct writing can be used to selectively expose the photoresist with

ultraviolet (UV) light. After exposure, the wafer can be immersed in a developer solution for removal of the unexposed areas of photoresist which leaves a pattern of bare and photoresist-coated areas of silicon oxide on the wafer. The areas exposed to the UV remain coated with the photoresist thereby providing us with a negative image of the mask. The wafer can be subsequently etched using an etchant like hydrofluoric acid which will etch away the unexposed bare oxide regions leading to cavities. The exposed area of photoresist prevents the etchant from reacting with the oxide layer underneath. The process of etching can be divided into two types viz., isotropic and anisotropic (fig. 2). After etching, the remaining photoresist can be stripped off with a solution like piranha (H_2SO_4:H_2O_2) which only attacks the photoresist and not the silicon and its oxide. The silicon wafer which has the required patterns thus fabricated can be used for a variety of applications.

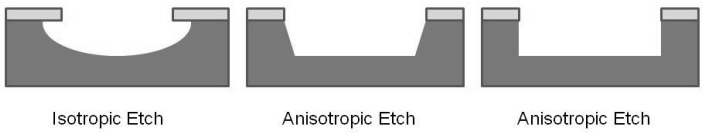

Figure 2 Schematic representation of isotropic and anisotropic etching techniques

The resolution of photolithography is limited by the wave length of light used and presently with the use of Deep UV sources resolutions as low as a few ten nanometers can be achieved. The processes involved in photolithography are described as follows.

2.1.1. Oxide growth

In many cases, an oxide layer is desired as a mask for subsequent processes (e.g. etching or ion implant process) or as an insulating layer. This is usually achieved by heating a silicon wafer to between 900 and 1150°C in a dry or humidified oxygen stream in a tube furnace.

2.1.2. Spin coating and soft-bake

Most photoresist used in silicon micromachining are polymeric compounds which are sensitive to UV radiation. When using oxidized silicon wafer, photoresist can be deposited on silicon wafers after oxidation. Usually, the resist in its liquid form is dispensed onto a wafer that is securely held by a vacuum chuck in a spin- coater. The wafer is then spun at desired speeds in one or more steps. Typically, spin speeds between 1500 and 8000 rpm allow the formation of a uniform film of the resist on a wafer depending on resist properties. The centrifugal forces caused by the spinning lead to homogeneous spreading and film formation on the wafer by allowing the resist to flow to the edges where it builds up and is later expelled due to increase in surface tension. The resulting resist thickness is hence a function of spin speed and time, concentration of the resist solution and molecular weight of the resist. The spin curves for various resists are provided by the manufacturers. Resist coating being the first step in silicon micromachining is extremely important as coating defects may lead to defects in the final device.

The resist thus coated contains residual solvent. It may also contain residual stress. Hence, the wafers should be soft-baked typically at 75-100°C for removal of solvent and stress. Soft baking also leads to better adhesion of the resist layer to the wafer.

2.1.3. Exposure and post-exposure treatment

Patterns can be designed using a variety of commercially available software. A multitude of methods are available to fabricate masks from the designed patterns. A widely used method for mask fabrication makes use of a laser beam to selectively expose the resist on a chromium layer which is coated on a glass plate.

Patterns can be transferred onto the photoresist by shining light through the mask (fig. 1c). Usually different wavelengths of light i.e. 435 nm (g-line), 405 nm (h-line) and 365 nm (i-line) of a mercury lamp are used for exposure of the photoresist. The exposure of photoresist to the light source either

increases or decreases the solubility of the resist in an appropriate developer depending on whether a positive or negative resist is used. Therefore, for a positive resist, the exposed areas will dissolved during resist development, and vice versa for the negative resist (fig. 3). The side wall profile of the developed photoresist layer (fig. 4) which is critical for applications like hard-to-etch metals (fig. 5) and mold fabrication depends on the resist tone, exposure dose, developer strength and development time amongst others. A desired side wall profile can be obtained by modifying these parameters.

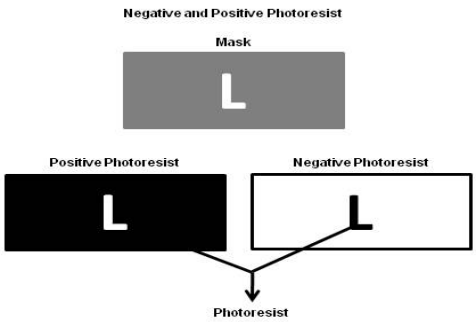

Figure 3 Final pattern transfer after resist development

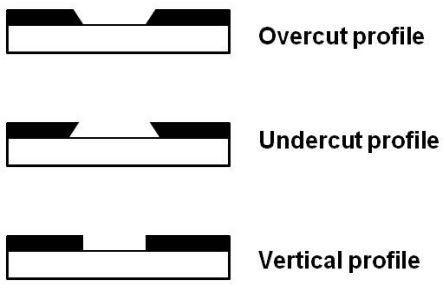

Figure 4 Illustration of different sidewall profiles of the photoresist

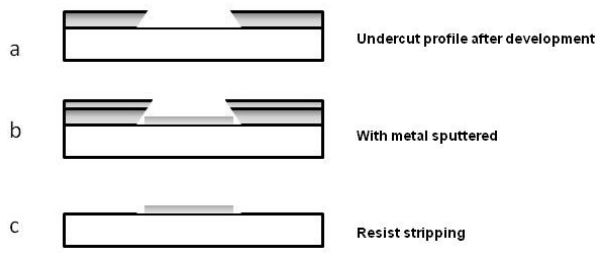

Figure 5 Schematic illustration of the use of undercut resist profile followed by sputtering of a metal which would otherwise be hard to etch (e.g., gold or palladium)

The polymerization reactions initiated during exposure do not always lead to completion leaving residues. Hence, very often a post exposure treatment is necessary to stop the reactions or to initiate new reactions. There are several post exposure treatments that are conventionally used. These include post exposure baking, flood exposure, also with other types of radiations, treatment with reactive gas and vacuum treatment.

2.1.4. Development, descumming, and postbaking

The development process of the resist involves selective dissolving of the resist (fig. 1d). Negative resists are developed using organic solvents and positive resists in aqueous alkaline solutions such as tetramethylammonium hydroxide. Sometimes, resist residues remain entrapped in the pattern even after development. For this, another process called descumming which makes use of mild plasma treatment is used to get rid of these residues. Energetic oxygen ions from the oxygen plasma react with the residual resist and burn it. Postbaking is a process which removes residual solvents and promotes adhesion of the resist film which has been weakened either due to the penetration of developer along the resist-substrate interface or by swelling of the resist. Postbaking is generally carried out at higher temperatures (120°C or similar). It is also referred to as hard baking. Postbaking is also desired as it increases hardness of the film and increases the resistance to subsequent etching and deposition steps.

Example: Lovmand et al. designed and fabricated combinatorial topographical libraries of tantalum surfaces for the screening of enhanced osteogenic expression and mineralization of MC3T3 cells (7) (fig. 6). This library of surface topographies which is known as BioSurface Structure Array (BSSA) contains 504 unique topographies.

In this study, the topographic libraries were first fabricated on boron-doped p-type silicon wafers. The designed arrays of patterns were transferred to the substrate using standard photolithography without the final hard bake, followed by a dry etch process with etch chemistries Cl_2, HBr and NF_3 leading to a side wall angle of approximately 85 degrees. After photoresist stripping, the surface was sputter-coated with tantalum.

Cells from the mouse osteoblastic cell line MC3T3 were seeded and cultured on these arrays. Osteocalcin and osteopontin activity of cells seeded on these arrays was analysed by immunostaining.

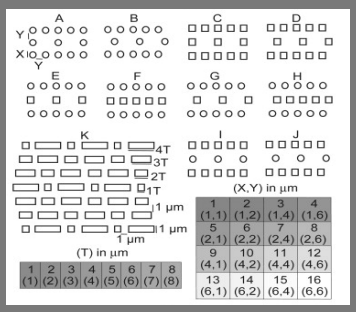

a

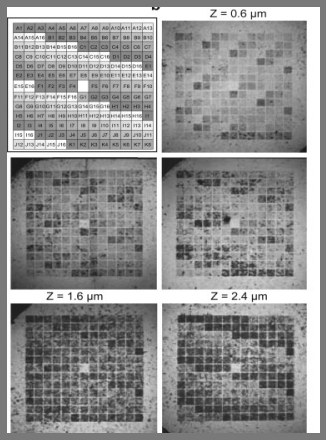

b

Figure 6 Wafer design and mineralization. (a) Series A–J; different patterns including square and round pillars. Each pattern series contains 16 different combinations of lateral dimension of the structure (X) and gap between the structures (Y). Series K; 8 different iterations of the lateral dimension of a "shark-skin"-like structure, all with the same gap between individual structures (1 µm). (b) Upper left illustration: location of series A–K on the wafer. White field in the middle of the wafer is the unstructured control field. Upper right and the two images in the middle: Induction of mineralization on three different vertical dimensions of the structures (Z = 0.6 µm, Z = 1.6 µm and Z = 2.4 µm) of the BSSA library described in A. Lower two images: repetition of the above-described experiment with two different heights (Z = 1.6 µm and Z = 2.4 µm). Note that structures 2 and 3 in a series are always located above structures 15 and 16 for the same series and that a small area of unstructured control surface separates each structure

Reprinted with permission from Elsevier Ltd. [Biomaterials] (Lovmand, J. et al. The use of combinatorial topographical libraries for the screening of enhanced osteogenic expression and mineralization. Biomaterials 30, 2015-2022) Copyright (2009)

2.2. Direct writing techniques

Direct writing techniques are a set of serial writing techniques. Unlike photolithography where the whole wafer can be patterned at once, serial writing processes incrementally write multiple small areas. Such processes make use of tools like a laser, an electron beam (e-beam), a focused ion beam or an atomic force microscope (AFM). These techniques are highly accurate in terms of feature dimensions. Using these techniques, resolutions down to 10 nm can be achieved.

These processes are relatively slow processes in terms of writing time and hence their use is limited to applications such as mask fabrication and patterning small areas. In a common usage scenario, these techniques can be efficiently employed to write areas of a few hundred square micrometers. The resolution of such a process is limited by the spot and step size of the beam and substrate properties. Furthermore, these techniques require expensive tools.

2.2.1. E-beam, focused ion beam and laser-based techniques

These techniques make use of light or particle beams. The wavelength of such beams except laser beams being extremely small allows fabrication of structures with dimensions in the range of a few ten nanometers. With the advent of systems with multiple e-beams, writing is increasingly becoming faster. Along with the use of multiple beams, the areas being written can be stitched together using corresponding software. The stitching method allows us to write areas in the range of a few square centimeters.

One of the ways to pattern a wafer using a light or particle beam involves use of this beam to expose photoresist-coated wafers in selective areas, similar as in the previously discussed conventional photolithography. Such a technique requires all the subsequent steps used in photolithography involving photoresist development, pattern transfer to the substrate beneath and resist stripping. Even though there have been numerous achievements with respect to the quality of beam being used, the

corresponding techniques are hampered by limitations due to the atomic or molecular structure of the substrate (see “proximity effect”) and in terms of etching of nanoscale features.

In a second type scenario, structures can be directly written on the substrate itself by means of a source like focused ion beam. Again, this technique is limited to the substrate chemistry.

Recently, it has been shown that using helium ions resolutions as low as 6 nm can be achieved (8) (fig. 7). Owing to the fact that helium ions are larger and heavier than electrons, they can be fired against the substrate surface with less speed and still deliver the same collision energy. Moreover, helium ions rebound less far off the surface and penetrate sideways less far into the structure itself and hence do much less damage to the surrounding material.

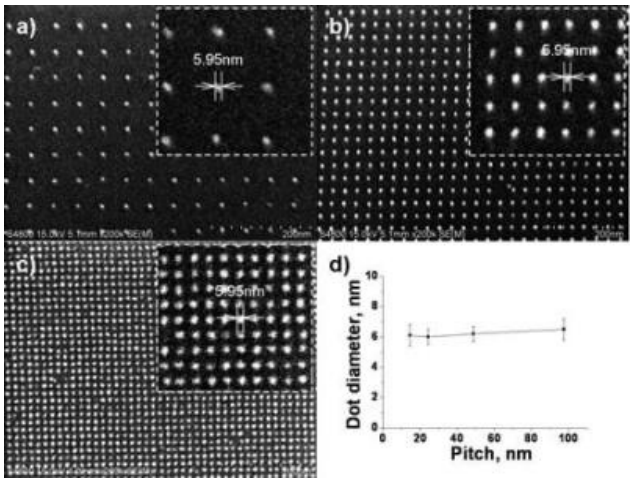

Figure 7 SEM images of dot exposures in hydrogen silsesquioxane (HSQ). a) 48 nm pitch, b) 24 nm pitch, c) 14 nm pitch, d) plot of dot diameter vs. pitch

Reprinted with permission from American Vacuum Society (Sidorkin, V. *et al.* Sub-10-nm nanolithography with a scanning helium beam. *Journal of Vacuum Science & Technology B: Microelectronics and Nanometer Structures* **27**, L18-L20) Copyright (2009)

Example: A study by Dalby et al. made use of topographic patterns on a silicon wafer using electron beam lithography (EBL)(9). Silicon substrates were fabricated using EBL to form arrays of 120 nm diameter pits of 100 nm depth and 300 nm pitch in hexagonal and square arrangements. Arrays of dots were also fabricated with near square order, but random displacements of ±20 nm and ±50 nm were introduced, maintaining an average 300 nm pitch. Finally, totally random arrangements were fabricated. The silicon substrates were subsequently used to prepare a nickel shim using electroplating. Using the nickel shims as molds, patterns were transferred to PMMA blocks using hot embossing.

Human mesenchymal stem cells (hMSC) were cultured on the patterned and non-patterned PMMA blocks, and osteopontin and osteocalcin expression was quantified using immunofluorescence staining (fig. 8). It was revealed that cells cultured on the disordered square array with dots displaced randomly by up to 50 nm on both axes (DSQ50 surface) resulted in higher expression of osteogenic markers compared to non-patterned substrates.

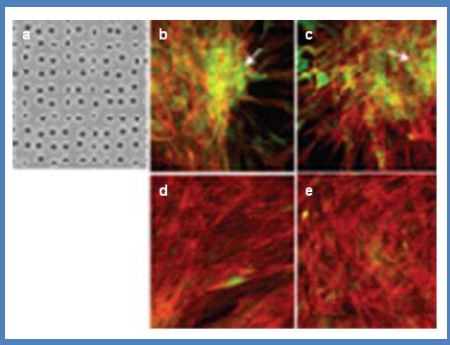

Figure 8 Comparison of osteocalcin and osteopontin staining on DSQ-50-patterned and non-patterned PMMA substrates a. SEM of DSQ 50 substrate, b&d. osteocalcin staining of hMSCs cultured on DSQ-50- and non-patterned PMMA, c&e. osteopontin staining of hMSCs cultured on DSQ-50- and non-patterned PMMA

Reprinted with permission from Macmillan Publishers Ltd. [Nature Materials] (Dalby, M. J. et al. The control of human mesenchymal cell differentiation using nanoscale symmetry and disorder. Nat Mater 6, 997-1003) Copyright (2007)

2.2.2. Atomic force microscopy based techniques

Atomic force microscopy (AFM), a technique conventionally used in surface and materials characterization, is increasingly used for nanoscale fabrication. For direct-writing-based techniques, the tip of an AFM can be used like a needle to displace or remove undesired material thereby forming point- or line-shaped craters. The tip can also be used in order to deposit material just like a conventional ink

pen. The latter is termed as dip pen nanolithography (DPN). The former may be used on relatively soft substrates like polymers for creating localized topographic patterns (fig. 9).

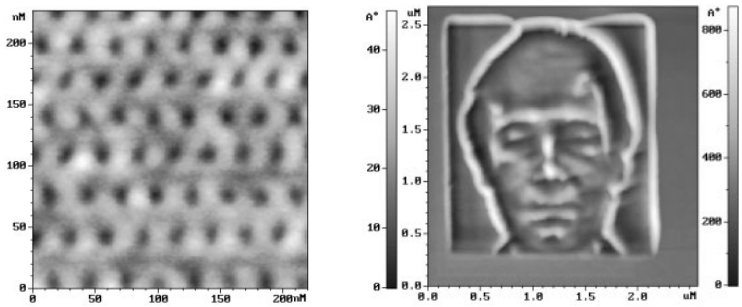

Figure 9 AFM picture showing a surface of a polycarbonate film on a silicon substrate after atomic force microscopy based direct writing technique. The distance between pits is about 25nm
(Image courtesy of Sergei N. Saunin , NT-MDT, Moscow, Russia)

AFM-based direct patterning techniques are generally considered slow and time-consuming. However, recently researchers from IBM have demonstrated that using a heated cantilever technique the throughput of such a technique can be improved (10). In their study, these researchers demonstrated that it is possible to reproduce a 25 nm high 3D replica of the Matterhorn (fig. 10) in less than three minutes.

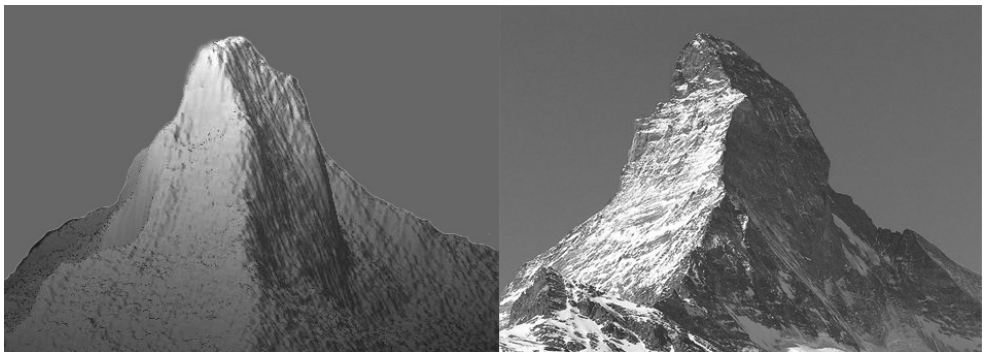

Figure 10 AFM scan of 25 nm tall rendition (left) of the Matterhorn, a 14,692 foot tall alpine mountain (right) (photographer: Marcel Wiesweg; source: Wikimedia Foundation), at a scale of 1-to-5 billion sculpted using AFM-based direct writing

Creating nanostructures using DPN is a single-step process which does not require the use of resists. Using a conventional AFM, it is possible to achieve ultra-high-resolution features – as small as 15 nm line widths and approximately 5 nm spatial resolution. For instance, using DPN, molecules of alkane thiols or proteins which bind strongly to gold can be selectively deposited in a defined format on gold substrates.

Techniques like AFM-based direct writing can be used for fabrication of a wide variety of 3D meta-materials. High-throughput screening of metamaterials and their properties largely remains unexplored. Development of fabrication techniques such as these will allow us to screen for metamaterials with distinct properties.

2.3. Polymer micromolding techniques

These are a set of techniques which make use of a mold or a master to replicate microstructures on moldable material generally polymer. Thermoplastic polymers which are a group of materials that have the ability to be reshaped when heated around or above the softening temperature of the material are frequently used for such processes. Typically, a molten thermoplastic polymer, a polymer solution or a thermally or photo-curable polymer resin can either be pressed, cast or drawn by capillary action into the mold space and subsequently solidified or cured there (in case of injection molding and some soft-lithographic molding processes), or polymer sheets or layers on wafers can be embossed by softening the polymer and applying pressure (in case of hot embossing or imprinting).

Micromolds, for example from silicon, can be fabricated using traditional photolithographic processes. Depending upon the dimensions to be achieved, the molds can also be fabricated using direct writing processes. Molding processes are fairly straightforward, fast and inexpensive, and can be easily up-scaled for bulk manufacturing.

2.3.1. Soft lithography

Soft lithography is a term suggested by Whitesides and coworkers and is an umbrella term for processes which make use of stamps, molds or masks from an elastomeric material, most commonly poly (dimethylsiloxane), (PDMS)(11). With the exception of microcontact printing, these processes are molding processes. Soft lithography has lately gained greater popularity because of the simplicity in fabrication. Molding processes among the soft lithography processes are replica molding (REM), microtransfer molding (μTM), micromolding in capillaries (MIMIC) or solvent assisted micromolding (SAMIM).

Soft lithography with PDMS involves pouring PDMS pre-polymer, a two-component mixture of base and cross-linking agent, directly onto a patterned silicon master and accelerated curing at an elevated temperature (100°C for 45 minutes, for example) to replicate the desired features. Soft-lithography-based processes can also be used for fabrication of multilayered integrated microfluidic biomaterials arrays with microfluidic channels for fluid transport such as channels for perfusion of cell culture media. The common procedure for making PDMS-based devices involves the fabrication of a silicon master in the form of a negative of the pattern to be copied on PDMS (fig. 11). The silicon master can be fabricated using the generic photolithographic process as explained previously.

Recently, PDMS stamps are used as molds for patterning hydrogels such as agarose and polyethylene glycol (12). Hydrogel-based well arrays can subsequently be used for high-throughput screening of, for instance, extracellular matrices (ECM) combinatorial chemistry arrays by virtue of their ability to incorporate functional groups. Different combinations of ECM components can be spotted in the wells of the hydrogel arrays using a robotic spotter. Subsequently, cells can be cultured on them and the interaction with combination of ECM molecules can be analyzed using high-content imaging(13).

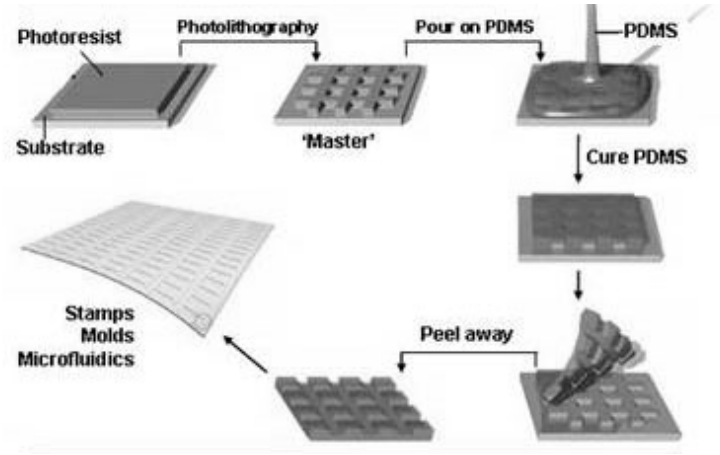

Figure 11 Fabrication of PDMS stamps, molds and devices for or by soft lithography

Example: Recently, Kobel *et al.* have described a process of soft lithography using polyethylene glycol (PEG) hydrogels (fig. 12). In this process, the researchers used a PDMS template as mold for patterning the hydrogels. For this, the PEG is allowed to partially cross-link and then subjected to embossing by PDMS mold under suitable pressure.

After 90 minutes of curing, the PEG gel was demolded from the PDMS template and used for culturing haematopoietic stem cells. Single cell proliferation kinetics was monitored using time-lapse imaging.

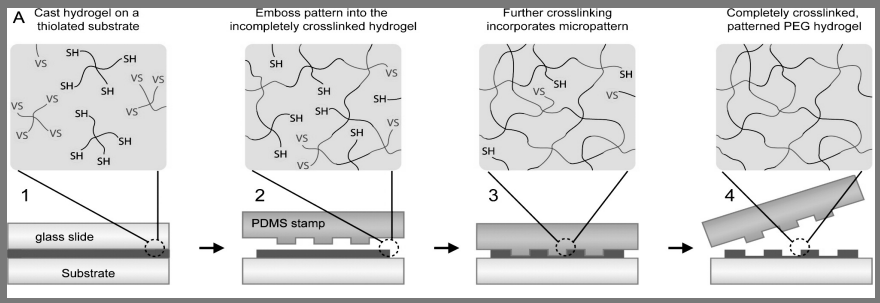

Figure 12 Illustration of the soft embossing concept. A PEG hydrogel film is cast from multiarm PEG precursors (for clarity, only four arms are shown) (1). After gelation, but before completion of cross-linking, a microfabricated PDMS mold is embossed into the surface (2). Further cross-linking irreversibly confines the embossed micropattern into the hydrogel surface (3) and the PDMS stamp can be removed (4)

Reprinted with permission from American Chemical Society [Langmuir] (Kobel, S., Limacher, M., Gobaa, S., Laroche, T. & Lutolf, M. P. Micropatterning of Hydrogels by Soft Embossing. Langmuir 25, 8774-8779) Copyright (2009)

2.3.2. Hot embossing

Embossing requires use of flat sheets from thermoplastic materials, which are patterned using a master (stamp) by applying pressure and heat. Thermoplastic materials routinely used for hot embossing include poly (methyl methacrylate), (PMMA), poly (lactic acid), (PLA), polycarbonate (PC), cyclic olefin copolymer (COC), polystyrene (PS), polyvinylchloride (PVC), and poly (ethylene terephthalate glycol), (PETG).

Example: Recently, Unadkat et al. have used hot embossing to fabricate a surface-topographic library (TopoChip) for analysing the effect of surface topographies on cell behaviour (fig. 13)The TopoChip is a library of 2178 randomly generated surface topographies. The topographies were designed using a mathematical algorithm. A chromium mask was fabricated and used for patterning a silicon wafer by conventional photolithography. Using the silicon master, hot embossing was performed on poly(D,L-lactic acid) sheets in a nano-imprint lithography tool.

Mitogenic effect and differentiation potential of surface topographies were evaluated by culturing human mesenchymal stem cells. Topographies with mitogenic and osteogenic differentiation potential were identified by high -content imaging and extensive data mining.

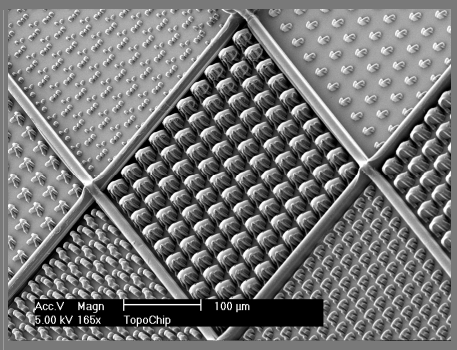

a.

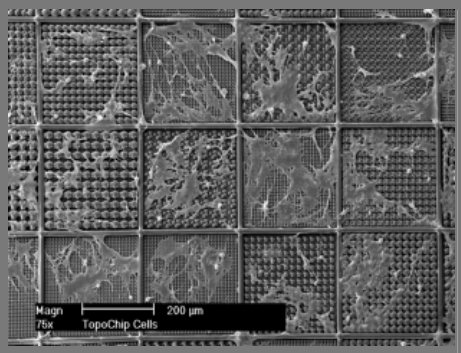

b.

Figure 13 a. SEM of a section of TopoChip b. SEM of mesenchymal stem cells exhibiting diverse morphologies when cultured on TopoChip

A master used for hot embossing can be fabricated using a silicon wafer or metals. Metal stamps can be fabricated by mechanical machining, laser ablation, electroplating on patterned silicon masters or using

the LIGA process (a German acronym for lithography, galvanoforming and molding). Upon fabrication of the stamp, the selected thermoplastic sheet is placed into a press. Typically, the thermoplastic sheet is sandwiched between a mold and a counter plate. Heat and pressure are applied to emboss the stamp into the thermoplastic substrate.

The only major requirement for embossing is press equipment and a patterned stamp. One stamp can be used for batch fabrication of devices. Some versions of embossing presses are accompanied with a vacuum system to eliminate air bubbles trapped between the substrate and stamp. The replication capability of embossing is mainly limited by the process used for fabrication of the stamp

2.3.3. Microthermoforming and SMART

Thermoforming refers to shaping of a heated semi-finished product in the form of a polymer film (or plate) by three-dimensional stretching. In thermoforming, a film of thermoplastic polymer is clamped at its edges or around the mold to be used. The stretching results in thinning of the semi-finished product compared to its initial thickness. Different variants of microthermoforming are described in literature (14). Here, we describe the process of micro pressure forming.

In micro pressure forming (Fig. 14a–c), a cut sheet of a thermoplastic film is inserted into a microthermoforming tool. The three-part tool consists of a plate-shaped micromold with mold cavities, a counter plate with openings for evacuation and gas pressurisation and an axial seal ring in between. The tool is mounted into a heated press. The press, and with it the tool, is closed to such an extent that vacuum sealing of the volume enclosed by the two tool plates and the seal is achieved, but the edges of the plastic sheet are not yet clamped between the plates. Then the entire tool is evacuated (Fig. 14a). The tool is completely closed, so that the sheet is now clamped, and heated up. Around the softening temperature of the film polymer, the film is formed into the evacuated microcavities of the mold by compressed nitrogen (Fig. 14b). Then the tool is cooled down. When, sufficiently below the softening

temperature of the polymer, the material is dimensionally stable again, the gas pressure is decreased. Then the tool is opened and the thermoformed film microstructure is demolded (Fig. 14c) and unloaded.

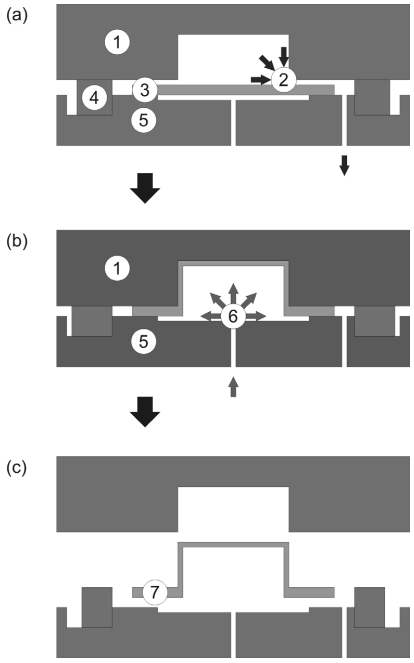

Figure 14 Micro pressure forming process with the following process steps: insertion of a thermoplastic film,

a. evacuation of the tool, heating up the tool,
b. forming of the film by compressed nitrogen, cooling down the tool and
c. demolding and unloading the film microstructure

(1) mold, (2) vacuum, (3) thermoplastic film, (4) seal, (5) counter plate, (6) compressed nitrogen, (7) thermoformed film microstructure; for (1), (5): blue/mid-grey and red/dark grey correspond to cold and heated, respectively

Example: Truckenmuller et. al. showed the application of microthermoforming for fabrication of cell culture chips in the form of film-based microcontainer arrays (fig. 15)(15). These chips were fabricated using a process which the authors refer to as SMART which stands for substrate modification and replication by thermoforming. In the process, still on the unformed, plane film, the material modifications of a preprocess define the locations where later, then on the thermoformed film, a postprocess generates the final local modifications. So, one can obtain highly resolved modification patterns also on hardly accessible side walls and even behind undercuts. The curved walls of the cell containers have been provided with micropores, cell adhesion micropatterns and thin film microelectrodes. With the SMART technology one can integrate libraries of micro- or nanopatterned material modifications into the curved or 3D wells of micro well arrays with each well representing an individual artificial microenvironment.

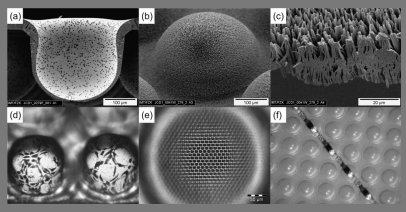

Figure 15 (a) Microporous cell container from PC with the pores perpendicular to the container walls (SEM micrograph; cross sectional view). (b) Highly porous PC microcontainer (SEM micrograph; back view). (c) Part of the highly porous container wall (SEM micrograph; cross sectional view). (d) PS microcontainers with fixed and crystal violet stained L929 cells (day 3 of cultivation) seeding only in the domains of the DUV irradiated chess board pattern (back view). (e) PMMA microcontainer with X-ray irradiated honeycomb mesh pattern. (f) PC microcontainers with crack-free conducting path from gold crossing (back view; conductor width between the containers: approximately 75 µm)

2.3.4. Micro injection molding

Unlike hot embossing and microthermoforming, injection molding does not use a softened or molten polymer sheet; instead molten polymer granules are used. The process of injection molding is usually employed for fabrication of 3-dimensional parts or for industrial scale production of devices.

In an injection molding process (Fig. 16), a sealable mold cavity is fabricated. The mold cavity is equipped with a nozzle for injection of molten polymer. The molten polymer is injected via the nozzle into the mold space. Upon ensuring the filling of the mold space, the assembly is allowed to cool which results in the solidification of the polymer melt. The assembly is subsequently opened and the fabricated parts are ejected.

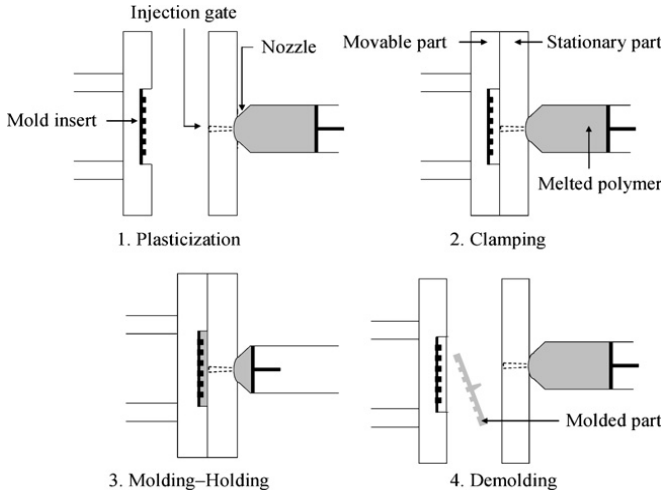

Figure 16 Schematic illustration of injection molding process

Reprinted with permission from OP Publishing Ltd. (Giboz, J. et al. Microinjection molding of thermoplastic polymers: a review. J. Micromech. Microeng. 17, 96-109) Copyright (2007)

3. Relation to Materiomics

Microfabrication techniques such as photolithography, micromolding and soft-lithography represent powerful approaches to generate precisely engineered scaffolds for tissue engineering applications. The cell-seeded porous scaffold approach led to significant advances over the past 20 years, but it is currently shifting from empirical approaches to precisely engineered systems based on mechanistic models, structures and chemistries(16). The actual challenge is the requirement for scalable engineered constructs reproducing the chemical, mechanical and biological microenvironment found *in vivo*. Microscale technologies are currently investigated as potential tools for addressing these issues, by the engineering structures and devices such as microelectromechanical systems (MEMS) that will help build 3D structures and monitor biological phenomenon occurring at the microscale.

3.1. Microfabrication techniques for scaffold fabrication

Photolithography and soft-lithography have considerably improved the control over the microarchitecture of scaffolding materials(17). These fabrication techniques have proven to be successful in allowing for the control of mechanical properties, porosity, interconnectivity, geometry and orientation of biodegradable polymers with micron-scale resolution(17). Microfabricated substrates were also shown to deliver drugs in a precisely controlled fashion by controlling the porosity and the crosslinking density of the delivery vehicle used for drug transport(18). Techniques like photolithography and micromolding have been applied for the fabrication of biodegradable scaffolds such as from poly (L-lactic acid), (PLLA), poly (lactide-co-glycolide), (PLGA) and poly (glycerol sebacate), (PGS), and were used to produce hydrogel-based scaffolds with tunable transport properties(19). They were also used to engineer surface topographies for guiding cell adhesion, orientation and migration(20-21). These approaches are contributing greatly to the actual efforts in the field of tissue engineering to reproduce cell-cell and cell-ECM interactions with fidelity in engineered tissues. They can also be used to control

the spatial distribution of molecules and cells, and to create physiologically relevant gradients in biomaterials. These physical, chemical and biological cues can later on be used to control cell adhesion, migration and proliferation. Therefore, these technologies can help to provide significant insights about cell behavior *in vitro* and can result into great technological advances *in vivo*.

3.2. High-Throughput Screening of Material Libraries

Materiomics is a recent powerful tool that will address multiple challenges in life sciences(22-23). It relies on microtechnologies and can be used in combination with biocompatible and biodegradable materials to generate material libraries with defined cell scale features to study cell-material interactions in a high-throughput fashion(24). By using microfabrication and microfluidics strategies, it is possible to create arrays of multiple materials, proteins, chemicals or stiffness gradients with high-resolution and spatial control(25). Therefore, Materiomics is aiming at design and exploration of a new generation of biomaterials having tailored properties that will enable the transfer of new technologies such as the engineering of 3D functional organs into clinical applications(26).

Materiomic studies and combinatorial approaches have greatly improved the rational design and the development of new classes of biomaterials. At the fundamental level, quantitative analysis of large sample size of micro-engineered materials helped identify most efficient designs for defined purposes(23, 27). These platforms have also provided high-throughput assays allowing the measurement of material properties such as wettability (indicates hydrophobicity-hydrophilicity of a sample, measured by contact angle), surface topography, surface chemistry and substrate stiffness(24, 28). It contributed to develop structure-function relationship between material properties and biological performance(25). Moreover, these technologies, allowing for the precise control of the cell-scale microenvironment, lead to the miniaturization of biological assays. This miniaturization capability has

proven to be efficient in the development of biologically relevant high-throughput assays, which resulted into multiple groundbreaking studies that would have not been previously possible(22, 29).

Microtechnologies can be used to miniaturize assays and enable high-throughput screening of libraries of materials and molecules, or to study the interplay of cells with multiple substrates or to various stimuli(23). Microfabricated micro-arrays greatly facilitate the rapid synthesis of libraries and high-throughput analysis enables the assessment of multiple conditions, providing a general framework for the combinatorial development of synthetic substrates for biomedical applications. Results obtained from these assays can then be used as a starting point to enhance the design of biomaterials for tissue engineering and regenerative medicine applications. This approach, which radically differs from previous strategies which relied on the development of, for example, a single polymer on which multiple experiments were conducted, represents a much more efficient way to develop and tailor the properties of new materials. In a recent study, a high-throughput analysis was performed using a library of 50,000 compounds to find the best substrate in order to promote self-renewal of mouse embryonic stem cells, greatly reducing the amount of time and effort required to obtain the optimal result(30).

In the future, it is not difficult to envision the evolution of biomaterial microarrays with an integrated fluidic systems for cell culture and metabolite removal. With addition of a microfluidic component, these arrays may also offer the advantage of performing multiple biological assays like quantitative polymerase chain reaction (qPCR) on the array itself.

4. Future perspective

Application of Materiomics and microfabrication to biotechnology has aided in the rapid expansion of various research fields such as cellular and molecular assays, diagnostic devices, drug discovery and chemical and biological detection (11, 31-35). New methods are moving towards robotic nanotechnology to deliver nano-liter volumes of many different molecules or materials. As the size of devices decreases, their surface-to-volume ratio increases. For this reason, the surface properties become very important in determining the performance of the assay. Therefore, it is necessary to engineer surface properties with molecular-level precision. The combination of microfluidics with photopolymerization chemistry has recently resulted into hydrogels containing gradients of crosslinking and signaling or adhesive molecules across the material, thus resulting in the regulation of cell behavior such as migration, adhesion and differentiation within the gel (36-38). These technologies could help to closely control the restoration of tissue morphology and function since they can be used to control the area, shape and locations of the substrate on which cells attach. They also have tremendous potential in overcoming key challenges such as engineering a microvasculature as well as introducing complexity in engineered tissues (39). Based on Materiomics and microscale technologies, a large set of tools are available to investigate cell-cell and cell-microenvironment interactions using high-throughput technologies and to test many environmental factors simultaneously. The application of these combinatorial approaches could lead to new ways to engineer biomimetic 3D constructs (40-42). Moreover, this biomimetic approach was recently used to generate large-scale tissues by assembling small building blocks (17). These repeatable blocks, comprising controllable and microengineered features, are mimicking the characteristics of native tissues which are often made of multiple functional units. These building blocks can later be assembled in an organized fashion, resulting in functional engineered tissues. For example, it was shown that cell-laden microgels could be molded in multiple

complementary micro-units and assembled into self-organizing larger patterns, allowing to engineer tissue complexity (43). By using Materiomics and microfabrication techniques, these building blocks could be comprised of precise biological or chemical cues or gradients that would promote tissue regeneration.

Future challenges confronting tissue engineers will include the design of novel matrices that can precisely control the cellular microenvironment. These materials will have to incorporate specific ligands, tailored mechanical cues and controlled release of growth factors. The development of these "smart" matrices will be designed to give the cells the appropriate signals in order to induce adhesion, migration, proliferation or differentiation, depending if the tissue is in a repair, regeneration or remodeling phase. Therefore, although microfabrication and Materiomics are already powerful tools for basic discoveries, they still need to be implemented to produce therapeutic outcomes for clinical applications and improve the efficiency of diagnostic devices.

References

1. Andersson H & Berg Avd (2004) *Lab-on-chips for cellomics : micro and nanotechnologies for life science* (Kluwer Academic, Dordrecht ; Boston) pp xv, 363 p.
2. Terry SC, Jerman JH, & Angell JB (1979) Gas-Chromatographic Air Analyzer Fabricated on a Silicon-Wafer. *Ieee T Electron Dev* 26(12):1880-1886.
3. Maerkl SJ & Quake SR (2007) A systems approach to measuring the binding energy landscapes of transcription factors. *Science* 315(5809):233-237.
4. Padilla WJ, Basov DN, & Smith DR (Negative refractive index metamaterials. *Materials Today* 9(7-8):28-35.
5. Gad-el-Hak M (2006) *MEMS: introduction and fundamentals* (CRC/Taylor & Francis).
6. Madou MJ (2002) *Fundamentals of microfabrication : the science of miniaturization* (CRC Press, Boca Raton, Fla.) 2nd Ed pp 723 p., [716] p. of plates.
7. Lovmand J*, et al.* (2009) The use of combinatorial topographical libraries for the screening of enhanced osteogenic expression and mineralization. *Biomaterials* 30(11):2015-2022.
8. Maas D*, et al.* (2010) Nanofabrication with a Helium Ion Microscope. *P Soc Photo-Opt Ins* 7638.
9. Dalby MJ*, et al.* (2007) The control of human mesenchymal cell differentiation using nanoscale symmetry and disorder. *Nat Mater* 6(12):997-1003.
10. Pires D*, et al.* (2010) Nanoscale Three-Dimensional Patterning of Molecular Resists by Scanning Probes. *Science* 328(5979):732-735.
11. Whitesides GM, Ostuni E, Takayama S, Jiang X, & Ingber DE (2001) Soft lithography in biology and biochemistry. *Annu Rev Biomed Eng* 3:335-373.
12. Kobel S, Limacher M, Gobaa S, Laroche T, & Lutolf MP (2009) Micropatterning of Hydrogels by Soft Embossing. *Langmuir* 25(15):8774-8779.

13. Gobaa S*, et al.* (2011) Artificial niche microarrays for probing single stem cell fate in high throughput. *Nat Meth* 8(11):949-955.

14. Truckenmuller R*, et al.* (2011) Thermoforming of film-based biomedical microdevices. *Adv Mater* 23(11):1311-1329.

15. Truckenmuller R*, et al.* (2008) Flexible fluidic microchips based on thermoformed and locally modified thin polymer films. *Lab on a Chip* 8(9):1570-1579.

16. Mikos AG*, et al.* (2006) Engineering complex tissues. *Tissue Eng* 12(12):3307-3339.

17. Khademhosseini A, Langer R, Borenstein J, & Vacanti JP (2006) Microscale technologies for tissue engineering and biology. *Proc Natl Acad Sci U S A* 103(8):2480-2487.

18. Richards Grayson AC*, et al.* (2003) Multi-pulse drug delivery from a resorbable polymeric microchip device. *Nat Mater* 2(11):767-772.

19. Khademhosseini A & Langer R (2007) Microengineered hydrogels for tissue engineering. *Biomaterials* 28(34):5087-5092.

20. Guillemette MD*, et al.* (2009) Surface topography induces 3D self-orientation of cells and extracellular matrix resulting in improved tissue function. *Integr Biol (Camb)* 1(2):196-204.

21. Alaerts JA, De Cupere VM, Moser S, Van den Bosh de Aguilar P, & Rouxhet PG (2001) Surface characterization of poly(methyl methacrylate) microgrooved for contact guidance of mammalian cells. *Biomaterials* 22(12):1635-1642.

22. Flaim CJ, Chien S, & Bhatia SN (2005) An extracellular matrix microarray for probing cellular differentiation. *Nat Methods* 2(2):119-125.

23. Anderson DG, Levenberg S, & Langer R (2004) Nanoliter-scale synthesis of arrayed biomaterials and application to human embryonic stem cells. *Nat Biotechnol* 22(7):863-866.

24. Underhill GH & Bhatia SN (2007) High-throughput analysis of signals regulating stem cell fate and function. *Curr Opin Chem Biol* 11(4):357-366.

25. Davies MC*, et al.* (High throughput surface characterization: A review of a new tool for screening prospective biomedical material arrays. *J Drug Target* 18(10):741-751.

26. Mei Y*, et al.* (2010) Combinatorial development of biomaterials for clonal growth of human pluripotent stem cells. *Nat Mater* 9(9):768-778.

27. Sundberg SA (2000) High-throughput and ultra-high-throughput screening: solution- and cell-based approaches. *Curr Opin Biotechnol* 11(1):47-53.

28. Mei Y*, et al.* A high throughput micro-array system of polymer surfaces for the manipulation of primary pancreatic islet cells. *Biomaterials* 31(34):8989-8995.

29. Soen Y, Mori A, Palmer TD, & Brown PO (2006) Exploring the regulation of human neural precursor cell differentiation using arrays of signaling microenvironments. *Mol Syst Biol* 2:37.

30. Chen S*, et al.* (2006) Self-renewal of embryonic stem cells by a small molecule. *Proc Natl Acad Sci U S A* 103(46):17266-17271.

31. Foquet M, Korlach J, Zipfel W, Webb WW, & Craighead HG (2002) DNA fragment sizing by single molecule detection in submicrometer-sized closed fluidic channels. *Anal Chem* 74(6):1415-1422.

32. Kennedy GC*, et al.* (2003) Large-scale genotyping of complex DNA. *Nat Biotechnol* 21(10):1233-1237.

33. Lipshutz RJ, Fodor SP, Gingeras TR, & Lockhart DJ (1999) High density synthetic oligonucleotide arrays. *Nat Genet* 21(1 Suppl):20-24.

34. Sia SK, Linder V, Parviz BA, Siegel A, & Whitesides GM (2004) An integrated approach to a portable and low-cost immunoassay for resource-poor settings. *Angew Chem Int Ed Engl* 43(4):498-502.

35. Rossier JS & Girault HH (2001) Enzyme linked immunosorbent assay on a microchip with electrochemical detection. *Lab Chip* 1(2):153-157.

36. Burdick JA, Khademhosseini A, & Langer R (2004) Fabrication of gradient hydrogels using a microfluidics/photopolymerization process. *Langmuir* 20(13):5153-5156.

37. King KR, Wang CCJ, Kaazempur-Mofrad MR, Vacanti JP, & Borenstein JT (2004) Biodegradable Microfluidics. *Advanced Materials* 16(22):2007-2012.

38. Bettinger CJ*, et al.* (2006) Three-Dimensional Microfluidic Tissue-Engineering Scaffolds Using a Flexible Biodegradable Polymer. *Advanced Materials* 18(2):165-169.

39. Ingber DE*, et al.* (2006) Tissue engineering and developmental biology: going biomimetic. *Tissue Eng* 12(12):3265-3283.

40. Kaihara S*, et al.* (2000) Silicon micromachining to tissue engineer branched vascular channels for liver fabrication. *Tissue Eng* 6(2):105-117.

41. Borenstein JT*, et al.* (2002) Microfabrication Technology for Vascularized Tissue Engineering. *Biomedical Microdevices* 4(3):167-175.

42. Huh D*, et al.* (2010) Reconstituting organ-level lung functions on a chip. *Science* 328(5986):1662-1668.

43. Du Y, Lo E, Ali S, & Khademhosseini A (2008) Directed assembly of cell-laden microgels for fabrication of 3D tissue constructs. *Proc Natl Acad Sci U S A* 105(28):9522-9527.

Chapter 3: An algorithm-based topographical biomaterials library to instruct cell fate

An algorithm-based topographical biomaterials library to instruct cell fate

Hemant V. Unadkat[1], Marc Hulsman[4], Kamiel Cornelissen[3], Bernke Papenburg[1], Roman K. Truckenmüller[1], Gerhard F. Post[3], Anne E. Carpenter[5], Matthias Wessling[6], Marc Uetz[3], Marcel J.T. Reinders[4], Dimitrios Stamatialis[2], Clemens van Blitterswijk[1], Jan de Boer[1*]

MIRA Institute for Biomedical Technology and Technical Medicine Departments of [1]Tissue Regeneration and [2]Biomaterials Science and Technology ,

[3]Department of Discrete Mathematics and Mathematical Programming,

University of Twente, Enschede, The Netherlands

[4]Delft Bioinformatics Lab, Delft University of Technology, Mekelweg 4, Delft, the Netherlands

[5]Imaging Platform Broad Institute of Harvard & MIT, 7 Cambridge Center, Room 6025, Cambridge, MA 02142, USA

[6]RWTH Aachen, Aachen, Germany

*Corresponding author
Email: j.deboer@utwente.nl
Phone: +31 53 489 3400

Abstract

It is increasingly recognized that material surface topography is able to evoke specific cellular responses, endowing materials with instructive properties that were formerly reserved for growth factors. This opens the window to improve upon, in a cost effective manner, biological performance of any surface used in the human body. Unfortunately, the interplay between surface topographies and cell behaviour is complex and still incompletely understood. Rational approaches to search for bio-active surfaces will therefore omit previously unperceived interactions. Hence, in the present study, we use mathematical algorithms to design non-biased, random surface features and produce chips of poly (D,L-lactic acid) with 2176 different topographies. With human mesenchymal stromal cells (hMSCs) grown on the chips and using high-content imaging, we reveal unique, formerly unknown, surface topographies that are able to induce MSC proliferation or osteogenic differentiation. Moreover, we correlate parameters of the mathematical algorithms to cellular responses, which yield novel design criteria for these particular parameters. In conclusion, we demonstrate that randomized libraries of surface topographies can be broadly applied to unravel the interplay between cells and surface topography and to find improved material surfaces.

Introduction

Biomaterials are applied for numerous clinical applications, ranging from stents, orthopaedic implants and sutures to contact lenses. In all these cases, the response of the human body to the material depends on the interface between the material and the cells. Often, interaction is not optimal. For instance, orthopaedic implants may get encapsulated by fibrous tissue upon implantation, rather than bonding directly with the bone which can result in implant failure. Hence, a lot of effort is dedicated to modify the surface of implants by either using coatings, e.g. using calcium phosphate coatings(1) on hip implants, or through physically modifying the surface of the implant by varying the surface roughness, e.g. by sand blasting and electropolishing(2). Considerable improvement of orthopaedic implant performance in the past decades signifies the potential of surface modification for optimizing medical devices in general. One of the drawbacks of these techniques is that they offer only limited control of surface characteristics. However, with the advent of new developments in micro- and nanotechnologies, it is possible to create surfaces with precisely designed feature sizes and shapes up to nanometre resolution. Some of the pioneering manuscripts in the field did not only provide proof-of-principle for micro- and nanopatterning of biomaterial surfaces but also disclosed unprecedented control of material surface on the behaviour of cells growing on them(3-4). For instance, using different concentrations of poly(2-hydroxyethyl methacrylate), Folkman and Moscona were able to control cell proliferation through the extent of cell spreading(5). Using micro pattering techniques, Chen and co-workers showed that the decision of a mesenchymal stromal cell (MSC) to either become a fat or a bone cell depends on the shape of the cell, which correlated with the activation of the RhoA signalling pathway(6). Micro- and nanotechnology can also be used to determine surface topography, a parameter which is known to influence the behaviour of cells growing on it (7). Micrometre-range patterning is used to align cells on biomaterial surfaces (8-10), whereas Dalby *et al*. reported that randomly placed nanotopographies were able to induce osteogenic differentiation of MSCs (11). Unfortunately, nature does not prescribe the

optimal surface topography for a given biomedical application, and the number of possible surface patterns that can be created is virtually unlimited, considering that cells are in the order of tens of micrometres whereas patterns can be created at nanometre resolution. The underlying mechanisms defining the interplay of cells with substrates are only partially understood (12-15). Additionally, the specific application of a biomedical device dictates the optimal surface as e.g. an orthopaedic implant requires a different biological response than a cardiovascular stent. Determining the distinct surface to elicit an appropriate biological response is thus a big challenge. Due to this complex interplay between cells and substrates, rational approaches may omit unperceived paradigms(16). Hence, in recent years, there has been a shift from the rational design of biomaterials to combinatorial screening approaches used typically in the pharmaceutical industry for drug discovery, which we and others refer to as materiomics(17-18). Thus, materiomics can be defined as large scale study of structure, function and properties of natural and synthetic materials. In a landmark study, Anderson *et al.* identified a host of unexpected material effects that offered new levels of control over human embryonic stem cell behaviour while evaluating an array of nearly 600 different co-polymer compositions(16). In this manuscript, we show that combining the power of high-throughput screening with mathematical design of micrometre- range surface topographies, enables deciphering the “Braille code” of cell-topography interactions.

Results

We created a library of 2176 distinct, randomly designed surface topographies using mathematical algorithms as a design tool (see Fig. 1a for an outline). They were reproduced in duplicate on a 2 by 2 cm^2 chip ("TopoChip") from poly (DL-lactic acid) (PLA) in areas of 290 by 290 μm^2, designated as "TopoUnits" (see Fig. 1b). First, a library of surface topographies was designed by generating topographic features, which are topography containing elements with a height of 5 µm arranged within an imaginary square with a size of either 10 by 10, 20 by 20 or 28 by 28 μm^2 (Fig. 1b). Topographic features are built up using three types of microscale primitive shapes: circles, isosceles triangles (with one angle of 36° and two angles of 72°), and thin rectangles (3 µm width). We choose these shapes because by combining these primitives, we can generate different types of patterns, e.g. circles can create large smooth areas, triangles can generate angles, and thin rectangles can result in stretched elements. With integral values for geometrical parameters (Tables 1 and 2) such as primitive type, primitive size and angle of rotation in the algorithm, 154,320,600 possible surface topographies can be defined. If we include non-integral values for these parameters, the possibilities are infinite. From the *in silico* library, 2176 topographic designs were randomly selected. In addition, four TopoUnits with a flat, non-patterned surface were included as reference surfaces. We divided the TopoChip into four quadrants (Fig. 1c) where quadrant A has identical TopoUnits to that of A_i and quadrant B is identical to quadrant B_i to assure that TopoUnits at the periphery have duplicates in the middle of the chip (Fig. 1c). With the TopoChip design, a silicon mould was fabricated using photolithography and etching, which was then used for imprinting of topographies onto PLA films. The chips were diced and further characterized using scanning electron microscopy (SEM; Fig. 2a and b). Upon characterization, we observed uniformity in the filling of the polymer into the mould cavities spaces. To assess the accuracy of replication of topographies, 32 TopoUnits were randomly chosen and height profile measurements of them performed using a Keyence VK9700 confocal laser scanning microscope. It is important to note

that the chips used in this study were composed of features with a height of 5 µm and 20 µm high walls between adjacent TopoUnits (Fig. 3). For each location, the measurements were performed on three chips. The average difference in height profile measurements was 99 nm with a standard deviation of 56 nm. TopoChips can also be coated with different materials used in tissue engineering. In Fig. 4, TopoChips are displayed with a layer of titanium oxide, deposited using plasma sputtering, and a calcium phosphate coating deposited using supersaturated simulated body fluids. Thus, we created a library of thousands of surfaces with unique physicochemical compositions.

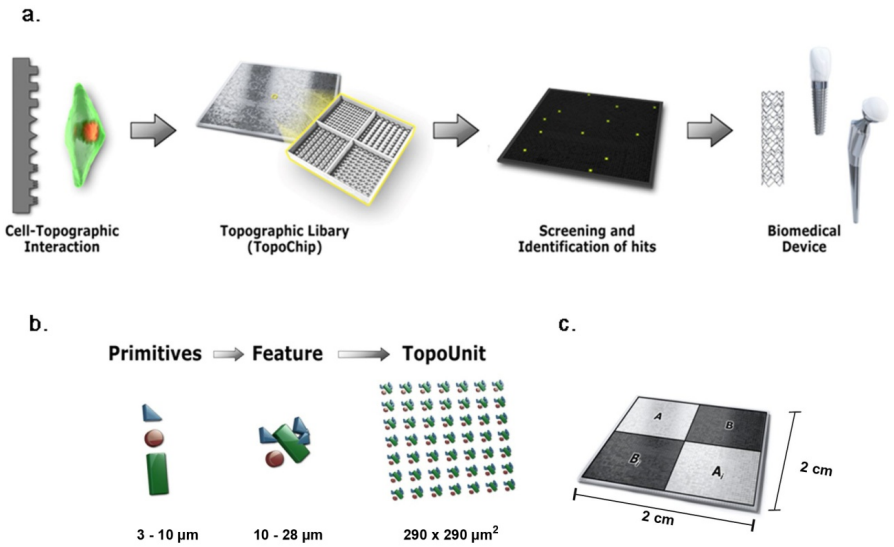

Figure 1 TopoChip design

a. A schematic representation of a sequence of events that is proposed to be followed for high-throughput screening of biomedical materials starting from initial design to clinical application.
b. Design of the TopoChip is based on the use of primitives. Three types of primitives, namely circles, triangles and lines were used to construct features. Repeated features constitute a TopoUnit and two times 2176 = 4352 TopoUnits constitute a TopoChip (size ranges are indicated). In addition, four flat control surfaces are included.
c. TopoChip is divided into four quadrants. TopoUnits in quadrant A are repeated in quadrant A_i and similarly TopoUnits in quadrant B are repeated in quadrant B_i in order to exclude site specific or localized effects.

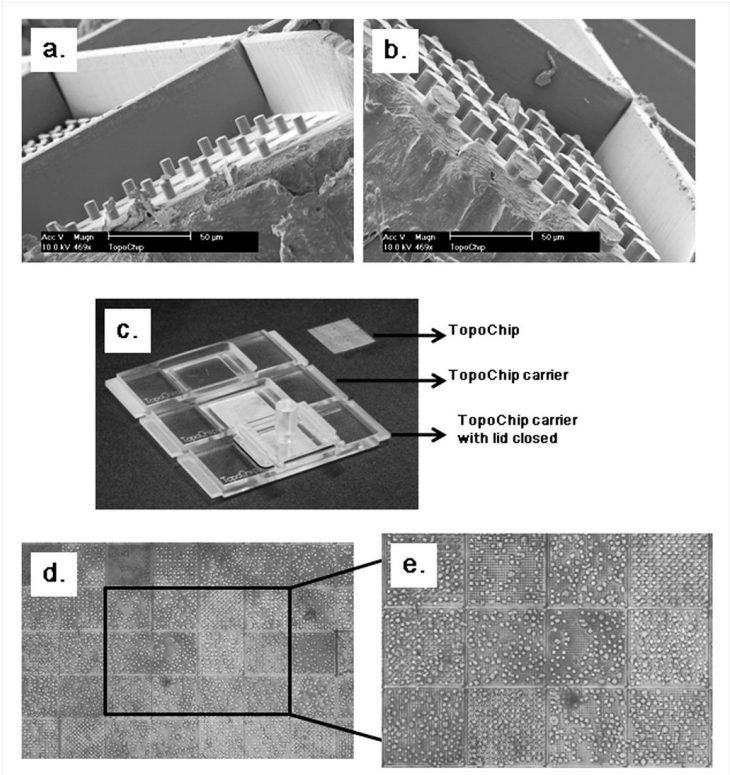

Figure 2 TopoChip fabrication and characterization

a. and b. SEM images of sections of TopoChips, displaying accurate feature replication on the TopoChip. Scale bar represents 50 µm.
c. The TopoChip carrier, lid and chip assembly. This chip carrier can even be used as a micro-bioreactor for perfusion culture of cells, or with a second set of attachment (not shown) for static cell culture.
d. and e. Light microscopic images of cells seeded using the chip carrier displaying homogeneity of cell distribution within and between TopoUnits.

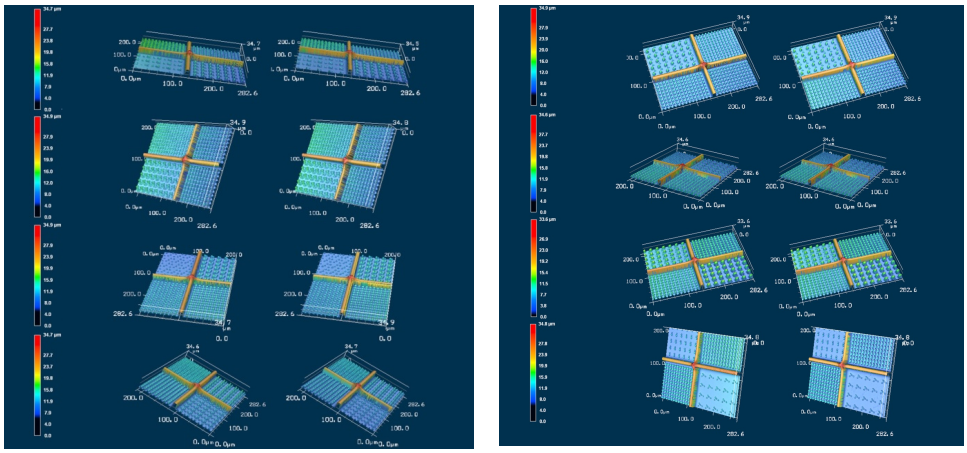

a. b.

Figure 3 Height profiles of TopoUnits measured using confocal laser scanning microscopy

a. and b. Each image has four representative areas of TopoUnits. In total 32 individual TopoUnits were analyzed for replication efficiency.

Table 1: The following table provides an overview of all parameter values and ranges used to construct features

Parameter	Value or range
Feature side length	10 µm, 20 µm, or 28 µm
Number of primitives used (10 µm)	3 - 5
Number of primitives used (20 µm)	3 - 12
Number of primitives used (28 µm)	3 - 16
Diameter of a circle primitive (10 µm)	3.0 µm - 4.0 µm
Diameter of a circle primitive (20 µm)	3.0 µm - 10.0 µm
Diameter of a circle primitive (28 µm)	3.0 µm - 10.0 µm
Shortest side length of a triangle primitive (10 µm)	3.0 µm - 4.0 µm
Shortest side length of a triangle primitive (20 µm)	3.0 µm - 8.0 µm
Shortest side length of a triangle primitive (28 µm)	3.0 µm - 10.0 µm
Top angle of a triangle primitive	36°
Length of a line primitive (10 µm)	3.0 µm - 8.0 µm
Length of a line primitive (20 µm)	3.0 µm - 16.0 µm
Length of a line primitive (28 µm)	3.0 µm - 23.0 µm
Thickness of a line primitive	3 µm
Standard deviation for the rotation of a primitive	0.0° - 180.0°

Table 2: The following table provides an overview of all additional parameter values used to develop algorithms for detecting the parameters leading to enhanced proliferation

Variable	Description
DC	The density of circle primitives
DT	The density of triangle primitives
DL	The density of line primitives
CA	The area of circle primitives scaled with their density
TA	The area of triangle primitives scaled with their density
LA	The area of line primitives scaled with their density
ROT	The scaled standard deviation of the rotation of primitives
CCD	Number of color changes of the feature over the diagonal
WN0.1	The fraction of energy in the signal with wavenumber approximately 0.1
WN0.2	The fraction of energy in the signal with wavenumber approximately 0.2
WN0.3	The fraction of energy in the signal with wavenumber approximately 0.3
WN0.4	The fraction of energy in the signal with wavenumber approximately 0.4
WN0.5	The fraction of energy in the signal with wavenumber approximately 0.5
WN0:7	The fraction of energy in the signal with wavenumber approximately 0.7
WN1	The fraction of energy in the signal with wavenumber approximately 1
WN1.5	The fraction of energy in the signal with wavenumber approximately 1.5
WN2	The fraction of energy in the signal with wavenumber approximately 2
WN3	The fraction of energy in the signal with wavenumber approximately 3
WN4	The fraction of energy in the signal with wavenumber approximately 4

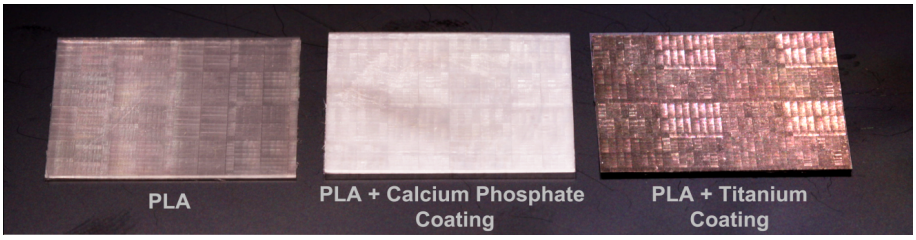

Figure 4 Conventional PLA TopoChip (left) as well as TopoChips coated with calcium phosphate (middle) and titanium (right)

Cell seeding and culture

To analyse the bio-activity of topographies, primary human mesenchymal stromal cells (hMSCs) were seeded onto PLA TopoChips and cell-material interaction was analysed by high-content imaging. We anticipated that quantification of cell behaviour relies on a critical number of cells per TopoUnit. Cell

seeding has to be homogenous across the chip and the seeding density needs to be controlled. To this end, we designed and fabricated a chip carrier by micromachining poly (methyl methacrylate) (Fig. 2c) to retain the chip in position. Design and quality control aspects of TopoChip seeding and the culturing device will be described in a separate manuscript. The chip carrier was fabricated with a removable closing lid which can be fixed within a slot which is placed 100 µm above the chip. Homogeneous distribution of the cell suspension across the chip area was observed upon closure of the lid and the cells were deposited into the TopoUnits by gravity (Fig. 2d and e). To confirm that the topographic features affect hMSC behaviour, we fixed the cells eight hours after seeding and stained their actin cytoskeleton. Visual inspection of the chip confirmed that a multitude of different cellular morphologies were induced by surface topography (Fig. 5a-j). For instance, TopoUnits were found in which hMSCs adopted an elongated shape, or in which cells spread extensively, but also TopoUnits were seen in which the hMSCs remained mostly rounded. In many TopoUnits, cells exhibited extensive filopodia and many cells were observed which clearly followed the outlines of the features.

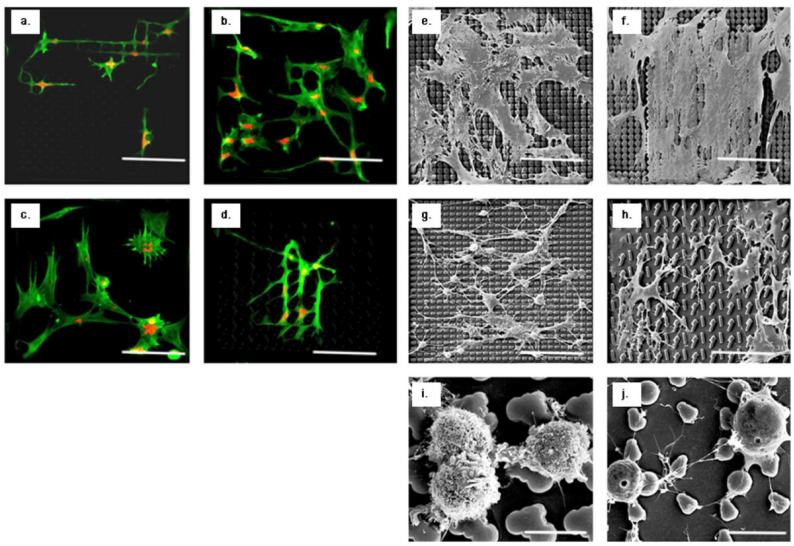

Figure 5 Morphology of hMSCs on different TopoUnits

a. to d. Fluorescent microscopic images of spread and elongated cells showing alignment on topographic features (pseudo coloured green: actin stained with Alexa Fluor 488 phalloidin; red: nuclear staining with TOTO-3; scale bar: 90 μm).
e. to h. SEM images of cells showing diverse cellular morphologies (scale bar: 90 μm).
i. and j. High magnification SEM images of rounded cells on two distinct TopoUnits showing differences in the texture of cell membrane (scale bar: 10 μm).

Mitogenic effect of surface topographies

To quantitatively screen for surface topographies that can exert a mitogenic effect on hMSCs, we seeded the cells, synchronized the cell cycle by serum deprivation and treated the cells with the nucleoside analogue EdU at the moment that serum was added to the cells. After eight hours of culture with serum, cells were stained for EdU and nuclei were stained with TOTO-3. Fluorescent images of the nuclei, proliferating nuclei and bright field images of TopoUnits were acquired for the whole chip area using an automated microscope. A pre-processing pipeline was designed in which the images were corrected for background and signal intensity distribution and quality control metrics were calculated in order to remove unreliable results (Fig. 6.). The images obtained from pre-processing were analyzed using a CellProfiler pipeline(19), which was used to count the total number of cells per TopoUnit as well as the number of proliferating cells per unit, represented by the number of EdU-positive cells. To improve reliability, the experiment was repeated five times, giving us for each of the 2176 units ten measurements (two per chip, n = 10). In Fig. 7a, the average number of cells per TopoUnit is represented. Similarly, the average number of EdU-positive cells is represented in a heat map (Fig. 8), which clearly shows that large differences occur between different TopoUnits confirming that surface topography influences cell proliferation(20). Finally, we analysed the number of EdU-positive cells per total cell number per TopoUnit (Fig. 7b). The surface patterns of top scoring units in terms of the number of proliferating cells are shown in Fig. 8c-f. Because all cells in the TopoChip share the same 5 ml of medium in the reservoir, it is possible that the biological response is not a direct effect of the surface topography but rather mediated through short-range signals produced by cells in adjacent units. Under these circumstances, a “colony” of positive TopoUnits would be expected, which we did not observe in

the heat maps. Furthermore, it is not very likely that the small numbers of cells in the TopoUnit are able to create a morphogen gradient in such a large volume of medium. However, to represent the extent to which the surface topography itself is predictive of class fate (proliferating or non-proliferating), we trained a nearest-neighbour classifier(21) (see “Materials and methods”) to distinguish between high- and low-scoring TopoUnits based on surface topography parameters using the highest and lowest ten percent of the observations. The classifier was employed in a tenfold cross-validation setting, in which it was trained with a subset of the TopoUnits, and afterwards used to predict the outcome of another subset of TopoUnits. By comparing predictions with the actual measurements, an area under curve score (AUC)(22) from the receiver operating characteristics (ROC) curve (see “Materials and methods”) of 0.68 (Fig. 9a) was obtained, confirming that surface topography correlates to the proliferation of hMSCs, and thus mitogenicity depends on surface topography.

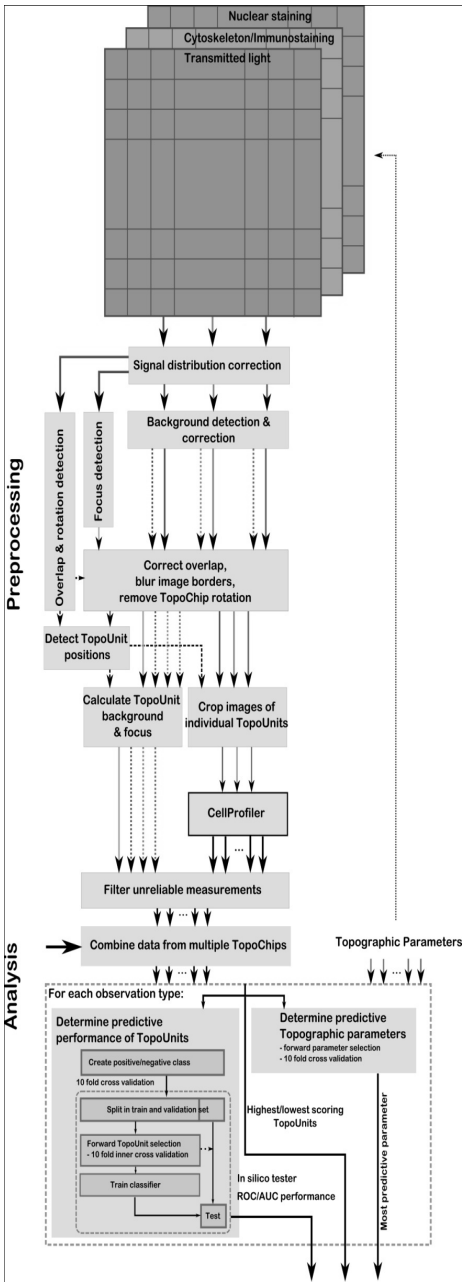

Figure 6 Schematic representations of image preprocessing, analysis and data analysis

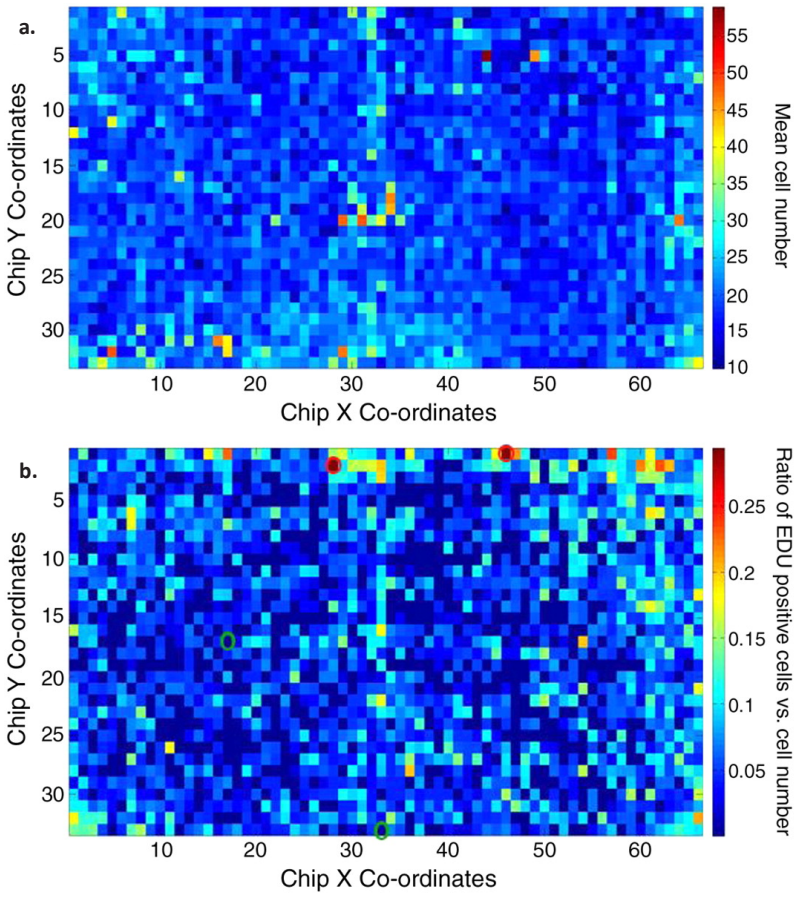

Figure 7 Cell proliferation assay

a. Heat map of the mean cell number per TopoUnit. The numbers represent the average of ten TopoUnits on five TopoChips (n = 10).
b. Heat map of the ratio of the mean number of proliferating cells over total cell number. TopoUnits marked with red circles indicate high scoring units in terms of cell proliferation ratio. Flat TopoUnits (without any features) are indicated with green circles.

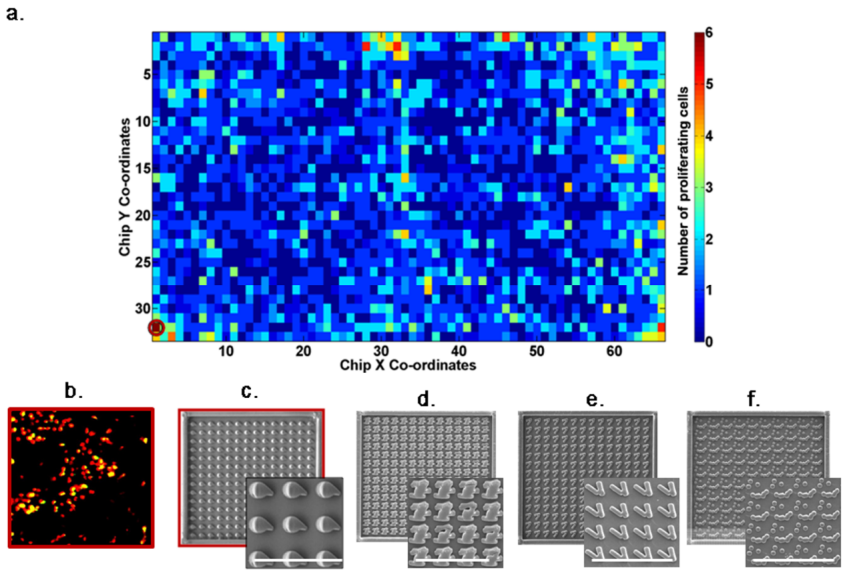

Figure 8 Mitogenic TopoUnits

a. This figure shows heat map of mean proliferating cell count of cells grown on different topographies. The TopoUnit showing maximum no. of proliferating cells is marked with a red circle.
b. Fluorescently stained pseudo coloured merged image of hMSC on the highest scoring TopoUnit. In this image the Alexa Fluor 488 EDU (representing proliferating cells) is pseudo coloured yellow whereas TOTO-3 (nucleic acid stain representing all the nuclei) is pseudo coloured red.
c. to f. SEM images of the TopoUnit showing the highest score for proliferating cells. In the inset higher magnification view of features (Scale bar: 50 µm)

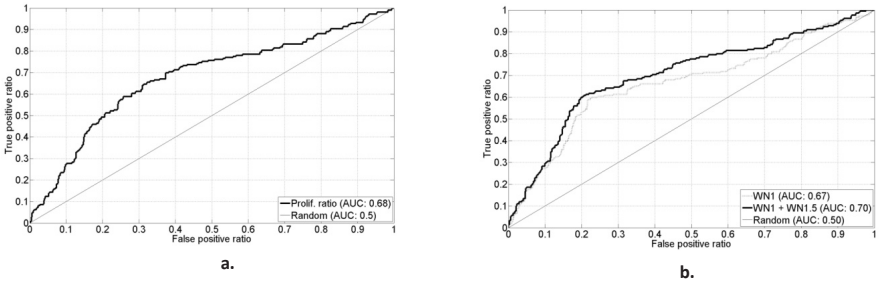

Figure 9 Data validation for the cell proliferation assay

a. ROC curve to rule out stochastic events for validation of proliferating cell count ratio as a function of surface topography after tenfold cross-validation.
b. ROC curve to determine surface topographic parameters responsible for enhanced proliferation with a machine-learnt model.

Machine learning algorithms for identification of important topographic parameters

At first sight, no apparent common design theme could be observed between the four topographic features that stimulate cell proliferation (Fig. 8c-f). To gain more insight in which (combination) of the 35 topographic parameters was most influential in determining proliferation, we performed a forward parameter selection. For this, a classifier algorithm was trained using only a subset of topographic parameters to distinguish between TopoUnits with high and low numbers of proliferating cells. This was again done for the 10% highest vs. 10% lowest measurements. The classifier was tested using a cross-validation strategy to give us an estimation of the predictive power of subsets of topographic parameters. As shown in Fig. 9b, we found that the best single parameter predictive of the number of proliferating cells was the Fourier-based parameter WN1 (AUC=0.67). Performance improved even further when forward selection included WN1.5 along with feature size and WN1 (AUC=0.70). The parameters WN1.5 and WN1 represent the fraction of the total energy contained in the feature after applying discrete Fourier transformation that is present in sinusoids with wave number approximately 1.5 and 1, respectively. These observations suggest that cell proliferation can be triggered by concentrating on designs that are composed of a certain spatial distribution.

Surface topography enhances osteogenic differentiation of hMSCs

High-content screening of TopoChips can be performed using virtually any fluorescence-based cellular staining. To further illustrate this, we analyzed the expression of alkaline phosphatase (ALP), a marker for early osteogenic differentiation, using hMSCs growing in basic medium on TopoChips. It has been shown in the past that surface topography is able to induce osteogenic differentiation in the absence of growth factors (11). Following cell culture, the cells were stained by immunofluorescence using a bone-specific anti-human ALP antibody. Immunofluorescence images of chips were acquired and ALP intensity was analyzed using CellProfiler software. First of all, we detected ALP-positive cells in less than 10% of

the TopoUnits. Fig. 10a represents mean ALP signal measured across five chips (n = 10), and immunofluorescent staining of hMSCs on the flat control is shown in Fig. 10b. The TopoUnit with the highest average/mean ALP intensity across ten measurements is shown in Fig. 10c and d. It has been reported that cell shape can influence osteogenic differentiation, and cell spreading seems to correlate positively to osteogenic differentiation(6). To investigate whether cell spreading was also related to ALP expression in our hit surfaces, we analysed the morphology of hMSCs on the top hit surface and flat reference surfaces using CellProfiler software (see Table 3). Of the 13 parameters analysed, cells on the hit surface displayed a significantly smaller cell area and a higher major axis length. Osteogenic differentiation is known to be enhanced in more compact 3-dimensional structures, such as nodules or spheroids(23) and the area of the ALP positive MSCs on the high scoring surface could be related to this, which is currently under investigation.

Table 3 CellProfiler analysis of hMSCs on a flat versus a hit surface[a]

Parameter	Flat surface	Hit surface	P value[c]
Area	2868[b]	2333	0.009
Compactness	1.45	1.51	0.06
Eccentricity	0.77	0.78	0.26
Center X	221	231	0.37
Center Y	222	225	0.39
Euler number	0.898	0.809	0.52
Extent	0.507	0.511	0.76
Form factors	0.235	0.227	0.47
Major axis length	78.9	84.2	0.004
Minor axis length	43.4	48.2	0.06
Orientation	-19.2	6.4	0.09
Perimeter	431	388	0.18
Solidity	0.76	0.75	0.25

[a] Cell profiler parameters were selected describing cell shape and measured in the flat reference surfaces and the hit surface with the highest ALP intensity.[b] On three TopoChips, about 40-50 cells were imaged per indicated TopoUnit. Average numbers are represented.[c] Student's T test on the average parameter values.

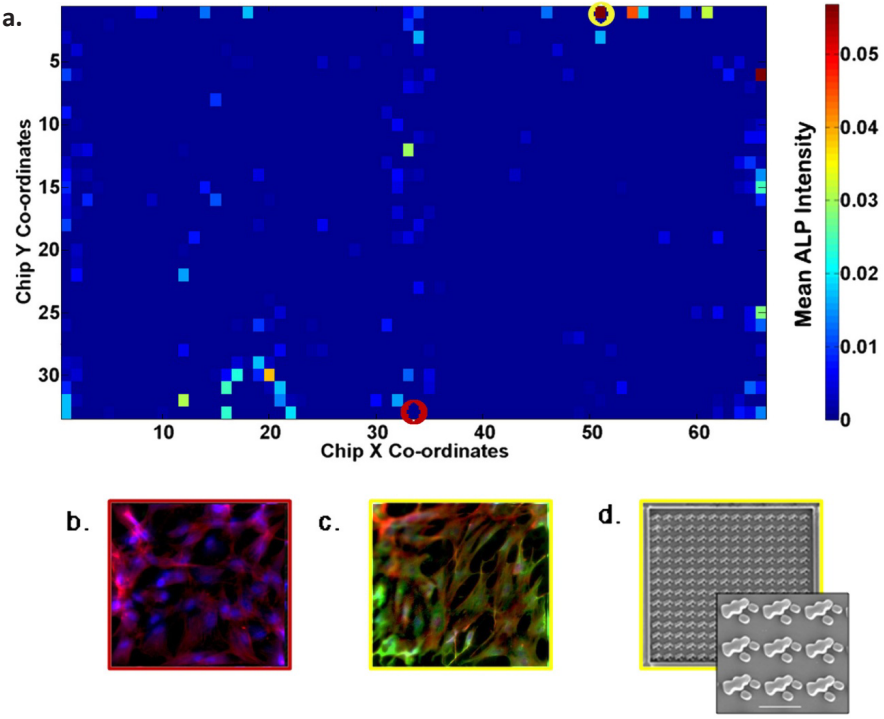

Figure 10 ALP expression of hMSC's

a. Heatmap of the mean intensity of fluorescently labelled ALP of hMSCs grown on different topographies.
b. Cells on/in a flat TopoUnit not expressing any ALP. In this image, actin staining is pseudo-coloured in red, ALP expression in green, and nucleic acid staining in blue.
c. Cells on the TopoUnit with the highest ALP expression. The corresponding TopoUnit is marked with a yellow circle on the heat map.
d. SEM image of the TopoUnit showing the highest intensity for ALP staining. The inset shows a higher magnification view of features (scale bar: 20 µm).

Discussion

Taken together, our data confirm the viability of a new approach to address the problem of unknown biological responses to a virtually unlimited number of potential surface pattern designs. In this manuscript, we have combined algorithmic generation of surface topographies with high-throughput screening of hMSCs, aiming at the identification of bio-active surface topographies.

An important pillar of the study is the use of high-content imaging and assay miniaturisation. The current TopoChip contains 2176 unique surface topographies, which we were able to screen and analyze simultaneously. Typically, research on the effect of surface topography on cell behaviour is characterized by low throughput, with some notable exceptions (24-25). Although exact calculations are difficult to make, we think that more unique surface patterns were screened for an effect on proliferation and osteogenic differentiation of hMSCs in this manuscript alone than ever published in literature. As such, we believe TopoChip screening can lead to a paradigm shift in research on surface topography, not only because of the throughput but also because our approach is based on the design of the surfaces. The current TopoChip comprises features down to a few micrometres, but future work will also focus on fabrication of TopoChips with nanometre scale topographic features, where the interaction with the cells may lead to yet another level of control.

Another powerful aspect of the TopoChip platform is its versatility. We used it to screen biological responses which are useful in bone regeneration strategies, i.e. hMSC proliferation and differentiation, but the platform can be used with different materials and cell types as well. For example, we have initiated experiments to screen for surfaces that support embryonic stem cell pluripotency, for surfaces that are favourable for proliferation of endothelial cells and surfaces with anti-adhesive properties for bacteria to prevent bio-film formation(26). With a well-defined biomaterial and biological read-out, straightforward screening projects for a myriad of different medical devices can be envisaged.

Beyond the use of TopoChip technology as a biomaterial development tool, we think it will also be instrumental in shedding new light on the scientific questions around the interplay between surface topography and cell behaviour. It is well recognized that cells respond to the surface they sit on, or in other words, we do know that cells can read a “Braille language” and respond to it. Analogous to the six simple dots that are enough to encode the Braille alphabet, it would be very interesting to decode the cell’s Braille script. How many unique cellular responses can be evoked by virtue of surface topography and what are the molecular mechanisms behind it? The algorithmic approach we used in the current study is particularly suited for this enterprise because the biological response can be correlated to design criteria of the materials. For instance, we did not anticipate that hMSC proliferation would correlate to the Fourier transform of certain features, a mathematical description of the spatial organization of topographic features on the surface(27). To fully explore the potential of this approach, systematic development of methodologies is needed that allows for generations of favourable surface topographies in environments with unpredictable response. This asks for development of new tools and insights in the design of (evolutionary) search algorithms, requires pushing the limits in imaging and nanoscale fabrication technologies, and most importantly, calls for a carefully designed hybrid of algorithmic and biological experiments. For instance, we are currently developing a nanoTopoChip for which e-beam lithography will be used, and we already produced TopoChips of various compositions including hydrogels. Moreover, we are developing the TopoChip into a device which is compatible with 6-well plates in order to make the technology more accessible for other research groups and to be able to screen even larger numbers of different TopoUnits. We believe that incorporation of iterative experimental and bioinformatics-based computational approaches for studying biomaterials will help us better understand cell-material interactions and develop better surfaces for medical devices.

Materials and methods

Design and fabrication:

As mentioned previously, topographies were designed using three types of primitive shapes, i.e., triangles, circles and rectangles. A feature was generated by first randomly selecting parameter values for its size, the number of primitives to be used and the distribution over the different primitive types, the size of the primitives, and the degree to which the primitives were to be aligned. Next, each primitive was placed at a random position inside the feature. Overlapping of primitives was allowed.

After designing the chip, a chromium mask was made and used for photolithography. The micro patterns were etched from the silicon wafer, generating a silicon master for hot embossing. To render a hydrophobic mould surface for easier demoulding, the master was coated with a layer of perfluorodecyltrichlorosilane (FDTS) (ABCR, AB111155) in an evacuated recipient. The master was subsequently used for hot embossing of PLA films (250 µm thick) (Folienwerk Wolfen GmbH, Germany) using an Obducat nanoimprint tool. Briefly, the silicon master was placed at the bottom and the PLA film was sandwiched between the silicon master and an Obducat UV Sheet Polyester (100 Micron 10638). Imprinting was carried out at 80°C with 30 bars of pressure for 10 min and then the assembly was allowed to cool down to 40°C prior to demoulding. The chips were diced from the imprinted PLA films using a wafer saw.

Cell culture:

HMSCs were isolated from a healthy donor and expanded as described previously(28). Briefly, cells were expanded in proliferation medium containing α-MEM (Gibco, 22-571-038), 10% foetal bovine serum (FBS; Lonza), 2 mM L-glutamine (Gibco, 25030), 0.2 mM ascorbic acid (Sigma, A8960), 100 U/ml penicillin + 100 g/ml streptomycin (Gibco, 15140-122) and 1 ng/ml basic fibroblast growth factor (bFGF; Instruchemie, PhP105). For the cell proliferation assay, hMSCs were trypsinised using 0.25% trypsin-EDTA (Invitrogen 25200-072), resuspended in basic medium (proliferation medium devoid of bFGF) and treated with Component A from a Click-iT™ EdU Alexa Fluor® 488 Imaging Kit (C10083) according to

manufacturer's protocol. For immunofluorescence staining of ALP, cells were resuspended in basic medium to a concentration of 1.2 million cells per millilitre and seeded on the chips. The cells were cultured in a humid 5% CO_2 environment.

Immunofluorescence staining:

After cell culture, the chips were washed with phosphate buffered saline and cells were fixed with 4% (w/v) paraformaldehyde for 10 min and permeabilised with 0.01% Triton X-100. Staining for EdU detection was performed using the EdU imaging kit according to manufacturer's protocol and cells were counter-stained with TOTO-3 iodide nucleic acid stain (Invitrogen, T3604) according to manufacturer's protocol. For ALP detection, following permeabilisation cells were incubated with a solution of 10% FBS for non-specific antibody blocking and stained for ALP using a bone-specific human ALP antibody (Developmental study hybridoma bank B4-78). The cells were counter-stained with Alexa Fluor 568 phalloidin (Invitrogen, A12380) and TOTO-3 iodide.

Image acquisition and analysis:

Images were acquired using a BD Pathway 435 automated microscope. A montage of a total of 221 montage images with respective filter sets for each fluorophore was acquired. Each image constituted a 3 by 5 montage of an area covering approximately 20 TopoUnits. All the 221 montage images were combined into one large montage (35000 by 35000 pixels) for each channel and corrected for rotation, overlap and intensity. Focus performance was determined using a Laplace operator and unreliable measurements were discarded. Subsequently, images of individual TopoUnits were cropped and analyzed using CellProfiler. For details see Fig. 6.

Data analysis:

To distinguish high-scoring TopoUnits from low-scoring ones, a nearest-neighbour classifier was applied. This is a method for classifying objects based on closest training examples (TopoUnits) in the (surface topography) parameter space and is widely used in the field of signal processing and pattern

recognition. To determine classifier performance, a tenfold cross validation strategy was employed, and ROC curves were constructed. ROC curves are a widely used standard for describing and comparing the accuracy of diagnostic tests. It represents the trade-off between the true and false positive rates for every possible classifier threshold. For each ROC curve, the AUC was determined, which is a measure of the probability that a classifier based on this label would rank a randomly chosen positive observation (e.g. enhanced proliferation) higher than a randomly chosen negative observation. AUC=1 is a perfect ranking classifier and AUC=0.5 depicts complete randomness.

References

1. Habibovic P, Barrere F, van Blitterswijk CA, de Groot K, & Layrolle P (2002) Biomimetic hydroxyapatite coating on metal implants. *J Am Ceram Soc* 85(3):517-522.
2. Meredith DO, Eschbach L, Riehle MO, Curtis ASG, & Richards RG (2007) Microtopography of metal surfaces influence fibroblast growth by modifying cell shape, cytoskeleton, and adhesion. *J Orthop Res* 25(11):1523-1533.
3. Huebsch N*, et al.* (2010) Harnessing traction-mediated manipulation of the cell/matrix interface to control stem-cell fate. *Nat Mater* 9(6):518-526 .
4. Lutolf MP & Blau HM (2009) Artificial Stem Cell Niches. *Adv Mater* 21(32-33):3255-3268.
5. Folkman J & Moscona A (1978) Role of cell shape in growth control. (Translated from eng) *Nature* 273(5661):345-349.
6. McBeath R, Pirone DM, Nelson CM, Bhadriraju K, & Chen CS (2004) Cell shape, cytoskeletal tension, and RhoA regulate stem cell lineage commitment. *Dev Cell* 6(4):483-495.
7. Ratner BD & Bryant SJ (2004) Biomaterials: Where we have been and where we are going. *Annu Rev Biomed Eng* 6:41-75.
8. Papenburg BJ*, et al.* (2007) One-step fabrication of porous micropatterned scaffolds to control cell behavior. *Biomaterials* 28(11):1998-2009.
9. Curtis A & Wilkinson C (1997) Topographical control of cells. *Biomaterials* 18(24):1573-1583.
10. Bettinger CJ, Orrick B, Misra A, Langer R, & Borenstein JT (2006) Micro fabrication of poly (glycerol-sebacate) for contact guidance applications. *Biomaterials* 27(12):2558-2565.
11. Dalby MJ*, et al.* (2007) The control of human mesenchymal cell differentiation using nanoscale symmetry and disorder. *Nat Mater* 6(12):997-1003.
12. Stevens MM & George JH (2005) Exploring and engineering the cell surface interface. *Science* 310(5751):1135-1138.

13. Lutolf MP, Gilbert PM, & Blau HM (2009) Designing materials to direct stem-cell fate. *Nature* 462(7272):433-441.
14. Lecuit T & Lenne PF (2007) Cell surface mechanics and the control of cell shape, tissue patterns and morphogenesis. *Nat Rev Mol Cell Bio* 8(8):633-644.
15. Marklein RA & Burdick JA (2010) Controlling Stem Cell Fate with Material Design. *Adv Mater* 22(2):175-189.
16. Anderson DG, Levenberg S, & Langer R (2004) Nanoliter-scale synthesis of arrayed biomaterials and application to human embryonic stem cells. *Nat Biotech* 22(7):863-866.
17. Mei Y*, et al.* (2008) Cell-Compatible, Multicomponent Protein Arrays with Subcellular Feature Resolution. *Small* 4(10):1600-1604.
18. Flaim CJ, Chien S, & Bhatia SN (2005) An extracellular matrix microarray for probing cellular differentiation. *Nat Methods* 2(2):119-125.
19. Carpenter AE*, et al.* (2006) CellProfiler: image analysis software for identifying and quantifying cell phenotypes. *Genome Biol.* 7(10) . Doi 10.1186/Gb-2006-7-10-R100.
20. Dalby MJ, Riehle MO, Johnstone HJH, Affrossman S, & Curtis ASG (2002) Polymer-demixed nanotopography: Control of fibroblast spreading and proliferation. *Tissue Engineering* 8(6):1099-1108.
21. Cover TM & Hart PE (1967) Nearest Neighbor Pattern Classification. *Ieee T Inform Theory* It13(1):21.
22. Hanley JA & Mcneil BJ (1982) The Meaning and Use of the Area under a Receiver Operating Characteristic (Roc) Curve. *Radiology* 143(1):29-36 .
23. Kale S*, et al.* (2000) Three-dimensional cellular development is essential for ex vivo formation of human bone. *Nat Biotech* 18(9):954-958.

24. Lovmand J*, et al.* (2009) The use of combinatorial topographical libraries for the screening of enhanced osteogenic expression and mineralization. *Biomaterials* 30(11):2015-2022.
25. Markert LD*, et al.* (2009) Identification of Distinct Topographical Surface Microstructures Favoring Either Undifferentiated Expansion or Differentiation of Murine Embryonic Stem Cells. *Stem Cells Dev* 18(9):1331-1342.
26. Statz AR, Meagher RJ, Barron AE, & Messersmith PB (2005) New peptidomimetic polymers for antifouling surfaces. *J Am Chem Soc* 127(22):7972-7973.
27. Assender H, Bliznyuk V, & Porfyrakis K (2002) How Surface Topography Relates to Materials' Properties. *Science* 297(5583):973-976.
28. Both SK, van der Muijsenberg AJ, van Blitterswijk CA, de Boer J, & de Bruijn JD (2007) A rapid and efficient method for expansion of human mesenchymal stem cells. *Tissue Eng* 13(1):3-9.

Chapter 4

A modular versatile chip carrier for high throughput screening of cell-biomaterial interactions

A modular versatile chip carrier for high throughput screening of cell-biomaterial interactions

Hemant V. Unadkat[1], Rohit R. Rewagad[1], Marc Hulsman[4], G.F.B. Hulshof[1,2], Roman K. Truckenmüller[1], Dimitrios Stamatialis[2], Marcel J. T. Reinders[4], Jan C. T. Eijkel[3], Albert van den Berg[3], Clemens van Blitterswijk[1], Jan de Boer[1*]

MIRA Institute for Biomedical Technology and Technical Medicine, Departments of [1]Tissue Regeneration and [2]Biomaterials Science and Technology,

[3]MESA+ Research Institute, BIOS/Lab-on-a-Chip group,

University of Twente, Postbox 217, 7500 AE Enschede, The Netherlands

[4]Delft Bioinformatics Lab, Delft University of Technology, Mekelweg 4, Delft, the Netherlands

*Corresponding author
Email: j.deboer@utwente.nl
Phone: +31 53 489 3400

Abstract

The field of biomaterials research is witnessing a steady rise in high throughput screening approaches, comprising arrays of materials of different physicochemical composition in a chip format. Even though the cell arrays provide many benefits in terms of throughput they also bring new challenges. One of them is the establishment of robust homogeneous cell seeding techniques and strong control over cell culture, especially for long time periods. To meet these demands, seeding cells with low variation per tester area is required, in addition to robust cell culture parameters.

In this paper we describe the development of a modular chip carrier which represents an important step in standardising cell seeding and cell culture conditions in array formats. Our carrier allows flexible and controlled cell seeding and subsequent cell culture using dynamic perfusion. To demonstrate the application of our device we successfully cultured and evaluated C2C12 premyoblast cell viability under dynamic conditions for a period of 5 days using an automated pipeline for image acquisition and analysis.

In addition, by using computational fluid dynamics, using lactate and BMP-2 as model molecules, we estimated that there is good exchange of nutrients and metabolites with the flowing medium, whereas no cross-talk between adjacent Test Units should be expected. Moreover, the shear stresses to the cells can be tailored uniformly over the entire chip area. Based on these findings we believe our chip carrier may be a versatile tool for high throughput cell experiments in biomaterials sciences.

Introduction

Biomaterials are being used for a wide range of clinical applications, ranging from sutures, stents and orthopaedic implants to contact lenses. In many cases, the interaction of the material surface with that of recipient's cells determines whether the material is accepted or rejected by the body. In addition, the field of biomaterials is changing from the use of bioinert materials to that of more bioactive materials. To realize the emergence of bioactive materials, different functionalization techniques such as topographic patterning, peptide patterning, plasma etching and combinatorial chemistry are being developed (1-2). Each of these emerging techniques generates enormous possibilities in terms of physicochemical variations. For instance, if we consider surface topographies alone, the geometrical possibilities in terms of shapes and sizes of surface features are virtually unlimited. Micro- and nano-technologies and robotics have been pivotal in enabling scaling down the assays and testing a multitude of materials and their properties (3-6). Often, this is approached by fabricating arrays of a variety of material properties, typically using a microscopic slide format in terms of dimensions (4, 7). For example, Anderson *et al.* have investigated the effect of embryonic stem cell behaviour on polymer libraries (8). We recently developed a high throughput platform for systematically studying the effect of thousands of surface topographies on cell behaviour (2). For studying a multitude of biomaterial properties, biological assays need to be miniaturized to accommodate a higher number of materials, which is similar to the drug discovery approaches used in the pharmaceutical industry (9). By growing cells on arrays of biomaterials, extensive control over the spatio-temporal features of the cellular microenvironment, requirement of low sample volumes, high throughput and shorter evaluation periods can be achieved. One of the challenges for high content imaging on arrays of biomaterials is determining the critical number of cells to acquire statistically significant data, which is hampered by the heterogeneity of the initial seeding density of cells. In contrast to screening using well plates where cells are dispensed per well, cell seeding on arrays is a stochastic phenomenon, similar to DNA microarrays. In the latter case

the cell lysate has to be distributed uniformly on the arrays to avoid inconsistent data. Recently we developed a chip for high throughput screening of surface topographies (10), i.e. TopoChip, with 4356 areas each with a given surface structure referred to as TopoUnits across a grid of 66 rows and 66 columns. Each TopoUnit is a 290 µm x 290 µm area separated by 10 µm thick and 50 µm high walls.

Here we describe fabrication of a generic microfluidic chip carrier for gravity driven cell seeding, which can also be used as a perfusion chip bioreactor for long term culturing. The cell seeding homogeneity and cell viability is studied while possible chemical communication between tester areas and the shear stress to the cells is estimated using computer fluid dynamics modelling.

The developed device maybe suitable for a variety of biomaterials arrays including (but not limited to) combinatorial polymer libraries, surface topographic arrays, microcontact printed protein/peptide arrays and is amenable to high content imaging.

Materials and Methods

Design and fabrication of the Chip Carrier

A computer aided design (CAD) was generated using SolidWorks 3D CAD/CAM software. The drawing of the assembly consisted of two units, being the chip carrier and the closing lid (see Figure 1a,b). The length and width of the slide part was designed similar to that of a conventional microscopic slide, i.e. 76 mm by 26 mm. The maximum height was 6 mm. One large chamber in the center of 21 mm by 21 mm and a depth of 0.5 mm was designed to secure the chip in position. All these dimensions can be suitably tuned according to the dimensions of the chip and the sizes of the features or testing areas on the chip. In the chamber, the chip can be slid into slots and kept in place.

The closing lid fits in the chip carrier and is designed to accommodate an O-ring around the border using a channel groove throughout the height. An O-ring is used as a packing to secure the closing lid in the right orientation and to prevent leakage during subsequent culture. Additionally, the closing lid was fabricated to accommodate two fluidic channels from the sides. One of the fluidic channels can act as inlet and the other as outlet for perfusion of cell culture medium. A channel of 0.1 mm depth, 23 mm width and 33 mm length was fabricated on the surface of the closing lid facing the chip to facilitate the flow of the medium (see Figure 1c,d). The depth of this channel can be tailored to control the cell seeding density.

The device components were fabricated by conventional computer-numerical-controlled (CNC) machining. The slide part was fabricated from anodized aluminium with a glass bottom for the chip chamber. The closing lid as well as the medium reservoir for static culture was fabricated from poly (methyl methacrylate) blocks.

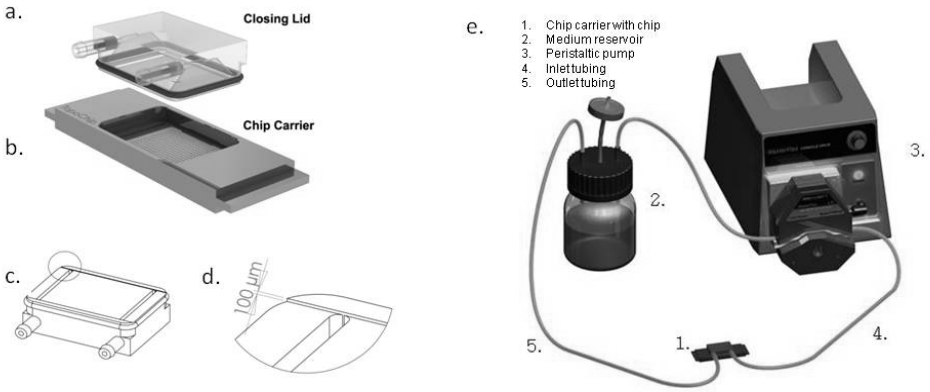

Figure 1 Chip carrier components

a. The closing lid with inlet and outlet ports for perfusion. The closing lid fits tightly on the chip carrier with an O-ring, fitted in a channel groove.
b. The chip carrier with dimensions of a conventional microscope slide of 76 by 21 mm, containing a chip, which is held in place by slots.
c. Schematic drawing of an inverted closing lid displaying inlet and outlet ports and the perfusion flow channel with a 0.1 mm depth, 23 mm width and 33 mm length, which determines medium volume on the chip.
d. Inset of the closing lid, showing perfusion flow channel in more detail.
e. Schematic representation of a closed chip carrier connected to a medium reservoir and a peristaltic pump to function as a flow micro bioreactor.

Chip design and fabrication

Briefly, the chips used in the present study were designed using Clewin 4.0 software. The 2 cm x 2 cm Chip incorporates a grid of small units (TestUnits). The lateral dimensions of the TestUnits are 290 µm x 290 µm and with a 10 µm wide and 50 µm high ridge separating adjacent units, leading to a total number of 4356 spread across a grid of 66 rows and 66 columns TestUnits per chip. The bottom of the TestUnits is uniform and unpatterned, in contrast to the previously reported TopoChip(10).

Chips were fabricated using a silicon mold processed by photolithography and etching. This mold was subsequently used to imprint the patterns onto sheets from poly (DL-lactic acid) (PDLLA, 250 µm thickness, Folienwerk Wolfen GmbH, Germany), by hot-embossing. For imprinting, a PDLLA sheet was loaded into a machine for hot embossing nanoimprint lithography (NIL 6”, Obducat AB, Sweden) together with the mold. First, the sheet was heated up to 80 °C, then 3 MPa pressure was applied for

10 min, later the temperature was reduced to 38 °C with subsequent release of the pressure. The sheet and the mold were allowed to cool down to room temperature prior to releasing the film from the mold.

Cell Culture and imaging

A pre-myoblast cell line C2C12 (ATCC CRL 1772) was used for cell culture studies. The cells were cultured in medium containing Dulbecco's Modified Eagle Medium (DMEM, Gibco), supplemented with 10% foetal bovine serum (FBS, Lonza) and 1% Penicillin and Streptomycin (Gibco) and grown at 37 °C in a 5% carbon dioxide humidified environment. Prior to seeding the cells were labeled with CM-DiI (Invitrogen D282) according to manufacturers protocol.

A peristaltic pump with a closed loop and medium reservoir as illustrated in Fig. 1e was used for continuous perfusion of the setup. The cells were cultured for 5 days with a flow rate of 100 µl/min. A live/dead assay (Molecular Probes) was used to access cell viability according to the manufacturer's protocol.

The chips were imaged with a BD Pathway 435 bioimager by designing a macro to autofocus on the fluorescent channel. Grey scale images were independently acquired by using the montage function. Individual montages were stitched together to obtain a composite image of the whole chip for each individual channel. The image was then subjected to background and alignment correction using a customized Matlab script. Out of focus TestUnits on the images were detected using Laplace filter and excluded from subsequent analysis. Images of individual TestUnits were then cropped from the composite image and subjected to analysis using CellProfiler over a computer cluster.

Computational fluid dynamics modeling (CFD)

Computational fluid dynamics (CFD) modeling was performed to evaluate the transport of secreted proteins and metabolites as well as the shear stresses generated by the flow within the chip. The study was carried out using commercial CFD software COMSOL Multiphysics® 3.5a, using bone morphogenic protein 2 (BMP-2) and lactate model components. BMP-2 is a molecule representative of secreted

proteins and if carried over to adjacent TestUnits in critical concentration may affect cell behavior (11). BMP-2 also plays a vital role in differentiation of a variety of cell types including C2C12 and mesenchymal stem cells (12). Lactate is a metabolite produced by all mammalian cell types and cell proliferation can be co-related to production of lactate. Taking into account the complex geometry of the chip and to reduce the load of computation, a two dimensional model (Cartesian coordinate system) was used to describe the chip geometry. Similarly, the problem was restricted to a series of 33 compartments instead of 66. Because the chip operation is continuous, a steady state was considered instead of time lapse and since the cell culture medium is liquid, the flow is assumed to be incompressible.

The momentum and mass transport phenomena occurring inside the chip were described by Navier-Stokes and mass balance equations respectively (11). In our case, the value of the source term for lactate was calculated to be 6.61×10^{-8} mol/m^2s, which represents the number of moles of lactate generated by 50 cells per unit time per cross sectional area at the bottom of the compartment (13). The source term for BMP-2 was presumed to be 1.66×10^{-16} mol/m^2s and the diffusion coefficient was considered to be 7.2×10^{-11} m^2/s. These coefficients are based on the values that have previously been determined for Decapentaplegic (Dpp), the drosophila homolog of BMP2 (14). In order to completely describe this transport phenomenon, conservation of momentum and mass was incorporated by using the continuity equation.

The chip geometry was divided into 470016 two dimensional nodal points by using a triangular mesh in the computational domain. The transport equations were solved over each nodal point by using a finite element method. Incompressible Navier-Stokes and convection diffusion modules available in COMSOL Multiphysics® 3.5a were used in this study. To satisfy the degrees of freedom of the set of equations, boundary conditions were specified for the inlet, outlet and the walls of the geometry. The value of the

horizontal x-directional velocity of the cell culture medium in m/s at the inlet was calculated from the time averaged velocity value corresponding to the given value of the flow rate in m^3/s.

Results and Discussion

Uniform cell seeding

To assess the uniformity of seeding on our chip, three homogenous cell suspensions of different densities (125,000, 250,000 and 750,000 cells per/ml) were seeded onto chips placed in chip carriers and the lid was closed. The chips incorporate a grid of small units (described in materials and methods), referred to as 'TestUnits'. Images were acquired 15 minutes after cell seeding and cells were counted automatically in each of the TestUnits using CellProfiler software. The uniformity of seeding was calculated using the following equation:

$$U(\%) = \left(1 - \frac{S}{M}\right) 100 \qquad (1)$$

where U is percent uniformity, S is standard deviation and M is the mean cell number per TestUnit. Figure 2a presents the results of cell seeding. We observed approximately 84% uniformity in cell distribution across the chip. We did not observe any site specific effects such as higher density of cells at the periphery of the chip, which is often the case in the seeding of well plates (data not shown). These results are very reproducible when the experiment is repeated multiple times and even with different cell types such as human mesenchymal stromal cells (data not shown).

Figure 2c presents the distributions of cells per TestUnit, seeded at different densities. Using the 125,000 cells/ml suspension more than 80% of the TestUnits were seeded with 8 to 12 cells per TestUnit. With higher cell counts of 250,000 and 750,000 per ml, the majority of TestUnits were seeded with 16 to 24, and 36 to 52 cells respectively. These results show that the chip carrier allows homogenous cell seeding, due to precise micromachining of the closing lid with a uniform channel depth. Any clumps of cells in the cell suspension should be avoided by using a cell strainer.

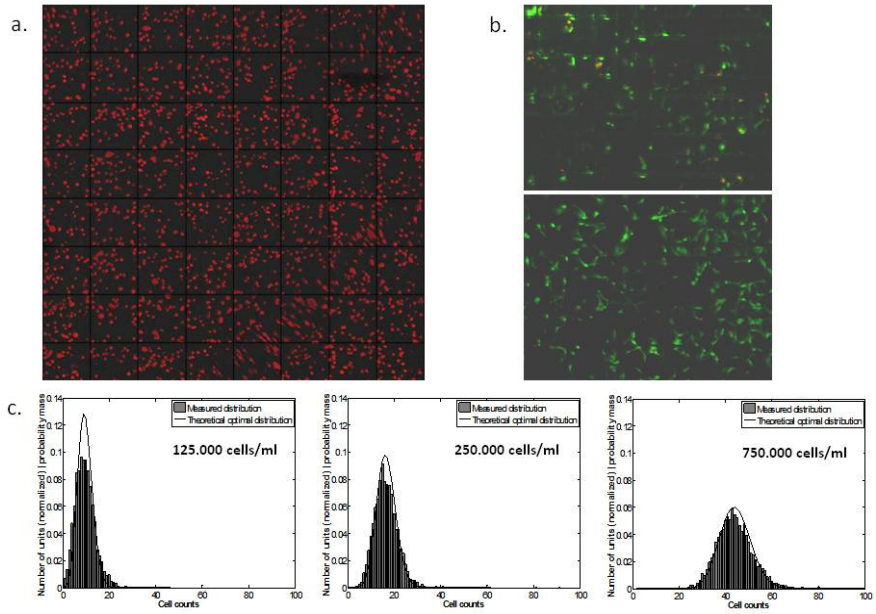

Figure 2 Cell seeding and perfusion culture

a. Typical fluorescent image of C2C12 cells 15 minutes after seeding onto the chip.
b. Live and dead staining of C2C12 cells following perfusion culture for 5 days.
c. Cell distributions on the chip using varying cell densities: 125,000, 250,000 and 750,000 cells/ml. Cell counts represent the number of cells measured with Cell profiler, within a TestUnit. In addition to the experimental data, the lines represent the estimated theoretical optimal distribution, based on the assumption that optimal cell seeding follows the binomial distribution.

To further understand the seeding process in our device, we also modeled the expected cell distribution for the three different cell densities used in the experiment. For this, we assumed that in an optimal case, each cell will be independently deposited in one of the TestUnits, i.e. without any bias for certain well or interference from other cells. The chance that a cell docks in a given TestUnit is represented by the equation:

$$P = \frac{1}{n} \qquad (2)$$

where *P* is the chance, and n the number of units, i.e. a Bernoulli variable. The number of cells in a TestUnit can then be modeled as the sum of *n* Bernoulli variables (one for each of the seeded cells on the chip), where each of the Bernoulli variables has the same chance of success (*P*). This is also known as a binomial distribution (15), with parameter *n* and *P*. As *P* is fixed (the number of units remains the same), we fitted the binomial distribution by simply setting *n* equal to the total number of counted cells on a chip. Figure 2 shows that our estimations are in excellent agreement with the experimental results, indicating that indeed well biases and/or cell interactions do not play an interfering role during seeding.

Cell culture

To assess cell viability in our seeding device under dynamic conditions, C2C12 cells were cultured for 5 days and analysed with a live/dead assay. The cells were allowed to attach for 6 hrs, prior to connecting the device to a peristaltic pump as illustrated in Fig. 1e. Figure 2b presents our results, showing that more than 95% of the cells are viable. This experiment has been performed also for human mesenchymal stem cells and Chinese hamster ovarian cell line with similar results (data not shown).

In a successful flow perfusion cell culture system the exchange of soluble factors and metabolites between the laminar flow and the cells should be adequate. The exchange is sufficient if the rate of convection of soluble proteins and metabolites is equal or greater than the uptake and metabolism. Peclet (Pe) number is in fact a measure of relative contribution of convection with respect to diffusion in the system. When Pe>1, the exchange of soluble molecules is dominated by convection and efficient exchange of nutrients and metabolites between the culture media and the cells is expected. In cases where Pe<1, diffusion is dominant and a high probability of accumulation of metabolites and hypoxia may be expected (16). Figures 3a and 4a show the Peclet number profile developed for BMP-2 and lactate respectively in the individual compartments of the chip. For all cases, Pe>1, suggests that convection is dominant and that a good exchange of soluble molecules near the chip surface is expected.

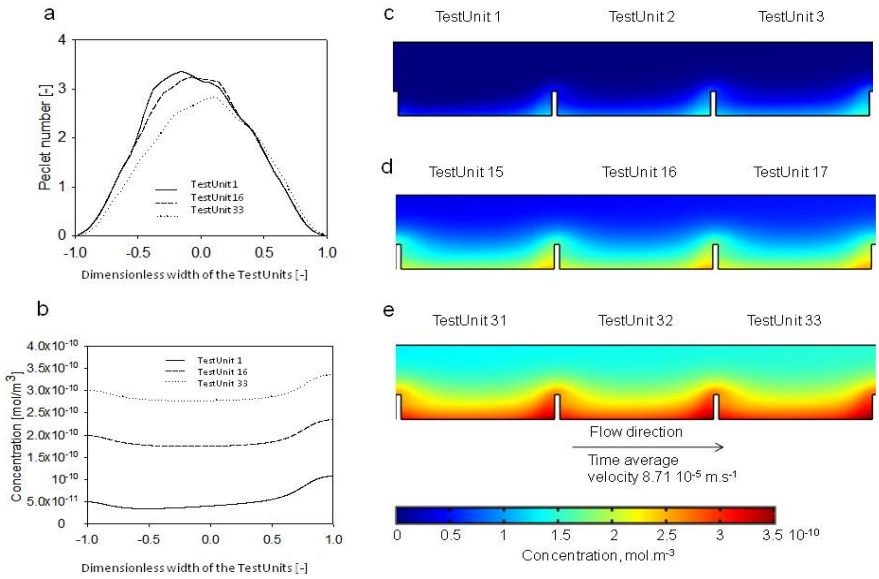

Figure 3 Peclet number profile and concentration profile of BMP-2: The concentration (in mol/m^3) profile of BMP2 on the chip was modeled by CFD.

a. Peclet number (Pe) profile across the width of TestUnit 1, 16 and 33 at a distance of 10 µm above the bottom of the TestUnits.
b. Concentration profile in mol/m^3 across the width of TestUnits 1, 16 and 33, at a distance of 10 µm above the bottom of the TestUnits.

(c-e) Concentration profiles of representative sections of the chip.

c. TestUnit 1 to 3, representing initial part of the chip.
d. TestUnit 15 to 17, representing the middle part of the chip.
e. TestUnits 31 to 33, representing the last part of the chip.

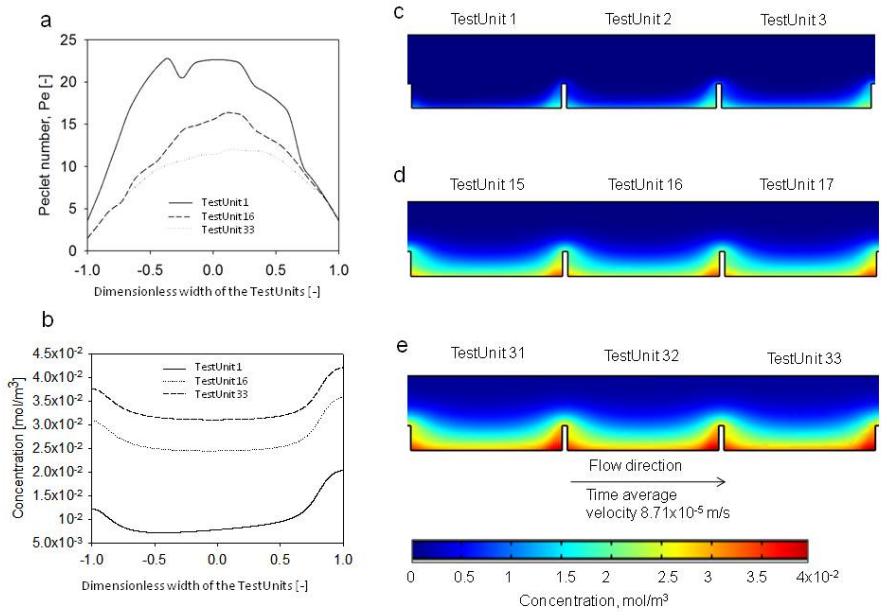

Figure 4 Peclet number profile and concentration profile of lactate: The concentration (in mol/m^3) profile of lactate on the chip was modeled by CFD.

a. Peclet number (Pe) across the width of the TestUnit 1, 16 and 33 at a distance of 10 µm above the bottom of the TestUnits.
b. Concentration profile in mol/m^3 across the width of the TestUnit 1, 16, and 33, at a distance of 10 µm above the bottom of the TestUnits.

(c-e) Concentration profiles of representative sections of the chip.

c. TestUnits 1 to 3 representing initial part of the chip.
d. TestUnit. 15 to 17 representing the middle part of the chip.
e. TestUnits 31 to 33 representing the last part of the chip.

Under the specific flow conditions (100 µl/min, the same flow rate which was also used in the cell culture experiments) a concentration gradient develops across TestUnits in the direction of the flow, with the bottom section of TestUnit 33 having higher concentrations compared to that of TestUnit 1 for both BMP2 and lactate (see Figure 3b-e, 4b-e). Nonetheless, the maximum concentration of BMP2 near the walls of TestUnit 33 is expected to be very low and in the order of 10^{-24}ng/ml. Having in mind that for most mammalian cell types BMP-2 is known to be active in the concentration range of 20-30 ng/ml, the accumulation of BMP2 there shouldn't have any biological effect. Similar conclusions can be made

about lactate. Its concentration at TestUnit 33 is expected to be 0.04 mol/m^3, which is more than three orders of magnitude lower than the value reported by Schop et. al. (35 mol/m^3) as to be the minimum for affecting cell proliferation (16). This indicates that the lactate gradient in the device would also not affect the proliferation activity of cells. All in all these previous estimations suggest that under the tested flow conditions chemical communication between the adjacent TestUnits is unlikely to happen.

Besides the concentrations of BMP2 and lactate, we also estimated the shear stresses on the cells caused by the medium flow**.** It is known from literature that shear stresses can influence gene expression profiles of cells (17) and the organization of tissue. Figure 5a presents the velocity profile within our chip. The contour plot of this profile shows that turbulence and recirculation are not present over the major part of the bottom surface of the TestUnits and only mild formation of eddies is expected at the bottom corners. The values of shear stress vary, increasing with flow rate, showing that the shear stress can be very well modulated by changing the flow rate and geometry of TestUnits depending upon the assay requirements. The maximum value of the shear stress developed for a flow rate of 100 µl/min is 0.028 Pa and the shear stresses developed for flow rates of 50 µl/min and 10 µl/min are 0.012 Pa and 0.0001 Pa respectively. Thus by simply regulating the flow rate, the height of the TestUnits and the height of the closing lid, multiple combinations of mass transport, different shear stress and cell distribution regimes are achievable. This makes our chip carrier attractive for detailed cell studies varying these parameters.

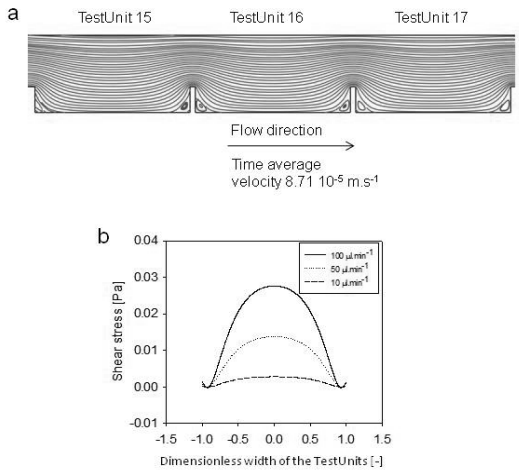

Figure 5 Velocity and shear stress profiles of the chip

a. Contour plot of the velocity profile developed in the chip for TestUnits 15 to 17 showing no turbulence, recirculation and eddies formation over the major part of the bottom of the compartments where cells are seeded.
b. Generic shear stress profile developed across the width of the compartments 10µm above the bottom of the TestUnits for different fluid flow rates.

Conclusion:

To address the challenges of standardising high throughput cell based chip assays we have developed a novel chip carrying device. The device provides robust cell culture conditions, uniform cell seeding and cell viability. In addition, CFD simulations suggest that there is good exchange of nutrients and metabolites with the flowing medium (Pe>1) whereas no cross-talk between adjacent TestUnits is expected. In fact, some local metabolite accumulation at the end of the chip is not expected to have a biological effect and the shear stress to cell can be tailored well via the flow conditions.

The developed Chip carrier is a relatively simple device and can be used for a multitude of applications in biomaterials screening and may be a great help in standardising cell based high throughput experiments in biomaterials science.

Acknowledgements

We would like to thank Dr. Gustavo Higuera Sierra for helpful discussion, Mr. Bjorn Harink for assistance with figures, Mr. Sip Jan Boorsma and Mr. Dominic Post for technical help with the fabrication. HVU received financial support from Marie Curie JOIN(ed)T early stage research fellowship.

References

1. Amis EJ (2004) Combinatorial materials science: Reaching beyond discovery. *Nat Mater* 3(2):83-85.

2. Unadkat HV*, et al.* (2011) An algorithm-based topographical biomaterials library to instruct cell fate. *Proceedings of the National Academy of Sciences* 108(40):16565-16570.

3. Amis EJ (2004) Combinatorial materials science: Reaching beyond discovery. *Nature Materials* 3(2):83-85.

4. Anderson DG, Levenberg S, & Langer R (2004) Nanoliter-scale synthesis of arrayed biomaterials and application to human embryonic stem cells. *Nat Biotech* 22(7):863-866.

5. Reynolds CH (1999) Designing Diverse and Focused Combinatorial Libraries of Synthetic Polymers. *Journal of Combinatorial Chemistry* 1(4):297-306.

6. Smith JR, Kholodovych V, Knight D, Kohn J, & Welsh WJ (2005) Predicting fibrinogen adsorption to polymeric surfaces in silico: a combined method approach. *Polymer* 46(12):4296-4306.

7. Flaim CJ, Teng D, Chien S, & Bhatia SN (2008) Combinatorial Signaling Microenvironments for Studying Stem Cell Fate. *Stem Cells and Development* 17(1):29-40.

8. Mei Y*, et al.* (2010) Combinatorial development of biomaterials for clonal growth of human pluripotent stem cells. *Nature Materials* 9(9):768-778.

9. Meredith JC (2009) Advances in combinatorial and high-throughput screening of biofunctional polymers for gene delivery, tissue engineering and anti-fouling coatings. *Journal of Materials Chemistry* 19(1):34-45.

10. Unadkat HV*, et al.* (An algorithm-based topographical biomaterials library to instruct cell fate. Submitted.

11. Zilberberg L, ten Dijke P, Sakai L, & Rifkin D (2007) A rapid and sensitive bioassay to measure bone morphogenetic protein activity. *BMC Cell Biology* 8(1):41.

12. Roelen BAJ & Dijke Pt (2003) Controlling mesenchymal stem cell differentiation by TGF? family members. *Journal of Orthopaedic Science* 8(5):740-748.

13. Higuera G*, et al.* (2009) Quantifying In Vitro Growth and Metabolism Kinetics of Human Mesenchymal Stem Cells Using a Mathematical Model. *Tissue Engineering Part A* 15(9):2653-2663.

14. Umulis DM, Serpe M, O'Connor MB, & Othmer HG (2006) Robust, bistable patterning of the dorsal surface of the Drosophila embryo. *Proceedings of the National Academy of Sciences* 103(31):11613-11618.

15. Box GEP (1978) *Statistics for experimenters : an introduction to design, data analysis, and model building / George E. P. Box, William G. Hunter, J. Stuart Hunter* (Wiley, New York :).

16. Schop D*, et al.* (2009) Growth, Metabolism, and Growth Inhibitors of Mesenchymal Stem Cells. *Tissue Engineering Part A* 15(8):1877-1886.

17. Glossop JR & Cartmell SH (2009) Effect of fluid flow-induced shear stress on human mesenchymal stem cells: Differential gene expression of IL1B and MAP3K8 in MAPK signaling. *Gene Expression Patterns* 9(5):381-388.

18. Figallo E, Cannizzaro C, Gerecht S, Burdick JA, Langer R, Elvassore N, et al. (2007) Micro-bioreactor array for controlling cellular microenvironments. *Lab on a chip* 7(6):710-9.

Chapter 5

High content imaging as a novel tool for automated analysis of biomaterial-induced cellular responses

High content imaging as a novel tool for automated analysis of biomaterial-induced cellular responses

Hemant V. Unadkat[1†], Natalie Groen[1†], Joyce Doorn[1], Bart Fischer[1], Ana M. C. Barradas[1], Marc Hulsman[2], Jeroen van de Peppel[3], Lorenzo Moroni[1], Johannes P.T. van Leeuwen[3], Marcel J. T. Reinders[4], Clemens van Blitterswijk[1], Jan de Boer[1*]

[1]MIRA Institute for Biomedical Technology and Technical Medicine, Department of Tissue Regeneration, University of Twente, P.O.box 217, 7500 AE Enschede, The Netherlands

[2]Delft Bioinformatics Lab, Delft University of Technology, Mekelweg 4, Delft, the Netherlands

[3]Erasmus MC, Department of Internal Medicine, Dr. Molenwaterplein 50, 3015 GE, Rotterdam, The Netherlands

[†]These authors contributed equally to this work.

* Corresponding author
Email: j.deboer@utwente.nl
Phone: +31 53 489 3400

Abstract

Upon contact with a biomaterial, cells respond in a manner dictated by the physicochemical and mechanical properties of the material. Traditionally, cellular responses are monitored using invasive analytical methods that report the expression of genes or proteins such as quantitative PCR or immunohistochemistry. These analytical methods involve assessing commonly used markers for a predefined readout, masking the actual situation induced in the cells. Hence, a broader expression profile of the cellular response should be envisioned, which technically limits up scaling to higher throughput systems. However, it is increasingly recognized that morphometric readouts such as cell shape are related to gene expression patterns. Moreover, morphometric data can be obtained and analyzed non-invasively without the use of molecular probes and thus are an interesting substitute for gene expression profiling. Here, we report the possibility to relate the morphological characteristics of mesenchymal stromal cells to their gene expression profile. The commonly used gene markers for osteo-, chondro- and adipogenesis did not allow the discrimination between 4 different materials with distinct surface roughness induced by oxygen plasma treatment whereas the morphological and genome wide expression profile revealed underlying cellular changes. Using 3 morphometric parameters, obtained by high content imaging, we were able to build a classifier and discriminate between oxygen plasma-induced modified sheets and non-modified PLA sheets. This approach indicates the feasibility to use noninvasive morphometric data in high-throughput systems to screen biomaterial surfaces indicating the underlying genetic biomaterial-induced changes.

Introduction

Recent progress in materials processing and chemical synthesis technology enables us to fabricate and synthesize biomaterials with virtually endless properties and compositions (1-4). Furthermore, advances in micro- and nanotechnology have provided us with enabling technologies to perform high-throughput screening of a multitude of material characteristics and properties using cell-based readouts (5-8). Similar to DNA microarray technology, these miniaturized platforms typically resemble an arrayed format for which technologies are being developed to achieve proper cell seeding and culturing. Another challenge in the field of high-throughput screening of biomaterials, designated materiomics, is to find the most efficient strategy to extract biological information from the cellular response to arrays of generated libraries. Traditionally, the field of biomaterials research uses a plethora of analytical techniques to report the expression of multiple molecular markers. Typically, in the case of mesenchymal stromal cells, one looks at osteogenic, chondrogenic or adipogenic differentiation pertaining to a given biomaterial behavior (9-10). This narrow view neglects other signaling pathways that may be involved in the differential response of cells to biomaterials. However, ideally, a broad picture is obtained indicating the overall response of cells to a certain material. For instance, gene expression profiling using DNA microarrays is able to provide a global insight in the cellular response. Unfortunately, to perform a DNA microarray analysis, a considerable amount of RNA needs to be extracted from the cells. On miniaturized biomaterial platforms the number of cells is often too low to isolate the required quantity of RNA. In addition, to probe a multitude of materials one needs arrayed isolation of thousands of RNA samples, which is technically not trivial. Therefore, microscopic analysis is currently the preferred strategy to screen material libraries (11-12). Obviously, the number of molecular markers that can be screened using fluorescent microscopy is limited to the number of available fluorescent channels on the high content bio-imaging equipment (nowadays typically four). Consequently, current assays for high content imaging focus on a relatively small subset of biological

markers, even though the broader molecular context for cellular behavior is known. Therefore, it would be desirable to be able to use single cell microscopic analysis of cells growing on biomaterials and extract other relevant data that can be associated with the cellular behavior. An interesting development within this respect is the evident link between morphological cellular parameters and complex biological responses of cells. For instance, using light microscopy, staining of the cytoskeleton and staining of nuclei, images of individual cells under different experimental conditions can be captured. Then, a morphological description comprising dozens of parameters can be compiled for individual cells using image analysis software (13-14). Next, using machine learning tools, morphological parameters that are predictive for the distinct experimental conditions, can be identified. For instance, morphological characteristics have been used to screen novel genes involved in the Rac signal transduction pathway (15). In another study, morphological characteristics obtained using light microscopy of fertilized oocytes have been correlated to successful development into the blastocyst stage of development (16). In the field of regenerative medicine, it has been demonstrated that it is possible to correlate the differentiation behavior of mesenchymal stromal cells using morphometric cytoskeletal parameters, which opens up the possibility to predict the behavior of mesenchymal stromal cells on a variety of biomaterial surfaces (13)

In this manuscript, we aim to provide proof of principle for the next step by combining microarray-based functional network analysis with that of morphometric cytoskeletal parameters. A combination of such analyses allows us to identify cellular morphometric parameters related to the expression of certain genes from genetic networks involved. As model systems, we analyzed different surface roughness of poly (DL-lactic acid) (PLA) sheets in comparison to smooth PLA surfaces. The surface roughness was introduced by applying different periods of oxygen plasma treatment. Mesenchymal stromal cells were cultured on the different sheets and two assays were performed; microarray analysis on one hand and fluorescence imaging-based single cell morphometric analysis on the other hand. We were able to

demonstrate that cells cultured on non-treated smooth sheets differed significantly from cells cultured on plasma-treated substrates using both morphometric and microarray analysis.

Materials and Methods

Oxygen plasma treatment

300 µm thick poly (DL-lactic acid) (Folienwerk Wolfen GmbH) sheets were treated with oxygen plasma, for which a radio frequency (RF) plasma reactor was employed. The sheets were subjected to this treatment for 10, 20 or 30 minutes and the electrode was powered with a current of 100 mA.

Surface topography of PLA sheets was observed by scanning electron microscopy (SEM) with a Philips XL 30 ESEM-FEG. Samples were gold sputtered (Carringdon) before SEM analysis. Using SEM data, pit diameters were measured for at least 10 spots per image and 3 images per condition were used. Further analysis of surface roughness was carried out using atomic force microscopy (AFM). All the samples were fixed with double-sided tape to magnetic stubs. All the images were obtained at ambient conditions using tapping mode, with a force of about 50 N/m (TESP tip, Veeco), a scan area of 2 µm × 2 µm and a resolution of 256 × 256 pixels. A plane fit was applied to the image and surface roughness was calculated in Nanoscope V7.30. 3-D images were generated using SPIP™ software (Image metrology A/S, Denmark). Then, pit depths were measured using the profilometric tool in Nanoscope V7.30. Ten random locations were chosen for each image and at least 3 images per condition were used. Statistical analysis was done by one-way ANOVA followed by Tukey's post-hoc test. Significance was set for $p < 0.05$.

Cell culture

Prior cell seeding, the sheets were diced to fit 24-well non-treated tissue culture plates (Nunc) for morphometric analyses and 6-well non-treated tissue culture plates (Nunc) for gene expression studies. Each experiment was performed in triplicate. The diced sheets were subsequently placed in respective culture wells, secured using an O-ring (Eriks), sterilized using 70 % ethanol for 15 minutes and washed three times with phosphate buffered saline solution.

Bone marrow aspirate (5-20 ml) was obtained from a healthy donor with written informed consent. Human mesenchymal stromal cells (hMSCs) were isolated and expanded as described previously (17). Briefly, the aspirate is resuspended using a 20-gauge needle, plated at a density of 5 x 10^5 cells/cm^2 and cultured in proliferation medium containing α-MEM (Gibco, 22-571-038), 10 % fetal bovine serum (FBS) (Lonza), 2 mM L-glutamine (Gibco, 25030), 0.2 mM ascorbic acid (Sigma, A8960), 100 U/ml penicillin + 100 g/ml streptomycin (Gibco, 15140-122) and 1 ng/ml basic fibroblast growth factor (bFGF) (Instruchemie, PhP105). The cells were trypsinized with 0.25 % Trypsin/EDTA solution prior to reaching confluence. Cells were suspended in basic medium (proliferation medium without bFGF), seeded on the PLA sheets at a density of 5000 cells/cm^2 and cultured for 5 days.

Gene expression analysis

After 5 days, total RNA was isolated from the cells cultured on different PLA sheets using a Nucleospin RNA II isolation kit (Machery Nagel) according to the manufacturer's instructions. The extracted total RNA was quantified spectrophotometrically using a ND 1000 spectrophotometer (Nanodrop technologies). mRNA levels from total RNA were determined by qPCR. cDNA was synthesized from 400 ng total RNA using iScript (Bio-Rad). 1 µl of undiluted cDNA was used for subsequent qPCR analysis which was performed on a Light Cycler real time PCR machine (Roche) using SYBR green I master mix (BioRad, Hercules, CA, USA). Data was analyzed using Light Cycler software version 3.5.3, using the fit point method by setting the noise band to the exponential phase of the reaction to exclude background fluorescence. Expression of marker genes was normalized to GAPDH levels and fold inductions were calculated using the comparative ΔCT method (18) Primer sequences are provided in table 1. Data were analyzed using one-way ANOVA followed by Tukey's multiple comparison test; $p < 0.05$ was considered significant.

Table 1 Primers sequences

Genes	Forward primer	Reverse primer
Osteogenic markers		
Osteocalcin	5'-GGCAGCGAGGTAGTGAAGAG-3'	5'-GATGTGGTCAGCCAACTCGT-3'
Osteopontin	5'-CCAAGTAAGTCCAACGAAAG-3	5'-GGTGATGTCCTCGTCTGTA-3'
Alkaline Phosphatase	5'-ACAAGCACTCCCACTTCATC-3	5'-TTCAGCTCGTACTGCATGTC-3'
Runx2	5'-GGAGTGGACGAGGCAAGAGTTT-3'	5'-AGCTTCTGTCTGTGCCTTCTGG-3
Chondrogenic markers		
Aggrecan	5'-AGGCAGCGTGATCCTTACC-3'	5'-GGCCTCTCCAGTCTCATTCTC-3'
Sox 9	5'-TGGGCAAGCTCTGGAGACTTC-3'	5'-ATCCGGGTGGTCCTTCTTGTG-3'
Collagen II	5'-CGTCCAGATGACCTTCCTACG-3'	5'-TGAGCAGGGCCTTCTTGAG-3'
Adipogenic marker		
Pparγ	5' GATGTCTCATAATGCCATCAGGTT 3'	5' GGATTCAGCTGGTCGATATCACT 3'
Housekeeping gene		
GAPDH	5' CGCTCTCTGCTCCTCCTGTT 3'	5' CCATGGTGTCTGAGCGATGT 3'

Fluorescent imaging

After culturing, cells on the different sheets were fixed with 4 % wt/v paraformaldehyde for 10 min, permeabilized with 0.1 % Triton X-100 and stained with Alexa Fluor 488 Phalloidin (Invitrogen) for the actin cytoskeleton and DAPI (Sigma) for nuclei. Images of cells were acquired automatically using a custom designed macro for a BD Pathway bioimager (BD Pathway 435, BD Biosciences). Briefly, the macro consisted of an autofocus algorithm based on the contrast of nuclear images. A set of two images, one for actin cytoskeleton and one for nuclei was acquired per sample. The images were automatically processed and analyzed using CellProfiler software. The CellProfiler pipeline consisted of measuring in total 555 different morphometric parameters such as area, perimeter, form factor, intensity and texture related to both nuclei and cytoskeleton for each cell. Forty-eight, 140, 108 and 106 hMSCs were measured for the non-treated and the 10, 20 and 30 min treated materials respectively. For the various surface modification comparisons, these morphometric parameters were ranked using a forward feature selection approach, using the logistic linear classifier to separate between non-treated and the 3 surface modifications.

Whole genome expression analysis

cRNA was synthesized from 400 ng RNA using the Illumina TotalPrep RNA amplification Kit (Ambion/Life Technologies), according to the manufacturer's protocol. Briefly, single stranded cDNA was synthesized using a T7 oligo (dT) primer followed by a second strand synthesis to obtain double stranded cDNA. Biotin-labeled cRNA was generated by *in vitro* transcription using T7 RNA polymerase. The RNA 6000 Nano assay was used to assess cRNA integrity on a Bioanalyzer 2100 (Agilent Technologies). Microarrays were performed using Illumina HT-12 v3 expression Beadchips (Illumina, Inc). First, 750 ng of cRNA was hybridized on each array overnight, then the arrays were washed and blocked followed by fluorescent signal development through addition of streptavidin Cy-3 (GE healthcare). Arrays were scanned on an Illumina iScan reader and analyzed with GenomeStudio (Illumina, Inc). For each type of surface treatment, 3 microarrays were performed (biological replicates). The measured raw intensity values were background corrected in BeadStudio (Illumina). Further data processing and statistical testing were performed using R and Bioconductor statistical software (http://www.bioconductor.org/). The probe-level raw intensity values were quantile normalized and transformed using variance stabilization (VSN). A linear modelling approach with empirical Bayesian methods, as implemented in Limma package (19), was applied for differential expression analysis of the resulting probe-level expression values.

The top 150 genes differentially expressed, having a p-value below 0.05, were considered for categorical analysis. Furthermore, a list of genes with p-values below 0.05 was uploaded to the Ingenuity Pathway Analysis (IPA) knowledgebase (Ingenuity Systems) and tested for over-representation of canonical signalling pathways. Statistical analysis of over-representation of a pathway was performed using a one-tailed Fisher's exact test. Pathways were ranked using these p-values and the top 25 was selected for functional genetic analysis of the treated surfaces (20).

Results and Discussion

Polymer surface modification by oxygen plasma treatment

hMSCs are able to respond to biomaterial surface topographies by changing both their morphology and gene expression profile. To investigate the correlation between both phenomena, we produced PLA sheets with different surface roughness by oxygen plasma treatment. Following oxygen plasma treatment, the PLA sheets were characterized using scanning electron microscopy (SEM) and atomic force microscopy (AFM). SEM helped us understanding the morphology of the modified surface and contact mode AFM allowed us to measure the pit depth. As can be seen from fig. 1 a-d different treatment times resulted in the modification of the surface of PLA sheets with variable degree of surface roughness. AFM data (fig. 1 e-j) further shows that upon higher exposure times of PLA to oxygen plasma, both the depth and mean feature diameter significantly increased. In conclusion, we produced materials with different surface topographies.

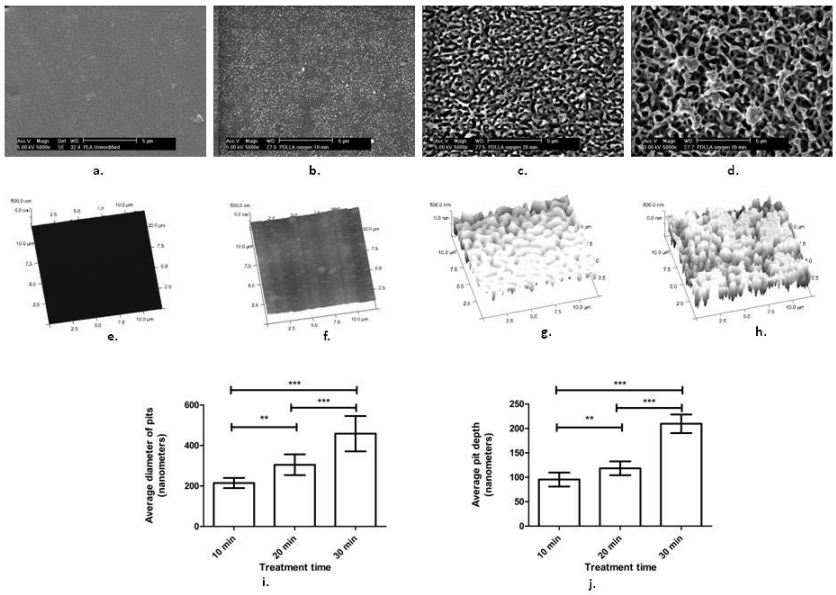

Figure 4 Characterization of oxygen plasma treated PLA sheets

a. to d. representative SEM images of PLA sheet following 0, 10, 20 and 30 minutes of oxygen plasma treatment respectively (scale bar 5 µm). Note the dose dependent increase in surface roughness upon oxygen exposure.
e. to h. AFM images of PLA sheets following 0, 10, 20 and 30 minutes of oxygen plasma treatment, respectively.
i. Average pit diameter on oxygen treated sheets, as determined using SEM images.
j. Average pit depth analyzed on oxygen treated sheets as determined using AFM images. ** represents $p < 0.05$ and *** represents $p < 0.01$.

No correlation between candidate genes and surface modification

From the literature it is known that hMSC differentiation can be influenced by surface topography (8, 21-22). To observe whether the surface topography in our set of sheets was able to induce differential gene expression, we assessed the expression of specific markers for osteogenic, adipogenic and chondrogenic differentiation. We isolated RNA from hMSCs grown for 5 days on the PLA sheets produced with different surface roughness and performed qPCR analysis for genes involved in osteogenic differentiation such as alkaline phosphatase, runx2, and osteocalcin. None of these genes showed significant differences ($p > 0.05$) in expression when cells cultured on the different PLA sheets were compared (fig. 2a). Similarly, no differences in expression of markers for chondrogenesis (i.e. Sox9, collagen II or aggrecan) or adipogenesis (PPARgamma) could be measured (fig 2b and c). Apparently, the topography induced by oxygen plasma did not result in significant differential expression of these lineage-specific marker genes. It should be noted, however, that the experiment was not performed under differentiation circumstances; no specific additives were included in the medium to drive differentiation and the expression of marker genes was assessed after 5 days.

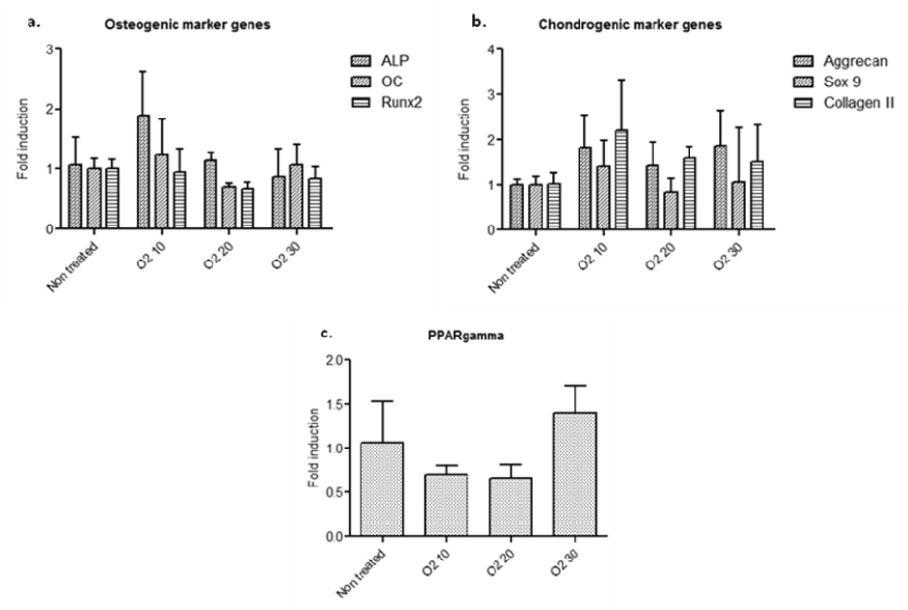

Figure 5 Marker gene expression in hMSCs cultured on oxygen treated PLA sheets

a. Relative expression of osteogenic marker genes alkaline phosphatase, osteocalcin and runx2 in hMSCs on oxygen plasma treated PLA sheets compared to non-treated sheets.
b. Relative expression levels of chondrogenic marker genes aggrecan, sox9 and collagen type 2.
c. Relative expression levels of adipogenic marker gene PPAR gamma.

All data were normalized to housekeeping GAPDH gene as described in the materials and methods section and with the expression in untreated sheets set to one. Statistical analysis was performed using ANOVA with Tukey's post testing but no significant differences ($p > 0.05$) were observed.

Cellular morphometric analysis

An alternative strategy to investigate the response of a cell to a surface is by observing their morphology. To determine whether the different surface characteristics resulted in different cell morphologies; hMSCs were seeded on the different PLA surfaces and cultured for 5 days. Next, we stained the cells with phalloidin to visualize the actin cytoskeleton. As represented in fig. 3 a and b, it appeared to us that cells cultured on the non-treated PLA sheets presented a more fibroblastic, elongated appearance compared to cells cultured on sheets treated for 30 min with oxygen plasma, which appeared to be spreading equally in all directions. Furthermore, the actin cytoskeleton appeared to be organized in more pronounced stress fibers on oxygen plasma treated sheets. Multiple cells were

imaged per sheet and CellProfiler software allowed us to describe and quantify their morphological appearance (shown in table 2). Indeed, we found statistically significant differences in cell morphology with cells on the oxygen treated surfaces having a lower perimeter and higher nucleus form factor, indicating that cells were indeed less elongated on oxygen treated surfaces. Using forward feature selection, we were able to readily distinguish cells growing on plasma treated and non-treated PLA sheets based on top three selected morphological parameters being nuclear texture, intensity of actin cytoskeletal staining and the perimeter of the cells (see fig. 4). By performing 10 fold cross-validation, we determined that a logistic classifier based on the top 3 selected features (determined for every cross validation fold using forward feature selection), was able to correctly separate the cells growing on treated and non-treated materials with an accuracy of 0.92 (92 % of the cells were classified correctly). The AUC score (Area Under the ROC curve) (23) of the determined classifier is 0.89, reflecting the chance that it will correctly distinguish two cells randomly chosen from either type of surface. Apparently, these three cellular parameters are affected by the surface roughness induced by the oxygen plasma treatment. To conclude, we are able to morphologically discriminate between hMSCs grown on oxygen-treated versus non-treated PLA sheets. The difference in morphological appearance hints at differences in cytoskeletal organization.

Table 2 Cell morphological analysis of hMSCs cultured on different PLA sheets [a]

Parameter	NT average	Treated average	p-value [b]
Cell–based			
Area	28574	26284	0.51
Area/Nucleus Area	11	8.6	0.07
Eccentricity	0.85	0.84	0.91
Extent	0.41	0.42	0.71
Form Factor	0.12	0.19	0.01
Intensity (lower quartile)	0.17	0.3	$1.98.10^{-011}$
Major Axis Length	347	300	0.03
Minor Axis Length	148	133	0.16
Orientation	-14.04	0.07	0.11
Perimeter	2342	1472	$8.83.10^{-010}$
Solidity	0.66	0.7	0.1
Nucleus-based			
Area	3287	3431	0.71
Eccentricity	0.58	0.64	0.01
Extent	0.73	0.7	0.01
Form Factor	0.78	0.62	$2.56.10^{-005}$
MajorAxisLength	72	74	0.58
MinorAxisLength	57	56	0.73
Orientation	-17.7	2.24	0.03
Perimeter	227	288	0.04
Solidity	0.96	0.93	0.003
Texture (Inverse Difference Moment)	0.79	0.75	$2.89.10^{-007}$

[a] Morphometric parameters were selected from a list of 555 parameters on their interpretability and uniqueness.
[b] p-values were determined using student's t-test comparing the parameters retrieved from cells cultured on non-treated sheets with the 3 different treated sheets. After Bonferroni multiple testing correction for a 0.05 threshold, p-values < 0.002 can be considered significant. Significant p-values are italicized.

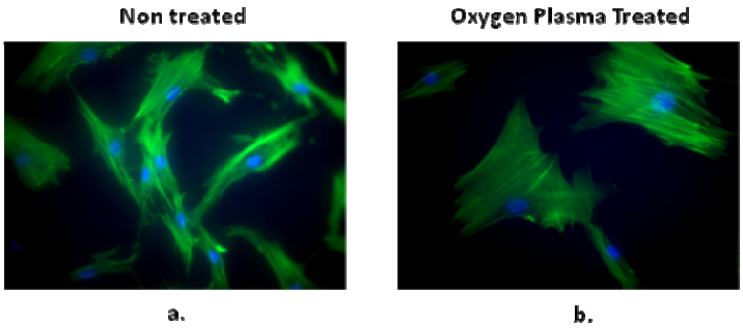

Figure 6 Cellular morphology of hMSCs cultured on PLA sheets

hMSCs were grown on the sheets for 5 days and subsequently stained with phalloidin (green) for the actin cytoskeleton nd DAPI (blue) for the nuclei. a. Representative image of hMSCs grown on untreated PLA sheets. b. Representative image of hMSCs grown on PLA sheets treated for 30 min with oxygen plasma.

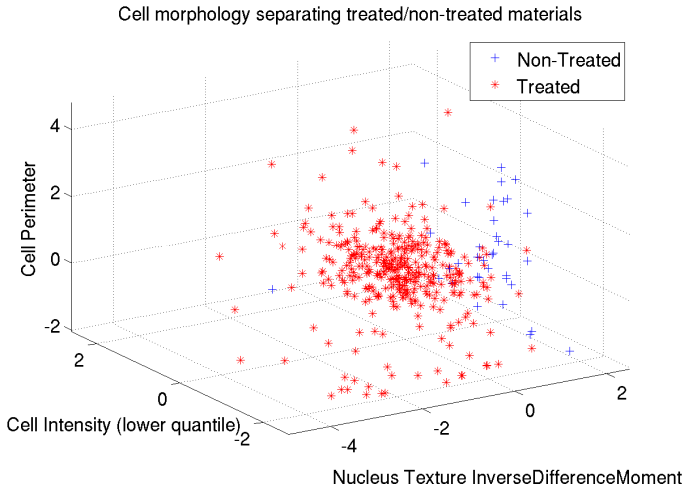

Figure 7 Phenotypical analysis of hMSCs growing on PLA sheets

Graphical representation of morphometric discrimination between hMSCs cultured on the 3 treated PLA sheets versus non-treated PLA sheets. The separation is based on the top three morphometric parameters obtained using forward feature selection. The separation accuracy was 0.92, as determined using 10-fold cross-validation and the AUC score of the 3 parameters to classify between the 3 surface treated sheets and the non-treated sheets is 0.89.

Whole genome gene expression profiling

The change we observed in cell morphology shows that the cells adapt to the surface they grow on, which is likely to be reflected by changes in their gene expression profile. Since candidate genes for osteo-, chondro- and adipogenesis did not expose this, we performed genome wide expression profiling using DNA microarray technology. To this end, a global overview of differential expressed genes between hMSCs grown on PLA sheets treated for 30 min versus non-treated PLA sheets was obtained. We analyzed the top 150 genes differentially expressed with a p-value below 0.05, on surfaces treated for 30 min with oxygen plasma. Interestingly, 24 of these top 150 genes were involved in cell adhesion, cell motility or actin cytoskeletal regulation, including for instance ACTC1, ITGA6 and several Keratins, indicating that the cells adapt their shape according to the surface they reside on (table 3). Moreover, 12 differentially expressed genes of the top list were cartilage related or involved in chondrocyte extracellular matrix production (table 4) such as COMP, COL10A1, HAS1 and DKK3 (table 4). In table 5,

an overview is given of miscellaneous genes differentially regulated on the surface treated for 30 min. From this table, we observe a down regulation of genes involved in bone remodeling in cells grown on PLA sheets treated for 30 min.

Table 3 Cell adhesion and cytoskeleton organization related genes differentially regulated in plasma treated versus non-treated surfaces[a]

Gene		Fold Regulation[b]	p-value[c]
PODXL	Podocalyxin-like	2.38	0.0146
CD74	HLA class II histocompatibility antigen gamma chain	-2.35	0.0134
LOC400578	keratin 16 pseudogene 2	2.01	0.0069
MGC102966	keratin 16 pseudogene 3	1.98	0.0029
KRT14	Keratin 14	1.88	0.0066
CSPG4	Chondroitin sulfate proteoglycan 4	1.81	0.0008
FAP	Fibroblast activation protein (Seprase)	-1.73	0.0146
MFGE8	Milk fat globule-EGF factor 8 protein (Lactadherin)	1.64	0.0002
JAG1	Jagged 1	1.62	0.0006
FRAS1	Fraser syndrome 1	1.61	0.0025
KRT16	Keratin 16	1.63	0.0043
PALM	Paralemmin	1.55	0.0179
LAMB1	Laminin beta 1	-1.52	0.0252
ITGA6	Integrin alpha 6	1.51	0.0216
RRAS	related RAS viral (r-ras) oncogene homolog	1.50	0.0059
SNTB1	Syntrophin beta 1	-1.48	0.0291
KRT7	Keratin 7	1.48	0.0125
HES4	Hairy and enhancer of split 4	1.47	0.0113
ACTC1	Actin, alpha cardiac muscle 1	1.47	0.0214
FLNB	Filamin B beta	1.47	0.0003
CDH15	Cadherin 15, type 1, M-cadherin	1.46	0.0007
RHOC	Ras homolog gene family, member C	1.46	0.0133
EMILIN1	Elastin microfibril interfacer 1	-1.43	0.0080
AFAP1	Actin filament associated protein 1	1.43	0.0023

[a] Genes of interested retrieved from the top 150 gene list differentially regulated between oxygen-treated (30 min) and non-treated surfaces.
[b] Fold difference in expression between the two studied conditions. Positive fold regulating indicates an up regulation in oxygen-treated surfaces while a negative fold difference represents an up regulation in non-treated surfaces.
[c] p-values were determined using student's t-test, corresponding to the statistical significance of fold regulation between the two conditions.

Table 4 Cartilage and cartilage matrix related genes differentially regulated in plasma treated versus non-treated surfaces[a]

Gene		Fold Regulation[b]	p-value[c]
COMP	Cartilage oligomeric matrix protein	2.41	0.0364
CLEC3B	C-type lectin domain family 3, member B (Tetranectin)	2.07	0.0134
COL10A1	Collagen, type X, alpha 1 (COL10A1)	-1.80	0.0007
ADM	Adrenomedullin	-1.71	0.0159
CTHRC1	Collagen triple helix repeat containing 1	-1.72	0.0005
HAS1	Hyaluronan synthase 1	1.67	0.0027
S100A4	S100 calcium binding protein A4	1.65	0.0429
STEAP1	Six transmembrane epithelial antigen of the prostate 1	-1.60	0.0267
PTGES	Prostaglandin E synthase	1.53	0.0019
HAPLN3	Hyaluronan and proteoglycan link protein 3	1.50	0.0103
DKK3	Dickkopf homolog 3	1.45	0.0448
P4HTM	Prolyl 4-hydroxylase	1.40	0.0037

[a] Genes of interested retrieved from the top 150 gene list differentially regulated between oxygen-treated (30 min) and non-treated surfaces.
[b] Fold difference in expression between the two studied conditions. Positive fold regulating indicates an up regulation in oxygen-treated surfaces while a negative fold difference represents an up regulation in non-treated surfaces.
[c] p-values were determined using student's t-test, corresponding to the statistical significance of fold regulation between the two conditions.

Table 5 Miscellaneous genes of interest differentially regulated in plasma treated versus non-treated surfaces[a]

Gene	Gene Name. *Gene description*	Fold Regulation[b]	p-Value[c]
COLEC12	Collectin sub-family member 12. *Scavenger receptor, binding antigens for host defense, possesses collagen-like sequences.*	-2.33	0.0290
CKB	Creatine kinase brain. *Cytoplasmic enzyme involved in energy homeostasis, reversibly catalyzes the transfer of phosphate from/to ATP.*	2.21	0.0011
APP	Amyloid beta (A4) precursor protein. *Brain related cell surface receptor and transmembrane precursor protein.*	-2.17	0.0274
APOE	Apolipoprotein E. *Scavenger of lipoproteins in blood and brain.*	-2.11	0.0177
MYL9	Myosin light chain 9, regulatory. *Regulates muscle contraction.*	-2.05	0.0176
PENK	Proenkephalin. *Neuropeptide hormone activity.*	2.02	0.0038
PKM2	Pyruvate kinase muscle. *Glycolysis, catalyzes phosphoryl group transfer to ADP.*	-1.98	0.0202
C10orf116	Chromosome 10 open reading frame 116 (Adipose specific 2). *Function unknown, exclusively expressed in adipose tissue.*	1.93	0.0006
WISP2	WNT1 inducible signaling pathway protein 2. *Possible role in modulating bone turnover.*	-1.74	0.0079
JAK1	Janus kinase 1. *Protein-tyrosine kinase involved in signal transduction pathways.*	-1.73	0.0244
PPP1R3C	Protein phosphatase 1, regulatory subunit 3C. *Catalyzes reversible protein phosphorylation.*	1.60	0.0087
SMAD6	SMAD family member 6. *Negatively regulates BMP and TGF-beta/activin signaling.*	1.58	0.0015
MYH11	Myosin heavy chain 11, smooth muscle. *Functions as a contractile protein.*	1.55	0.0011
CTSK	Homo sapiens cathepsin K. *Involved in bone remodeling and resorption.*	-1.54	0.0079
MDK	Midkine (neurite growth-promoting factor 2). *Promotes angiogenesis.*	-1.52	0.0028
CD248	CD248 molecule (Endosialin). *Related to tumor angiogenesis.*	1.49	0.0009

[a] Genes of interested retrieved from the top 150 gene list differentially regulated between oxygen-treated (30 min) and non-treated surfaces.
[b] Fold difference in expression between the two studied conditions. Positive fold regulating indicates an up regulation in oxygen-treated surfaces while a negative fold difference represents an up regulation in non-treated surfaces.
[c] p-values were determined using student's t-test, corresponding to the statistical significance of fold regulation between the two conditions.

Next, we analyzed the function of genes differentially regulated with a p-value lower than 0.05, resulting in 2613 genes, using Ingenuity Pathway analysis (table 6). Interestingly, from the top 25 pathways in which these genes are involved, 4 relate to actin (top ranked) and integrin signaling (ranked fifth). Regulation of actin based motility by Rho and Integrin signaling were also pathways in the list of genes. These data confirm that the morphological response of MSCs to the different surface roughness was induced by plasma treatment.

Table 6 Top 25 list of Ingenuity Pathway analysis of genes differentially expressed between oxygen plasma treated and non-treated surfaces[a]

Ingenuity Canonical Signaling Pathways	p-Value[b]	Ratio[c]
Actin Cytoskeleton Signaling	0.0006	0.173
Role of JAK1 and JAK3 in γc Cytokine Signaling	0.0007	0.246
IL-9 Signaling	0.0009	0.289
Agrin Interactions at Neuromuscular Junction	0.0009	0.254
ILK Signaling	0.0010	0.187
p70S6K Signaling	0.0011	0.205
Mitochondrial Dysfunction	0.0016	0.188
Germ Cell-Sertoli Cell Junction Signaling	0.0019	0.189
Virus Entry via Endocytic Pathways	0.0041	0.207
Regulation of eIF4 and p70S6K Signaling	0.0052	0.174
Interferon Signaling	0.0071	0.265
AMPK Signaling	0.0087	0.173
IGF-1 Signaling	0.0095	0.186
Myc Mediated Apoptosis Signaling	0.0107	0.217
Small Cell Lung Cancer Signaling	0.0112	0.179
EGF Signaling	0.0112	0.229
EIF2 Signaling	0.0151	0.176
JAK/Stat Signaling	0.0162	0.203
Molecular Mechanisms of Cancer	0.0182	0.139
Regulation of Actin-based Motility by Rho	0.0186	0.184
Integrin Signaling	0.0219	0.151
Docosahexaenoic Acid (DHA) Signaling	0.0219	0.225
Role of JAK2 in Hormone-like Cytokine Signaling	0.0219	0.229
IL-4 Signaling	0.0234	0.188
Semaphorin Signaling in Neurons	0.0240	0.212

[a] Uncorrected p-value < 0.05, resulting in a list with 2613 genes
[b] p-Value calculated based on the Right-tailed Fisher's Exact test, defining the statistical significance of over-representation of the pathway in the gene list compared to a reference gene list
[c] Ratio is the number of genes from the gene list that participate in the canonical signaling pathway divided by the total number of genes involved in the pathway.

Conclusion

We have been able to evoke changes in the morphology of hMSCs by changing the surface properties of the PLA sheets on which the cells grew. Using fluorescent labeling, high content imaging and forward feature selection, we were able to describe the morphology of the cells, based on three parameters, i.e. nuclear texture, intensity of actin cytoskeletal staining and the perimeter of the cells. The morphological data indicate a change in the cytoskeletal organization and may hint at the differential activity of signaling pathways. Nevertheless, qPCR analysis on osteogenic, chondrogenic and adipogenic markers did not reveal significant differences in gene expression. On the other hand, whole genome gene expression profiling identified differential expression of genes involved in cell adhesion and cytoskeletal organization and additionally identified differential regulation of genes related to cartilage and chondrocyte matrix production. By precisely defining the cellular phenotype, high content morphological imaging is a powerful tool to screen libraries of biomaterials without the use of molecular markers.

Acknowledgements

The authors acknowledge the Marie Curie Early Stage training program JOIN(ed)T for funding of H.U., STW for funding JdB, TeRM for A.B. and J.D. and the BMM program for N.G. We wish to acknowledge Anne Carpenter and colleagues for their kind assistance with CellProfiler software, Dr. Auke Renard from Medisch Spectrum Twente for kindly providing us with bone marrow aspirates, André Uitterlinden for access to and assistance with Illumina microarray facility. We are also grateful to Martin Bennink and Kim Sweers for assistance with atomic force microscopy and Dr. René Kalio from Folienwerk Wolfen GmbH (Wolfen, Germany) for kindly providing the materials.

References

1. Anderson DG, Levenberg S, & Langer R (2004) Nanoliter-scale synthesis of arrayed biomaterials and application to human embryonic stem cells. *Nat Biotechnol* 22(7):863-866.
2. Dankers PY, Harmsen MC, Brouwer LA, van Luyn MJ, & Meijer EW (2005) A modular and supramolecular approach to bioactive scaffolds for tissue engineering. *Nat Mater* 4(7):568-574.
3. Lovmand J*, et al.* (2009) The use of combinatorial topographical libraries for the screening of enhanced osteogenic expression and mineralization. *Biomaterials* 30(11):2015-2022.
4. Silva GA*, et al.* (2004) Selective differentiation of neural progenitor cells by high-epitope density nanofibers. *Science* 303(5662):1352-1355.
5. Lutolf MP, Gilbert PM, & Blau HM (2009) Designing materials to direct stem-cell fate. *Nature* 462(7272):433-441.
6. Mei Y*, et al.* (2010) Combinatorial development of biomaterials for clonal growth of human pluripotent stem cells. *Nat Mater* 9(9):768-778.
7. Tare RS*, et al.* (2009) A microarray approach to the identification of polyurethanes for the isolation of human skeletal progenitor cells and augmentation of skeletal cell growth. *Biomaterials* 30(6):1045-1055.
8. Dalby MJ*, et al.* (2007) The control of human mesenchymal cell differentiation using nanoscale symmetry and disorder. *Nat Mater* 6(12):997-1003.
9. Yuan H*, et al.* (2010) Osteoinductive ceramics as a synthetic alternative to autologous bone grafting. *Proc Natl Acad Sci U S A* 107(31):13614-13619.
10. Benoit DS, Schwartz MP, Durney AR, & Anseth KS (2008) Small functional groups for controlled differentiation of hydrogel-encapsulated human mesenchymal stem cells. *Nat Mater* 7(10):816-823.

11. Tourovskaia A, Figueroa-Masot X, & Folch A (2006) Long-term microfluidic cultures of myotube microarrays for high-throughput focal stimulation. *Nat Protoc* 1(3):1092-1104.

12. Markert LD*, et al.* (2009) Identification of distinct topographical surface microstructures favoring either undifferentiated expansion or differentiation of murine embryonic stem cells. *Stem Cells Dev* 18(9):1331-1342.

13. Treiser MD*, et al.* (2010) Cytoskeleton-based forecasting of stem cell lineage fates. *Proc Natl Acad Sci U S A* 107(2):610-615.

14. Logan DJ & Carpenter AE (2010) Screening cellular feature measurements for image-based assay development. *J Biomol Screen* 15(7):840-846.

15. Wang J*, et al.* (2008) Cellular phenotype recognition for high-content RNA interference genome-wide screening. *J Biomol Screen* 13(1):29-39.

16. Wong CC*, et al.* (2010) Non-invasive imaging of human embryos before embryonic genome activation predicts development to the blastocyst stage. *Nat Biotechnol* 28(10):1115-1121.

17. Alves H*, et al.* (2010) A link between the accumulation of DNA damage and loss of multi-potency of human mesenchymal stromal cells. *J Cell Mol Med* 14(12):2729-2738.

18. Livak KJ & Schmittgen TD (2001) Analysis of Relative Gene Expression Data Using Real-Time Quantitative PCR and the 2−ΔΔCT Method. *Methods* 25(4):402-408.

19. Wettenhall JM & Smyth GK (2004) limmaGUI: a graphical user interface for linear modeling of microarray data. *Bioinformatics (Oxford, England)* 20:3705-3706.

20. Tusher VG, Tibshirani R, & Chu G (2001) Significance analysis of microarrays applied to the ionizing radiation response. *Proc Natl Acad Sci U S A* 98(9):5116-5121.

21. Unadkat HV*, et al.* (2011) An algorithm-based topographical biomaterials library to instruct cell fate. *Proc Natl Acad Sci U S A* 108(40):16565-16570.

22. Olivares-Navarrete R*, et al.* (2010) Direct and indirect effects of microstructured titanium substrates on the induction of mesenchymal stem cell differentiation towards the osteoblast lineage. *Biomaterials* 31(10):2728-2735.

23. Hanley JA & McNeil BJ (1982) The meaning and use of the area under a receiver operating characteristic (ROC) curve. *Radiology* 143(1):29-36.

Chapter 6

Materiomics: Where we are and where can we go?

General discussion and future outlook

Materiomics: Where we are and where can we go?

The primary goal of this work was to develop screening technology for the identification of bioactive surface topographies which would enable us to modulate, steer and study cell behaviour in a high throughput manner. The secondary goal was to fill in some technological voids by development of enabling technologies which would lead to the realization of the Materiomics paradigm.

Cell behaviour is a complex phenomenon and numerous attempts in the past to realise *in vivo* scenario have focussed on development of biomimetic materials. The primary intention of the high throughput approach has been to achieve functional biomimetics rather than structural biomimetic properties. In other words identifying right surface topography for an implantable biomaterial which would be able to evoke a functionally desired biological response rather than relying merely on replicating the physical structure of the tissue being replaced with biomaterials. The TopoChip technology has helped us identify functional design attributes for biologically active surface topographies that were previously not known thereby bringing a paradigm shift where screening of topographic libraries revealed numerous insights about cell behaviour.

The TopoChip:

In the third chapter we describe the development of mathematical algorithms for designing a randomized library of 2178 surface topographies (TopoChip). In addition, the influence of topographic features on the growth and differentiation of human mesenchymal stem cell was studied in a high throughput manner. With this work we demonstrate a streamlined work flow of high throughput study of stem cells-surface topography interactions including randomized library design, high throughput surface feature fabrication, cell seeding and manipulation, high content image analysis, and data analysis.

The TopoChip technology can be used for a wide range of applications beyond identification of surface topographies for implantable biomaterials. For instance studying cell-surface topographic interactions can be a cornerstone for studying cell-matrix interactions. The signal propagation of cell-surface topographic responses can be used as a tool for mimicking other aspects of contact guidance in cells such as morphology, directed migration, and effects on proliferation. Studying these interactions as synergistic cues to direct and enhance complex processes such as stem cell differentiation shall prove to be extremely useful.

Some additional applications for the future along with the challenges are in sections below.

Enabling technologies for Materiomics:

In the fifth chapter of this thesis we demonstrate the fabrication of oxygen-plasma treated surfaces and the screening of their effects on cell behaviour. The aim of this study was to identify robust and reliable assays for determination of cellular responses to different topographies. Initially, we sought to rely on the traditional approach of qPCR to look at genes of interest. However, narrowing down the research question to genes of interest may omit the understanding of other dominant interactions. It is widely acclaimed that biomaterial properties can lead to genome wide changes in cells grown on them. If the goal is to understand genome wide changes within cells grown on biomaterials one needs a good, fast and reliable way to identify the alterations in phenotype that result from the effect of biomaterials on cells. Even though many large scale studies in the past have been designed and performed on a multitude of biomaterials by manually analyzing the images either by effective design of assays or tenacity of scientists there is little doubt that the field of Materiomics will be greatly benefited from the development of automated or semiautomated phenotypical assays. When it comes to high throughput these assays are limited to two dimensional cell culture systems. With the advent of novel and faster

algorithms especially for fast, reliable deconvolution and 3D image reconstruction the phenotypical assays will play a vital role in the development of 3D high throughput screening systems.

The present generations of high throughput biomaterial screening systems rely on chip based arrays. Miniaturizing to a chip format comes with other significant hurdles, firstly the distribution of cells within tester areas need to be identical and second the cross talk between adjacent test areas has to be biologically limited. In the fourth chapter we present a modular chip carrier technology which can potentially be used for next generation of biomaterials arrays. We have successfully used this chip carrier technology to overcome the hurdles presented by biomaterials arrays by being able to seed cells with very low variation in seeding density and limiting the cross talk between adjacent test areas by using a flow regime. The modular nature of this device also allows for static cell culture and the microscope slide format is suitable for a range of automated microscopes. This technology and its subsequent revisions will allow for efficient seeding and culturing of cells amongst others on combinatorial biomaterials libraries, surface topographic arrays and microcontact printed peptide arrays.

TopoSensor Chips or MMP responsive TopoChip:

The TopoSensor chip was based on a concept of introducing a sensing element on the TopoChip itself. It is expected that this platform would help us understand if topographical cues by means of mechanotransduction could induce an effect on matrix metallo protease (MMP) activity of cells. The technology was aimed at fabricating these chips out of poly (ethylene glycol) (PEG) hydrogel by soft embossing. A Michael type addition reaction can be used for crosslinking PEG-vinyl sulphone and PEG-thiol by incorporating a MMP sensitive peptide. In this project a commercially available MMP FRET peptide (520 MMP FRET Substrate XIV, Anaspec Inc,CA) consisting of a 5-FAM fluorophore and QXL 520 quencher is used (Figure 1). Fluorescence Resonance Energy Transfer (FRET) peptides carry a

fluorophore-quencher pair in which respectively the emission and excitation spectra overlap. Since these spectra overlap and the fluorophore-quencher pairs are within a short range distance of each other (smaller than the wavelength of the emitted photon), virtual photons emitted due to excitation of the fluorophore are non-radioactive absorbed by the quencher. Photons absorbed by the quencher will not result in another emitted electron thus no fluorescent signal can be detected. On the contrary when the peptide will be cleaved by the MMPs released from the cells, the distance between the quencher and the fluorophore will increase resulting in emission of a fluorescence signal.

A schematic explaining the fabrication of this chip is depicted in fig. 2. It is expected that this technology will help us understand the effect of surface topographies on the MMP activity of cells by means of mechanotransduction. These proteases play an important role in the foreign body response (FBR) leading to failure of implants and are moreover involved in various human pathophysiological conditions. Modulation of cellular MMP activity and corresponding biological processes involved in the FBR by regulating MMP is an attractive strategy to improve implant performance and reduce disease progression.

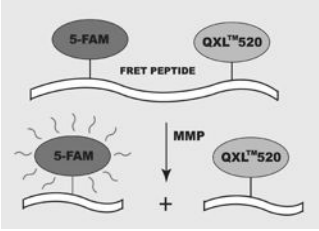

Figure 8 5-FAM/QXL520 fluorophore/quencher pair and MMP cleavage point. Before cleavage the pair is in a short range of distance and the emitted photons from the fluorophore are quenched. Upon cleavage the distance increases and the fluorescent signal is recovered

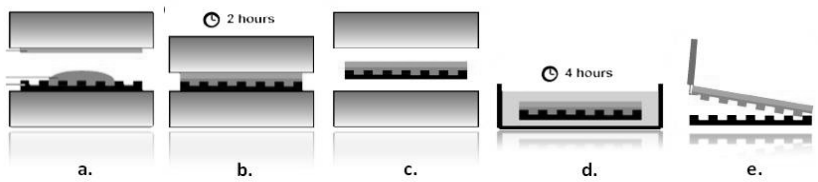

Figure 2 Schematic of TopoSensor chip fabrication (Image courtesy MSc. internship report Frank Assen)

a. Dispensing a required amount of solution prior to gelation
b. Embossing
c. Releasing the pressure
d. Immersion in deionised water
e. Demolding

Biofouling surfaces:

Biomaterials are used for a variety of procedures in a hospital ranging from catheters, rubber drains, tracheostomy tubes, blood bags to implants. In spite of extensive sterilization protocols biomaterial associated infections are one of the main causes for the failure of medical devices, with the incidence ranging from 1% to 30%, depending on the biomaterial and its application. Significant efforts are being dedicated towards the development of surfaces which can prevent bacterial adhesion. We are currently investigating the use of TopoChip technology to screen for surfaces preventing bacterial adhesion. However the present size of features on the TopoChip is much larger compared to the size of bacteria. Hence, development of TopoChip with features in the range of 100-500 nm is vital for studying these interactions. Some of the challenges and development of nano-TopoChips are described in the following sections.

Finite element modelling of surface topographies:

In chapter 4 we studied the influence of feature shapes on cell behavior. It is also known that mechanical rigidity influences cell morphology, focal adhesion, cytoskeletal contraction, stem cell proliferation and differentiation. It is possible to speculate that the effect of surface topographies that

we observe in chapter 3 might also be due to the variation in rigidity of the features. In order to better understand the phenomenon finite element modeling of different shapes of features may be vital.

Nano TopoChip:

The size of surface topographic features on the present TopoChip ranges from 10 µm to 30 µm. However cells are sensitive to nano scale cues like antibody binding. It has also been shown that molecular imprinting in the range of nanometers can significantly alter cell behavior. Hence efforts are being dedicated for the fabrication of a TopoChip with features in the range on 80 to 300 nm. There are significant technical hurdles in order for such a chip to see the light of the day the most important being the huge size of the design files generated using mathematical algorithms. The lack of proprietary software meant for E-beam systems which can handle such huge design files is an impending hurdle at the moment.

qPCR on TopoChip:

The first generation of micro total analytic systems in chemistry were aimed at addressing the problems associated with sample analysis and eventually complex systems with fluid handling capability evolved which allowed for automated and efficient sample handling and manipulation. With the advances in microfluidic technologies it is possible to perform qPCR's on a chip based format. Fluid handling and manipulation technologies when incorporated with the TopoChip platform would enable us to perform DNA extraction and qPCR with cells seeded on the TopoChip. This would allow us not just to answer specific biological questions but also to verify the hits identified by immunostaining or fluorescent reporter assays.

Pseudo 3D TopoChip:

The application of the present TopoChip is limited to analyzing behavior of cells in two dimensional setup and can be efficiently translated to applications requiring two dimensional cell biomaterial interactions for instance vascular stents, contact lenses etc. Understanding the three dimensional interactions between cells and their environment is vital for understanding underlying developmental mechanisms. For instance it is known that organization of embryonic stem cells in their niche regulates their self renewal and/or differentiation. With this intent we fabricated a pseudo 3D TopoChip (fig. 3) to modulate the organization of embryonic stem cells thereby allowing us to identify niches regulating either the self renewal or differentiation of mouse embryonic stem cells. We hypothesize that in the future it will be possible to study further challenges in developmental biology including organogenesis using this technology.

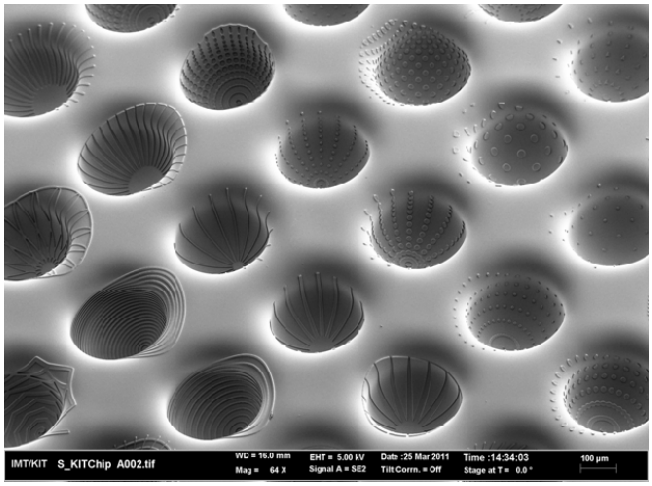

Figure 3 SEM of the pseudo 3D TopoChip displaying hemispherical containers with assorted topographies (In collaboration with Dr. Stefan Giselbrecht, KIT)

3D Translation:

It may very well be argued that cell behavior on two dimensional substrates may not necessarily be the same as that on three dimensional substrates. However, development of three dimensional substrates with controlled surface topographies is itself a challenge. In order to overcome this we performed some pilot experiments for patterning of three dimensional substrates. In these experiments a 3 dimensional scaffold fabricated by rapid prototyping technique was used. The scaffold was then subjected to ablation of fibers for creating surface topographies using a femtosecond pulse laser as shown in figure 4. The scaffold used in our study was made from poly(ethylene oxide terephthalate)–poly(butylene terephthalate) (PEOT/PBT) copolymers. Although the study was performed on a prefabricated scaffold a hybrid rapid prototyping setup comprising ablation lasers and mirrors is not a farfetched reality.

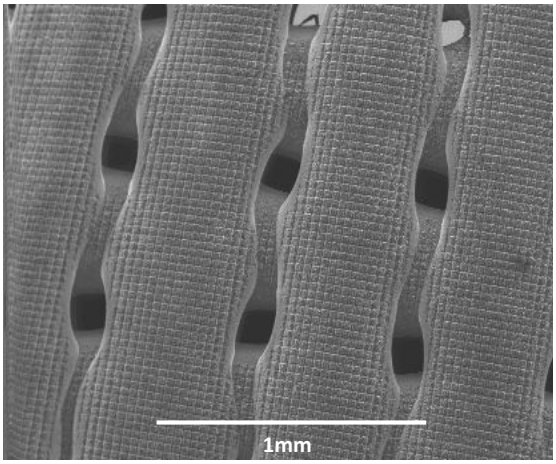

Figure 4 SEM of PEOT/PBT scaffold fabricated by rapid prototyping and patterned using femtosecond laser

Summary

The technological advances in the field of material science coupled with the improved understanding of cell behaviour have brought us to the era of smart or instructive biomaterials. In contrast to the bioinert materials this new generation of materials rely on the technological advances from the evolving field of Nanotechnology. It has long been known that the surface topography of a biomedical implant is able to dictate the response of tissue surrounding it. The increasing trend of using stem cells in combination with biomaterials requires materials with predictable instructive properties. Surface topography of an implant can provide such instructions to stem cells in a reliable manner. However, the endless possibilities for the creation of surface topographies make it difficult to choose the best one for a given implant.

The field of Materiomics, which deals with high throughput screening of natural and synthetic materials and their properties, provides us with tools to better understand cell behaviour on a library of surface topographies. This thesis describes the TopoChip platform, a high-throughput screening system for studying the interaction of cells with surface topographies.

Chapter 2 describes the microfabrication techniques considered to be vital for the development of Materiomics. It also describes the possible uses of such techniques by providing relevant examples.

In Chapter 3 elaborates the algorithmic design and fabrication of surface topographic library called TopoChip. The identification of surface topographies with instructive activity for proliferation as well as osteogenic differentiation of mesenchymal stem cells is also explained. We were able to correlate the algorithmic design parameters to cellular responses, which yield novel design criteria for these particular parameters. It is proved that randomized libraries of surface topographies can be broadly applied to unravel the interplay between cells and surface topography and to find improved material surfaces.

Chapter 4 describes the design, fabrication and use of a microfluidics based chip carrier to address the challenges of standardising high throughput cell based assays for chip based biomaterial screening. The device provides robust cell culture conditions, uniform cell seeding and cell viability. In addition, CFD simulations suggest that there is good exchange of nutrients and metabolites with the flowing medium (Pe>1) whereas no cross-talk between adjacent TestUnits is expected. Moreover, the shear stresses to the cells can be tailored uniformly over the entire chip area. Based on these findings we believe our chip carrier may be a versatile tool for high throughput cell experiments in biomaterials sciences.

Chapter 5 aims at showcasing the development and versatility of a fairly easy phenotypical assay to monitor and predict the response of cells when grown on different biomaterial surfaces. We have been able to evoke changes in the morphology of hMSCs by changing the surface properties of the PLA sheets on which the cells grew. Based on cellular morphometric parameters we were able to classify cells cultured on treated as well as untreated surfaces with 92 % accuracy. The morphological data indicate a change in the cytoskeletal organization and may hint at the differential activity of signaling pathways. By precisely defining the cellular phenotype, high content morphological imaging has proven to be a powerful tool for screening of biomaterials libraries without the use of molecular markers.

Chapter 6 reviews the conclusions and discussion of each chapter. In this chapter we also propose some new technologies which make use of surface topography as a tool to investigate fundamental intricacies of cell behaviour and organisation.

Samenvatting

De technologische vooruitgang in materiaalwetenschap heeft door het bestuderen van cel gedrag de deur geopend voor een tijdsperk van slimme biomaterialen. In tegenstelling tot bio-inerte materialen gebruikt deze generatie technologie die voortkomt uit het veld van Nanotechnologie. Het is bekend dat de topografie van een biomedisch implantaat de locale respons van het omliggende weefsel kan beïnvloeden. Voor het gebruik van stamcellen in combinatie met biomaterialen, zoals gebruikt bij implantaten, zijn materialen nodig die gedrag van weefsel kunnen sturen. De topografie van het biomateriaal kan een robuuste manier zijn om stamcellen te beïnvloeden. Het kiezen van de juiste topografie voor een specifieke toepassing blijft echter lastig aangezien er uit oneindig veel mogelijkheden gekozen kan worden, dit leidt tot uiteenlopende resultaten wanneer het wordt toegepast op een implantaat.

In het onderzoeksveld van Materiomics wordt onderzoek gedaan naar de eigenschappen van natuurlijke en synthetische materialen door middel van high-throughput screening. Hiermee wordt een bibliotheek opgebouwd van de effecten van topografie op het weefsel, dit kan gebruikt worden bij toekomstige onderzoeken en toepassingen. In deze thesis wordt het “TopoChip” platform beschreven dat gebruikt kan worden voor high-throughput screening van interacties tussen cellen en oppervlakte topografieën.

Hoofdstuk 2 beschrijft de microfabricatie technieken die vitaal zijn voor de ontwikkeling van Materiomic. Verder wordt de toepassing van deze techniek voorgesteld met enkele relevante voorbeelden.

In hoofdstuk 3 wordt verder ingegaan op het ontwerp en vervaardigen van de bibliotheek van cellulaire responsen op oppervlakte topografieën die de naam “TopoChip” heeft. Het identificeren van oppervlakte topografieën die de proliferatie of osteogene differentiatie kunnen sturen van

mesenchymale stamcellen wordt verder toegelicht. Het is mogelijk gebleken specifieke eigenschappen van ontwerpen te koppelen aan cellulaire responsen, waardoor het mogelijk is deze eigenschappen mee te nemen in toekomstige ontwerpen. Het is bewezen dat het gebruik van gerandomiseerde oppervlakte topografieën breed kan worden toegepast om de interactie tussen cellen en oppervlakte topografie te bepalen, waarmee uiteindelijk betere materiaal oppervlakten gemaakt kunnen worden.

Hoofdstuk 4 beschrijft het ontwerp, de fabricatie van een micro-vloeistof chip platform voor high-throughput screening van biomaterialen door middel van cel culturen. Het apparaat levert een omgeving die nodig is voor het kweken van cellen wat leidt tot goede levensvatbaarheid. Bovendien is het ook mogelijk is om de cellen uniform te verspreiden tijdens het zaaien. Verder indiceren CFD simulaties dat er een goede uitwisseling is van voedingsstoffen en metabolieten met de stroom van medium (Pe>1) terwijl er geen uitwisseling tussen aanliggende testeenheden wordt verwacht. Bovendien kan de schuifspanning van de cellen uniform aangepast worden over het gehele oppervlak van de chip. Op basis van deze uitkomsten denken we dat ons chip platform een veelzijdig stuk gereedschap is voor high-throughput cel experimenten op biomaterialen.

Hoofdstuk 5 laat de ontwikkeling en veelzijdigheid van een eenvoudige analyse methode zien die het gedrag van cellen die gekweekt worden op biomaterialen kan meten en voorspellen. We zijn in staat geweest om veranderingen in morfologie van hMSCs op te roepen door de oppervlakte eigenschappen van PLA sheets aan te passen die gebruikt werden voor cel cultuur. Aan de hand van morfologische eigenschappen bleek het mogelijk om met 92% nauwkeurigheid cellen te onderscheiden die op behandelde en onbehandelde sheets waren gekweekt. Het verschil in morfologie geeft een verandering het cytoskelet van de cellen aan, wat een indicatie kan zijn van veranderingen in activiteit van biochemische reactieketens. Door het precies bepalen van het cellulaire fenotype, is het gebruik van

digitale scans een krachtig gereedschap om eigenschappen van biomaterialen te testen zonder het gebruik van biologische markers.

Hoofdstuk 6 kijkt terug op de discussie en conclusies van ieder hoofdstuk. In dit hoofdstuk stellen we ook nieuwe technieken voor die gebruik maken van oppervlakte topografieën om de fundamentele complexiteit van cellulaire organisatie te onderzoeken.

Acknowledgements

It is a pleasure to thank the many people who made this thesis possible.

It is difficult to overstate my gratitude to my supervisor, Dr. Roman Truckenmuller. With his enthusiasm, his inspiration, and his great efforts to explain things, he helped to make science fun for me. Roman, you have been a walking, talking encyclopedia of microfabrication for me. Throughout my thesis-writing period, he provided encouragement, sound advice, good teaching, good company, and lots of good ideas. I would have been lost without him. It is due to Prof. Jan Feijen's co-operation and kind advice that this thesis is seeing the light of the day.

I would like to thank the many people who have taught me science: my high school teachers (especially Chandrashekhar Kashikar and Chandrakant Raut), my undergraduate teachers at Sawangi (especially Prof. Dr. Anil Wanjari and Prof. Dr. Rajiv Borle), and my graduate teachers (especially Dr. John Hedley and Prof. Ken Snowdon). For their kind assistance with writing letters, giving wise advice, helping with various applications, and so on, I wish to thank in addition Prof. Dr. Vinod Subramaniam and Prof. Dr. Jan Eijkel who have been inspirational in showing me the right way.

I am indebted to my many student colleagues for providing a stimulating and fun environment in which to learn and grow. I am especially grateful to Bart Fischer, Frank Assen, Andy Hoffner, Daniel Leisen, Michiel Croes. Niek Molenkamp was particularly helpful with Matlab programming, patiently teaching me. Bart and Niek thanks for all the wonderful time in and out of the lab. Niek and Natalie, thanks a lot for the samenvatting as well.

I also wish to thank my collaborators, particularly Mark Hulsman, Prof. Marcel Reinders, Dr. Matthias Lutolf, Prof. Jeffrey Hubbell, Prof. Albert van den Berg, Dr. Dimitrios Stamatialis, Dr. Anne Carpenter, Dr. Robert Gauvin, Prof. Ali Khademhosseini and Dr. Stefan Gieselbracht without their fruitful contributions this work would have been difficult.

It was a pleasure to share life with wonderful people like Nico, Renuka-Anand, Andre, Aliz,Veda-Ram, Clara-Gustavo, Juan & Björn among others who are very close friends now.

Thanks are also due to members of TR group Jun, Lorenzo, Joyce, Mijke, Anindita, Hugo, Ana, Febriyani, Eelco, Emilie, Ellie, Guilia, Janneke, Nicole, Tim, Bin, Ling, Anouk, Jacqueline, Parthiban, Pamela, Jeroen Rouwkema, Jeroen Leijten, Liliana, Karolina, Wim, Anne, Erik, Bach, Andreas and Charlene. You guys rock! Thanks for all the wonderful time in and out of the lab.

I also wish to thank Tom Groothuis and Maryana Escalante for their timely help in troubleshooting and helping me with problems I would come across. I wish to thank the cleanroom staff in particular Huib van Vossen and Rene Wolf in teaching and helping me with the cleanroom work. This work would be impossible without the help and input of Sip Jan Boorsma and Dominique Post.

Thanks to excellent support from Audrey and Karin for all the administrative work. I wish to thank my friends in Enschede who made the stay worthwhile in particular Marco, Simon, Leunis, Dirk and Cindy Kruse. My roommates Abhi, Mahendra, Amol, Rohit, Mahendra, Amneet and Yash thanks guys for being in my support group.

I wish to express my gratitude to my Indian friends in Enschede particularly, Falguni-Jigar, Hinal-Dhaval, Shashank, Vijay, Nishant and Sushil.

Thank also to my family, especially my mother Nirmala, my uncles and sisters, who have been patient and supportive to see me, progress with my aims in life. Thanks to my father, whose memory has only increased after so many years of his death, when I was a boy wishing to save the world. I am working on it, still.

Last but not least, a big thank you to my wife, Monika. Without her I would be a very different person today, and it would have been certainly much harder to finish a PhD. Still today, learning to love her and to receive her love makes me a better person.

I finish with a final silence of gratitude for my life.

Hemant Unadkat (born 1979, Nagpur, India), finished his bachelors in Dental Surgery from Sharad Pawar Dental College and Hospital, Nagpur University in India. Following which he worked as a research fellow in the Biomaterials and Biointerfaces Laboratory at the Indian Institute of Technology Bombay (IIT Bombay). His work at the IIT Bombay was related to nanoparticulate delivery of Surfactant for neonatal respiratory distress syndrome. After his brief stay at IIT Bombay he went on to do his Masters in Biomedical Nanotechnology at INSAT, University of Newcastle upon Tyne. His Master's project was related to engineering self assembled protein surfaces for tissue culture of neuronal cells. The experimental work of his masters' project was carried out at Orla Protein Technologies Ltd, Newcastle upon Tyne.

Hemant, joined as a Marie Curie Fellow at the University of Twente in October 2006. His research at Twente was focussed around the areas of high content and high throughput screening of biomaterials, micro-nanotechnologies for tissue engineering applications and stem cell bioengineering.

ISBN: 978-90-365-3321-8